Crystal Engineering for Metal-Organic Frameworks

Thèse présentée à la Faculté des Sciences
Institut de Chimie
Université de Neuchâtel

Pour l'obtention du grade de Docteur ès Sciences

Par

Déborah González Mantero

Chimiste diplômée de l'Université de Granada (Espagne)

Acceptée sur proposition du jury:

Prof. H. Stoeckli-Evans, directrice de thèse
Dr. A. Neels, rapporteur
Prof. K. Fromm (Bâle), rapporteur
Prof. F. Stoeckli, rapporteur
Prof. J.-M. Bourgeois (Fribourg), rapporteur

Soutenue le 10 novembre 2005

Université de Neuchâtel

2006

Université de Neuchâtel

IMPRIMATUR POUR LA THESE

Crystal Engineering for Metal-Organic Frameworks

Déborah GONZÁLEZ MANTERO

UNIVERSITE DE NEUCHATEL

FACULTE DES SCIENCES

La Faculté des sciences de l'Université de Neuchâtel,
sur le rapport des membres du jury

Mmes H. Stoeckli-Evans (directrice de thèse),
A. Neels, K. Fromm (Bâle)
MM. F. Stoeckli
et J.-M. Bourgeois (Fribourg)

autorise l'impression de la présente thèse.

Neuchâtel, le 12 décembre 2005

Le doyen :

Le Doyen
de la Faculté des sciences

J.-P. Derendinger

A mis padres

A mis hermanos

A Marcel

Remerciements

Le présent travail a été effectué de janvier 2002 jusqu'à novembre 2005 dans les laboratoires de Chimie Physique II de l'Université de Neuchâtel, sous la direction de Madame le professeur Helen Stoeckli-Evans.

Premièrement, j'aimerais exprimer ma gratitude à ma directrice de thèse, Madame le professeur Helen Stoeckli-Evans, pour m'avoir donné l'opportunité de travailler dans son groupe ainsi que pour sa confiance, son encouragement, sa disponibilité et sa constante bonne humeur et gentillesse. Il a été et il sera toujours un plaisir travailler pour une personne si exceptionnel.

Je remercie les membres de mon jury de thèse, Madame le professeur Katharina Fromm (Université de Basel), Monsieur le Professeur Jean-Marc Bourgeois (HES Fribourg), Madame le Docteur Antonia Neels et Monsieur le Professeur Fritz Stoeckli d'avoir accepté d'être membres du jury de cette thèse et de m'avoir prodigué leurs précieuses suggestions pour l'achèvement de ce travail.

Mes remerciements s'adressent aussi à tous les membres du groupe Chimie Physique I et II, les anciens et les nouveaux. Parmi ces personnes, j'aimerais en citer, en particulier: Jessica, Elena, Gilles et Alejandro. Je les remercie pour leur amitié très enrichissante que j'espère garder très longtemps.

Je remercie aussi mes amis en Suisse et en Espagne pour leur soutien et encouragement.

Enfin, j'aimerais très particulièrement remercier mes parents, mes sœurs, mon frère, et Marcel pour m'avoir écouté, « supporté » et pour être toujours là pour moi. Muchísimas gracias!

Je remercie l'Etat de Neuchâtel et le Fonds National Suisse de la Recherche Scientifique de m'avoir confié un poste d'assistant ainsi que pour leur soutien financier.

Table of Contents

Abbreviations

1D, 2D, 3D	One-, two-, three-dimensional
MOF	Metal-Organic Framework
XRPD	X Ray Powder Diffraction
a, b, c	Unit-cell lengths in Å
α, β, γ	Unit-cell angles in °
V	Unit-cell volume in $Å^3$
Z	Number of molecules per unit cell
D_c	Calculated density in g/cm^3
R1, wR2	Final structure agreement factors
τ	Five coordinate distortion parameter
4,4'-bpy	4,4'-Bipyridine
dpdo	4,4'**-**Dipyridyl-N,N′-dioxide
Apy	4-aminopyridine
Apyz	2-aminopyrazine
ClApy	4-amino-2-chloropyridine
H_4-BCTA	benzene-1,2,4,5-tetracarboxylic acid
ETOH	Ethanol
DMSO	Dimethyl sulfoxid
THF	Tetrahydrofurane
MW	Microwave
IR	Infrared
$\tilde{\nu}$	Vibration frequency in cm^{-1} (IR)
s, m, w, br	Strong, medium, weak, broad (IR)
ESI-MS	Electrospray Ionization - Mass Spectrometry

EI-MS	Electronic Impact - Mass Spectrometry
T	Temperature
t	Time
TG	Thermogravimetric analysis
EA	Elemental analysis
$\mathbf{N_a}$	Amount of gas adsorbed in moles per gram of solid when the relative pressure is p/p_0
$\mathbf{N_{a0}}$	Total amount of gas adsorbed in moles per gram of solid
p	Pressure
$\mathbf{p_0}$	Saturation vapour pressure of the adsorptive
A	Polanyi adsorption potential
B	Structural constant of the adsorbent
β	Affinity coefficient
$\mathbf{E_0}$	Characteristic energy of the solid in kJ/mol
α	Expansion coefficient of the adsorbate
Γ	Gamma function
$\mathbf{-\Delta h_i}$	Enthalpy of immersion in J/g
$\mathbf{W_0}$	Micropore volume in cm^3/g
$\mathbf{S_e}$	External surface area in m^2/g
$\mathbf{-h_i}$	Enthalpy of immersion of the external surface in J/m^2
$\mathbf{V_m}$	Liquid molar volume in cm^3/mol
MW	Molecular weight in g/mol
L	Molecule width in nm
μ	Dipole moment in D
Q	Electric quadrupole moment in multiples of barns [$\cdot 10^{-24}$ cm^2]
k	Kinetic rate constant

Keywords: Metal-organic frameworks, Nanoporous, Crystal Engineering, Adsorption, Green Chemistry.

Mot clés: Structures métal-organiques nanoporeuses, Assemblage ciblé, Adsorption, Chimie verte.

Résumé

La porosité est une caractéristique des matériaux solides qui détermine leur performance comme catalyseurs, adsorbants, etc. Pour cette raison, le control de la taille des pores et leur forme sont des facteurs déterminants pour leur efficacité pendant le processus d'adsorption. L'assemblage ciblé des structures métal-organiques, cristallines et nanoporeuses permet obtenir un large nombre de nouveau matériaux ainsi que une vaste variété de propriétés, fonctions et applications. Ces structures peuvent être synthétisées par simple modification des composants ou des conditions de réaction.

Ce travail a eu comme but la synthèse de nouveau matériaux métal-organiques et cristallines, spécialement ces qui possèdent une grande porosité et qui peuvent être utilisés comme adsorbants. La technique de diffraction de Rayons X nous a permit déterminer les structures cristallines de un grand nombre de composés ainsi que les transformations que certaines parmi eux soufrent sous déterminées conditionnes.

La réalisation des isothermes d'adsorption ainsi que des expériences de calorimétrie d'immersion nous a permit déterminer le caractère permanent de la porosité pour plusieurs structures métal-organiques. Ces deux techniques ont apporté également d'information essentielle sur le type des interactions qui contrôlent le processus d'adsorption.

La synthèse de quelques ligands organiques a été réalisée en considérant les principes de la *Chimie Vert*. La condensation des produits initiaux sans l'utilisation de solvants génère des ligands qui possèdent des atomes susceptibles de coordiner au centres métalliques pour former des structures métal-organiques, cristallines et nanoporeuses.

Overview of Synthesized Products

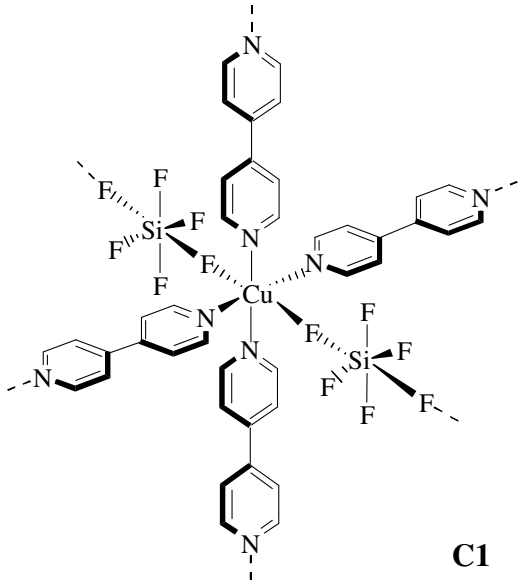

C1

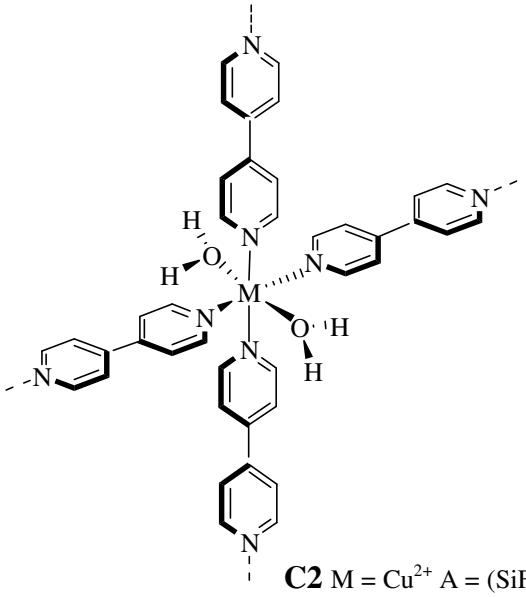

C2 M = Cu^{2+} A = $(SiF_6)^{2-}$
C9 M = Cu^{2+} A = $(S_2O_6)^{2-}$
C10 M = Co^{2+} A = $(SO_4)^{2-}$

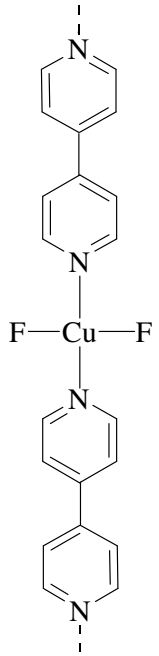

C3

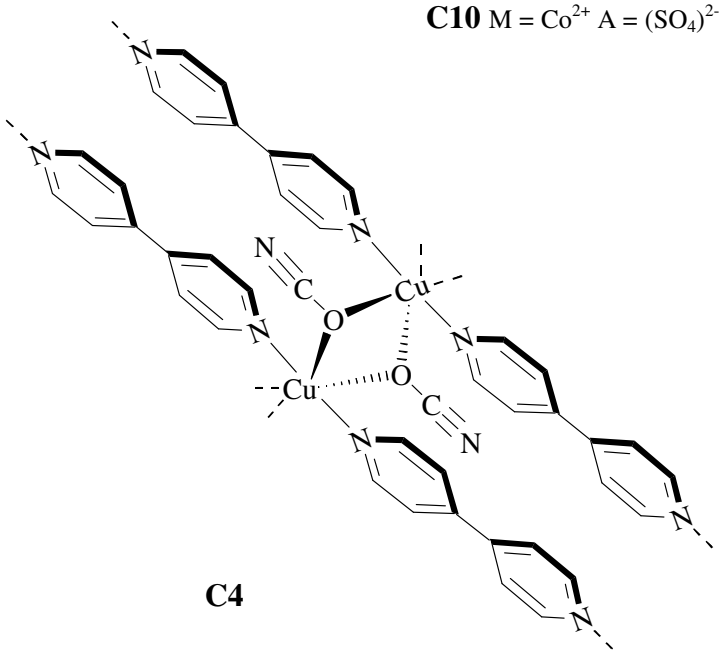

C4

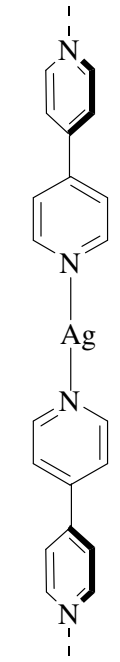

C5 A = $(SiF_6)^{2-}$

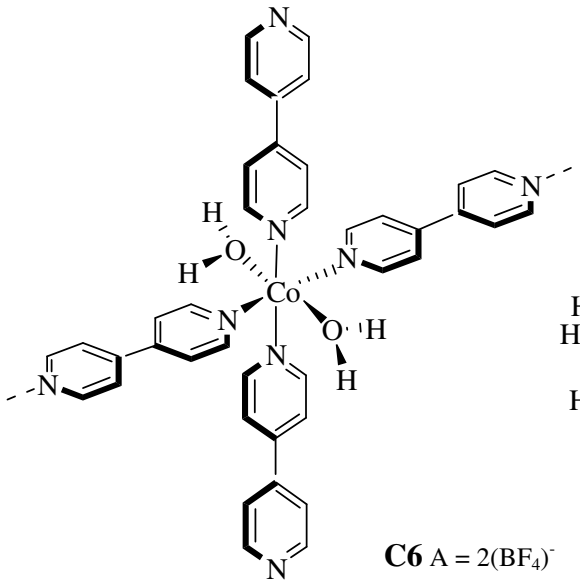

C6 A = $2(BF_4)^-$

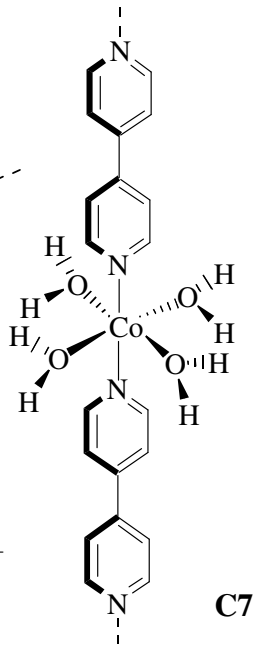

C7 A = $2(BF_4)^-$

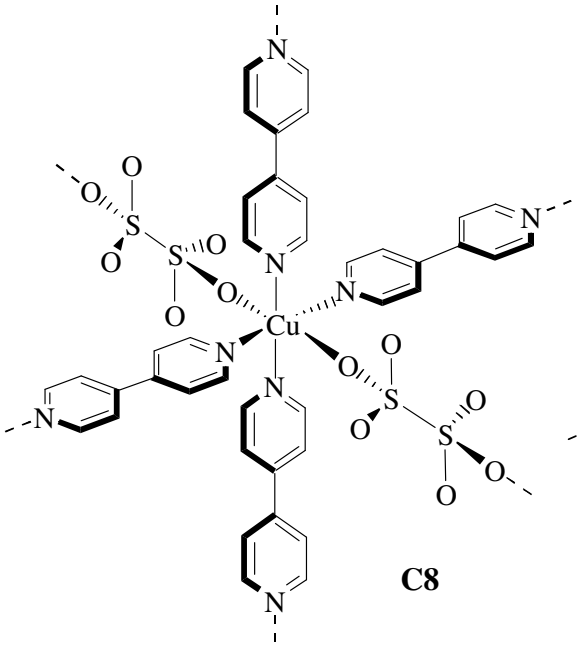

C8

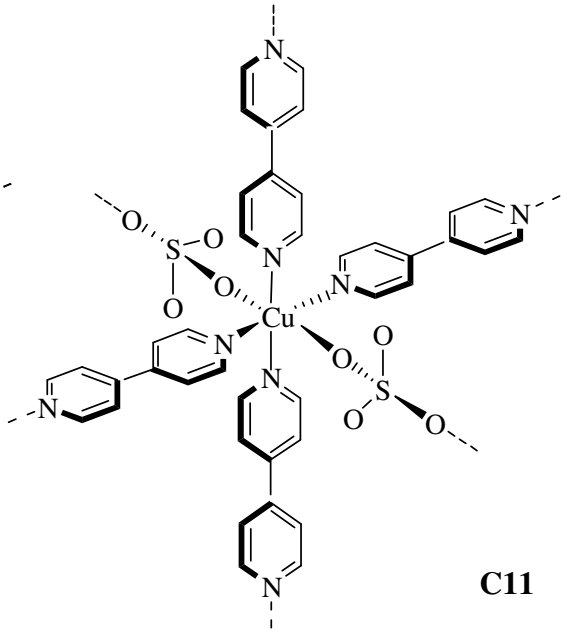

C11

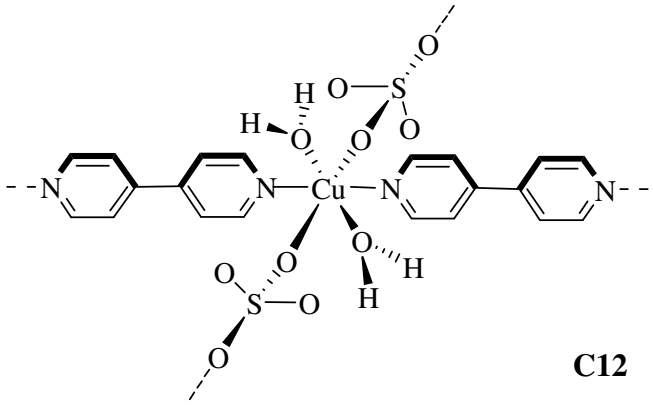

C12

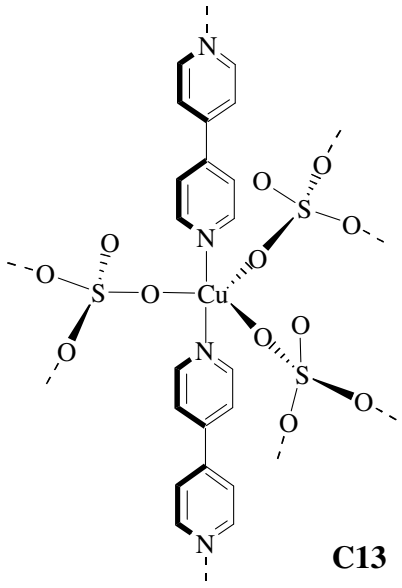

C13

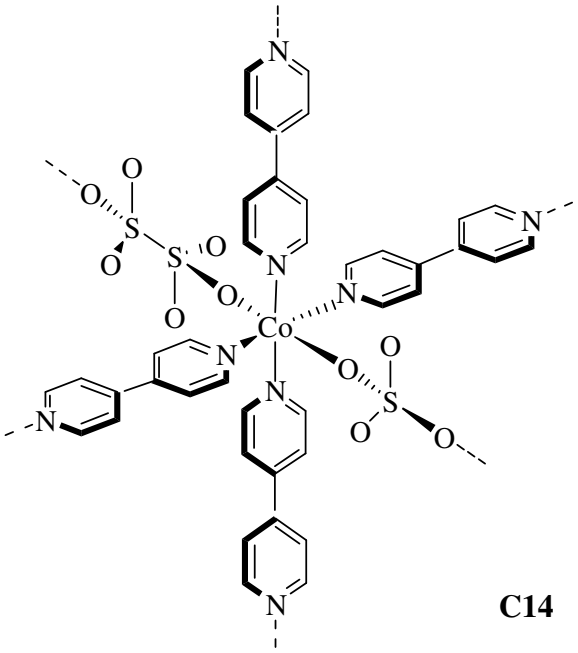

C14

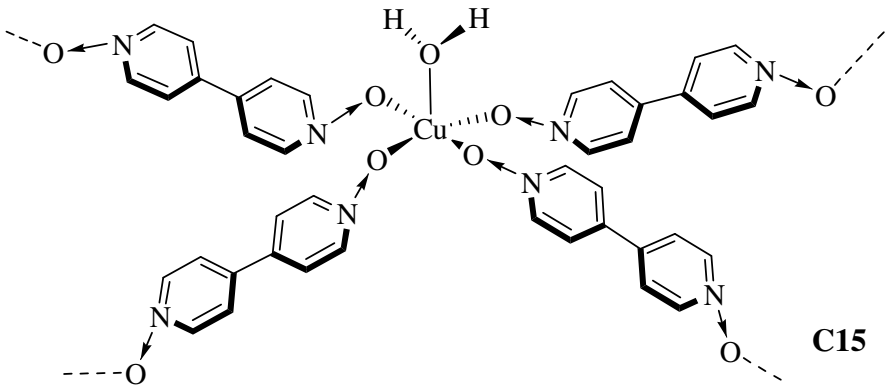

C15

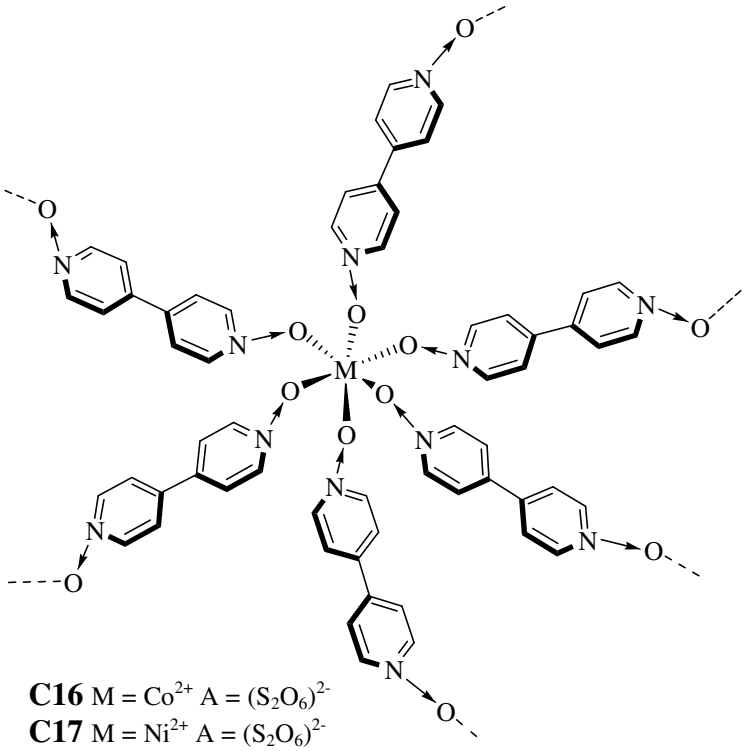

C16 M = Co^{2+} A = $(S_2O_6)^{2-}$
C17 M = Ni^{2+} A = $(S_2O_6)^{2-}$

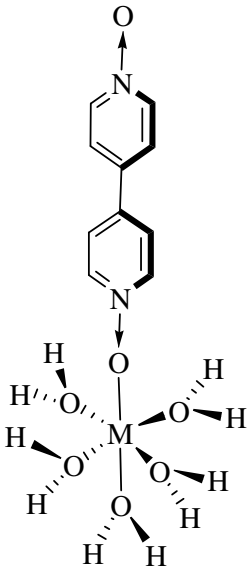

C18 M = Co^{2+} A = $(SO_4)^{2-}$
C19 M = Ni^{2+} A = $(SO_4)^{2-}$

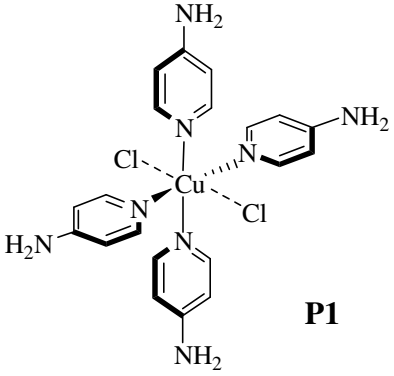

P1

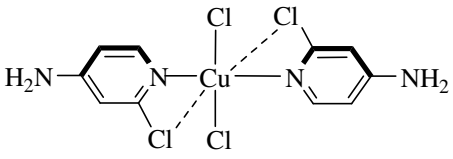

P2

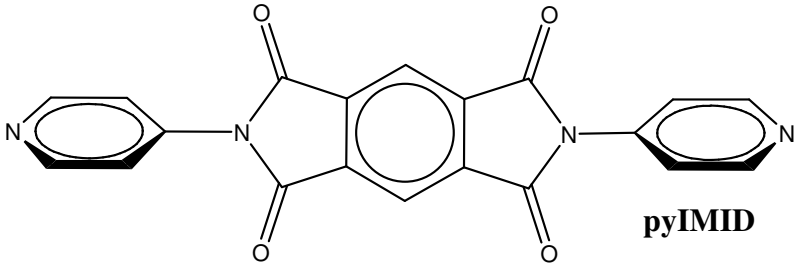

pyIMID

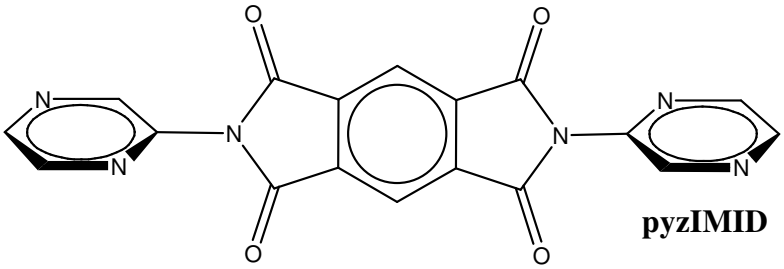

pyzIMID

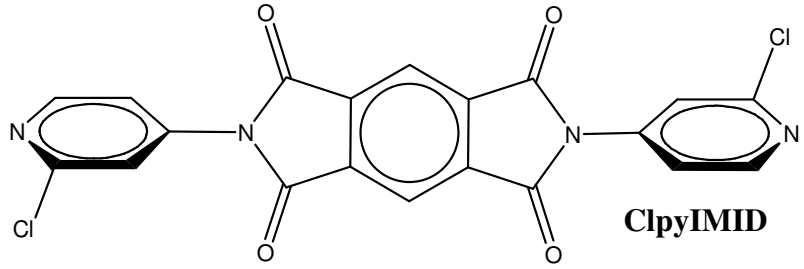

ClpyIMID

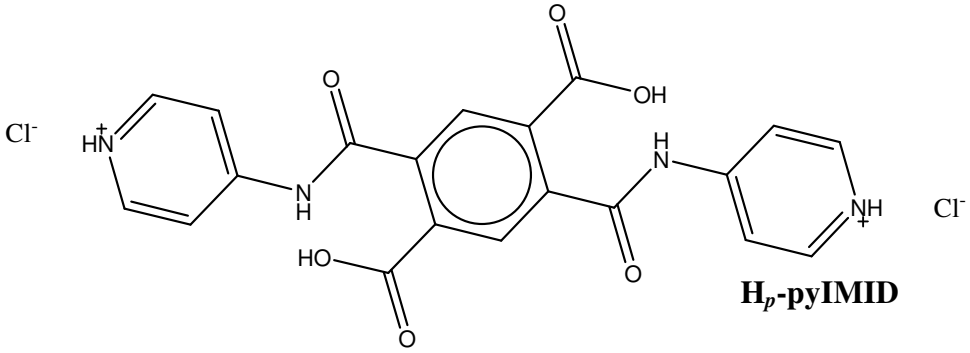

H$_p$-pyIMID

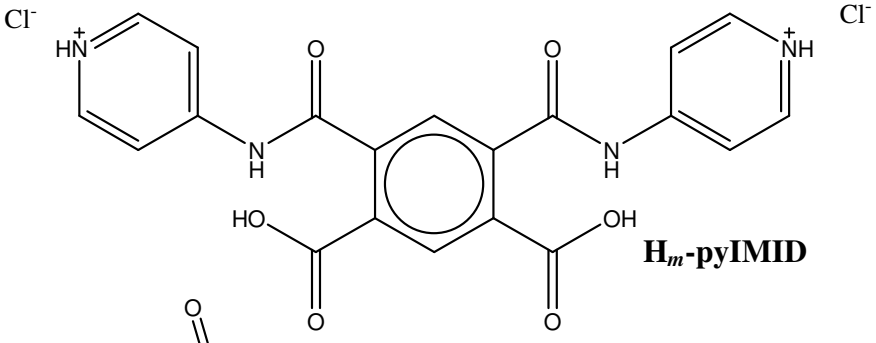

H$_m$-pyIMID

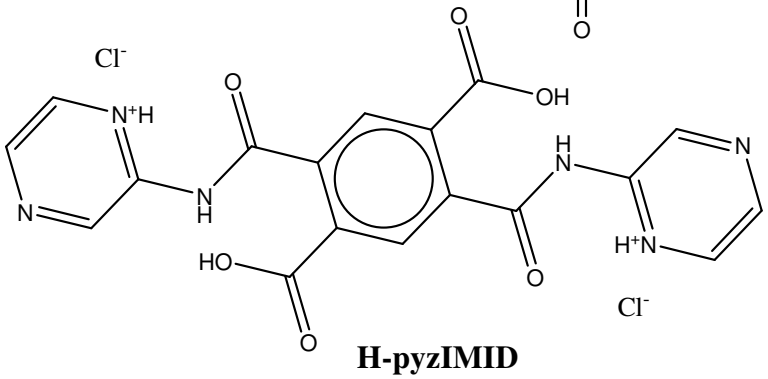

H-pyzIMID

1. Introduction

1. Introduction

1.1 Coordination Polymers: From the Molecule to the Network

Coordination Chemistry has also gone *supramolecular* [1-3] and *Crystal Engineering* is the tool for the design of these new supramolecular structures by self-assembly from the initial components [1, 4-9]. Molecular self-assembly occurs through interactions of a very wide energy range [10].

- Isotropic interactions, which are responsible for gross shapes and close packing effects (medium range).
- Anisotropic interactions and those of electrostatic origin like hydrogen bonds, which are responsible for all the fine effects and intermolecular interactions (long range).
- Strong metal-metal bonds and metal-ligand coordination bonds.

The understanding of these interactions constitutes the first step in the control of the organisation in supramolecular structures.

In the construction of coordination polymers, polydentate organic ligands, inorganic anions and metal centres are frequently used, expanding coordination in one, two and three dimensions [11-13] (Figure 1.1). The diversity of structures that can be obtained from the simplest of components is quite remarkable.

The self-assembly approach applies equally well to all levels of dimensionality. The dimension of the metal-organic polymer is, in the first step, determined by the metal

ions coordination geometry, e.g., linear, T-shaped, octahedral, etc. Then, the tendency of counteranions to coordinate to the metal centres, the ligand size and its steric bulk, and the solvent used in the synthesis, among other factors (e.g., temperature, pH, pressure, etc.) can determine the dimensionality of the polymer.

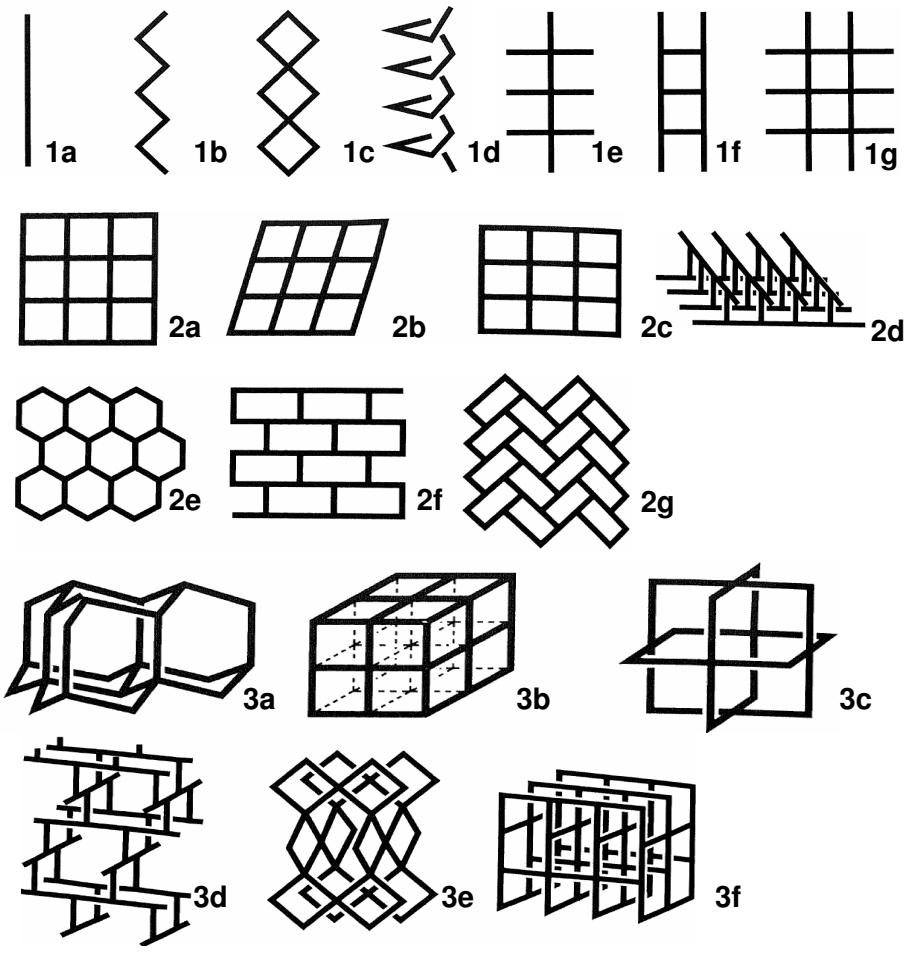

Figure 1.1 Multidimensional structures [11]; (1a) linear chain, (1b) zigzag chain, (1c) double chain, (1d) helix, (1e) fish-bone, (1f) ladder, (1g) railroad, (2a) square grid, (2b) rhombic grid, (2c) rectangular grid, (2d) bilayer, (2e) honeycomb grid, (2f) brick wall, (2g) herringbone, (3a) diamondoid net, (3b) octahedral net, (3c) NbO net, (3d) $ThSi_2$ net, (3e) PtS net and (3f) $CdSO_4$ net.

1.2 Porous Materials

Porosity and surface area are important characteristics of solid materials and determine their properties and performance as catalysts, sorbents, medicines, etc. and the

efficiency of their activity is related to these characteristics. For this reason, the control of the pore size and pore shape in these materials are determinant factors for the ulterior adsorption process [14-17]. Although these compounds are usually useful, some of them present some limitations. For example, the pore size of the zeolites is difficult to control due to the inherent geometry of the alumino-silicates and the framework of inclusion compounds often collapses after removal of the guest.

Crystal Engineering involves the design and the development of new crystalline materials named *metal-organic frameworks* (MOF's). They possess a broad variety of properties, functions and applications [11, 18-20] such as materials chemistry, heterogeneous catalysis, gas storage, polymer magnets, etc. This functionality can be modulated by an easy and rational modification of the building block components or reaction conditions [20].

For a solid to be labelled a MOF, it should display the inherent attributes that the term implies [21], namely,

- Strong bonds, providing robustness
- Linking units, that are available for modification by organic synthesis
- A geometrically well-defined structure

There is also some debate about the minimum dimensionality that is necessary to constitute a MOF. 1D or 2D structures do not fit the connotation of "framework"; nevertheless, some of these structures have shown adsorption properties [16, 22]. Consequently, these structures will be denoted as "MOF" only if they fulfil all the related conditions [21].

Porosity is frequently assumed in MOF's but it is erroneous for frameworks where the co-crystallized solvent molecules cannot be removed or exchanged without loss of framework integrity. For this reason, a classification of the porous coordination compounds into three categories was performed [23, 24].

- First generation compounds have microporous structures, which are sustained only with guest molecules and show irreversible framework collapse on removal of guest molecules.
- Second generation compounds have stable and robust microporous structures, which show permanent porosity after removal of guest molecules.
- Third generation compounds have flexible and dynamic structures, which respond to external stimuli such as pressure, guest molecules, light, etc.

Adsorption studies can be carried out only on samples which belong to the second and third generation of porous coordination compounds.

In summary, this new class of porous materials is attracting attention due to their accessible pore structure, high apparent surface areas, selective uptake of small molecules, anion and solvent molecule exchanges, and optical or magnetic responses to the adsorption of the guest [25-28].

1.3 Adsorption Theory

When a gas comes into contact with a solid surface, molecules of the gas will adsorb ("*stick*") to the surface in quantities that are a function of the temperature and of their partial pressure in the system. The adsorption of a gas by solid results from the forces of attraction between the individual molecules of the gas and the atoms or ions composing the solid [29]. The measurement of the amount of a gas adsorbed, N_a (molg^{-1}), over a range of partial pressures and a given temperature leads to a graph known as an adsorption isotherm, where

$$N_a = f(p)_{T,gas,solid} \tag{1.1}$$

If the temperature is below the critical temperature of the gas, the Equation 1.1 leads to

$$N_a = f(p/p_0)_{T,gas,solid} \qquad (1.2)$$

where p_0 is the saturation vapour pressure of the adsorptive.

Isotherms can have different shapes depending on the type of adsorbent, the type of adsorbate, and the intermolecular interactions between the gas and the solid (Figure 1.2) [30].

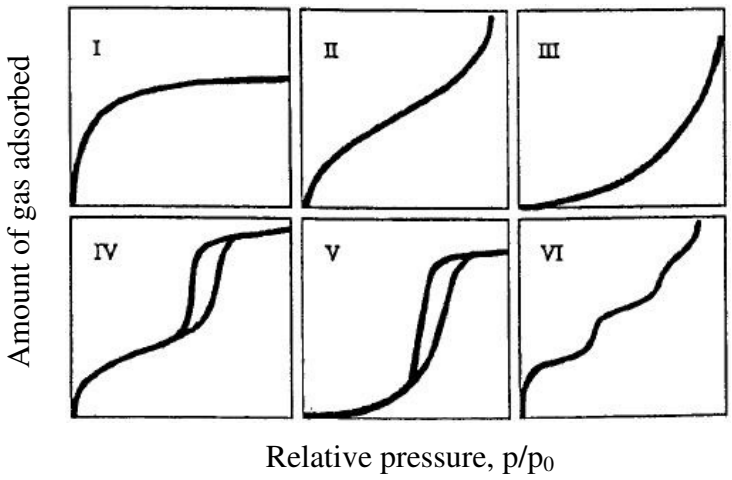

Figure 1.2 The IUPAC classification for adsorption isotherms.

Type I isotherms characterize microporous adsorbents with pore widths smaller than 2nm. Types II and III describe adsorption on open substances. Types IV and V represent adsorption isotherms on mesoporous adsorbents with pore widths between 2 and 50 nm. The hysteresis loops reflect capillarity condensation in the pores of radii > 1.8 nm. Types III and V isotherms present a weak adsorbate-adsorbent interaction. Finally, the type VI has steps and is relatively rare [29,30].

Dubinin's theory [31] for the volume filling of micropores is used to describe the gas-solid adsorption by our solids. The theory postulates the temperature invariance of the relative adsorption plotted as a function of the adsorption potential A = -ΔG (free energy of adsorption) [32].

$$A = RT \ln\left(\frac{p_0}{p}\right) \tag{1.3}$$

It is a direct consequence of the Polanyi potential theory of adsorption (Equation 1.3) [33].

Dubinin, in collaboration with Radushkevich (DR), put forward an equation based on the earlier Polanyi theory of adsorption. The equation is

$$N_a = N_{a0} \exp\left[-B\left(\frac{T}{\beta}\right)^2 \log^2\left(\frac{p_0}{p}\right)\right] \tag{1.4}$$

where B is a parameter which depends on the solid structure and β is a parameter called affinity coefficient which depends on the adsorbate nature. Dubinin chose benzene for the standard adsorbate, therefore, $\beta(C_6H_6) = 1$.

In 1971, Dubinin and Astakhov (DA) proposed a more general equation (Equation 1.5) [34] to extend the scope of the DR treatment (Equation 1.4) to a variety of porous solids.

$$N_a = N_{a0} \exp\left[-\left(\frac{A}{\beta E_0}\right)^n\right] \tag{1.5}$$

where E_0 is the characteristic energy of the solid and n is an exponent, the value of which is between 1.5 – 3.0 for active carbons and 3 – 6 for zeolites.

Although the DA equation applies essentially to microporous solids, some non-microporous solids follow an equation (Equation 1.6) similar to DA equation (Equation 1.5), usually with exponent n = 2, called equation of Dubinin, Radushkevich and Kaganer (DRK).

$$N_a = N_{a0} \exp\left[-\left(\frac{A}{E}\right)^n\right] \tag{1.6}$$

Dubinin's theory can be extended to immersion calorimetric studies [32, 34, 35] of microporous solids. This approach provides a constructive complement to adsorption isotherm experiments. Immersion calorimetry is based on the determination of the enthalpy change occurring on immersing an out-gassed sample into a liquid [30]. The enthalpy change is related to the chemical and structural *nature* of the surface and the enthalpy immersion value is equal to the integral of the net heat of adsorption [32, 35].

$$-\Delta h_i\left(Jg^{-1}\right) = Na_0 E(1+\alpha T)\Gamma(1+1/n) \tag{1.7}$$

where α is the expansion coefficient of the adsorbate and Γ is the tabulated "Gamma" function. In the case of the DR equation, where n = 2 and the micropore volume $W_0 = Na_0\ V_m$ and taking into account the wetting of the external and non-porous surface area S_e, Equation 1.7 leads to

$$-\Delta h_i\left(Jg^{-1}\right) = \beta E_0 W_0(1+\alpha T)\sqrt{\pi}/2V_m + h_i S_e \tag{1.8}$$

where $-h_i(J/m^2)$ represents the enthalpy of wetting of the external (non-microporous) surface.

Immersion calorimetry has the advantage of being sensitive and accurate, but it requires the preparation of sealed thin-walled or brittle-ended glass bulbs enclosing the out-gassed sample.

1.4 Green Chemistry Approach in Synthesis of New Ligands for Metal-Organic Frameworks

As previously said, different physical and chemical properties of solids can be obtained by applying *Crystal Engineering* principles to the construction of coordination polymers. For this reason, the design and synthesis of new organic ligands, which are susceptible to coordination with metal centres, is fundamental in *Supramolecular Chemistry* and *Crystal Engineering*. Moreover, there is a new "*green*" way of synthesising molecular and supramolecular solids called *Green Chemistry* [36-39], which focuses upon the reinvention of chemistry in an environment friendly way.

.

Green Chemistry or *Environmentally Benign Chemistry* is defined by the IUPAC as the invention, design, and application of chemical products and processes to reduce or eliminate the use and generation of hazardous substances [40, 41]. The new *Green Chemistry* reactions are broad in scope and they range from natural processes (biosynthesis, biocatalysis) to solid state reactions and are based on an ideal synthetic method (Figure 1.3) [42].

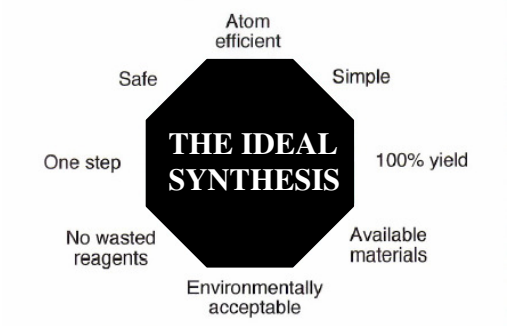

Figure 1.3

To determine how *green* a method is, Anastas and Warner have developed the *Twelve Principles of Green Chemistry* [41]. They are

1. It is better to prevent waste than to treat or clean up waste after it is formed.

2. Synthetic methods should be designed to maximize the incorporation of all materials used in the process into the final product.
3. Wherever practicable, synthetic methodologies should be designed to use and generate substances that possess little or no toxicity to human health and the environment.
4. Chemical products should be designed to preserve efficiency of function while reducing toxicity.
5. The use of auxiliary substances (e.g. solvents, separation agents, etc.) should be made unnecessary whenever possible and, innocuous when used.
6. Energy requirements should be recognized for their environmental and economic impacts and should be minimized. Synthetic methods should be conducted at ambient temperature and pressure.
7. A raw material feedstock should be renewable rather than depleting whenever technically and economically practical.
8. Unnecessary derivatization (blocking group, protection/unprotection, and temporary modification of physical/chemical processes) should be avoided whenever possible.
9. Catalytic reagents (as selective as possible) are superior to stoichiometric reagents.
10. Chemical products should be designed so that at the end of their function they do not persist in the environment and break down into innocuous degradation products.
11. Analytical methodologies need to be further developed to allow for real-time in-process monitoring and control prior to the formation of hazardous substances.
12. Substances and the form of a substance used in a chemical process should be chosen so as to minimize the potential for chemical accidents, including releases, explosions, and fires.

Green Chemistry involves the development of chemical products and synthetic procedures, which are environmentally friendly and have reduced health risks with the search for more efficient methods to do chemistry. Like Dr. Terry Collins, Professor of

Chemistry of the Carnegie Mellon University said, "Chemistry has an important role to play in achieving a sustainable civilization on earth." [43].

1.5 Scope of the Present Investigation

The scope of this work is the design of MOF's especially those which present a rigid three-dimensional structure with a high degree of porosity suitable to work as adsorbents. They are constructed from transition metal ions, inorganic anions and bridging linear organic ligands derived from pyridine, such as 4,4'-bipyridine and 4,4'-dipyridyl-N,N′-dioxide.

Reversible physisorption of small molecules experiments such as gas isotherms and immersion calorimetry studies have also been carried out on the above mentioned polymers which will establish the attainment of permanent porosity after guest removal.

Another related subject of the investigation is the synthesis of new linear ligands based on *Green Chemistry*, a new emerging field in modern chemistry. These new ligands are potential bridging ligands which could be used to build MOF's applying the principles of *Crystal Engineering*. They have been synthesized by the condensation of the starting materials and the final product contains nitrogen donors suitable for coordination to metal centres.

1.6 References

[1] Braga D., *Chem. Commun.*, 22, 2751-2754, **2003**.

[2] Lehn J.-M., *Pure Appl. Chem.*, 66, 1961-1966, **1994**.

[3] Ward M. D., *Annu. Rep. Prog. Chem. Sect. A: Inorg. Chem.*, 97, 293-329, **2001**.

[4] Brammer L., *Chem. Soc. Rev.*, 33, 476-489, **2004**.

[5] Braga D., *Chem. Rev.*, 98, 1375-1405, **1998**.

[6] Sherman J., *Chem. Commun.*, 14, 1617-1623, **2003**.

[7] Erk P., Hengelsberg H., Haddow M. F., van Gelder R., *Cryst. Eng. Comm.*, 6(78),

474-483, **2004**.

[8] Braga D., Maini L., Polito M., Scaccianoce L., Cojazzi G., Grepioni F., *Coord. Chem. Rev.*, 216-217, 225-248, **2001**.

[9] Ball P., *Nanotechnology*, 13, R15-R28, **2002**.

[10] Desiraju G. R., *J. Mol. Struct.*, 656, 5-15, **2003**.

[11] Kitagawa S., Noro, S., *Comp. Coord. Chem. II*, 7,231-261, **2004**.

[12] Moulton B., Zaworotko J., *Chem. Rev.*, 101, 1629-1658, **2001**.

[13] Blake A.J., Champness N. R., Hubberstey P., Li W.-S., Withersby M. A., Schröder M., *Coord. Chem. Rev.*, 183, 117-138, **1999**.

[14] Bradshaw D., Prior T. J., Cussen E. J., Claridge J. B., Rosseinsky, *J. Am. Chem. Soc.*, 126, 6106-6114, **2004**.

[15] Férey G., Latroche M., Serre C., Millange F., Loiseau T., Percheron-Guégan A., *Chem. Commun.*, 2976-2977, **2003**.

[16] Kitaura R., Seki K, Akiyama G., Kitagawa S, *Angew. Chem. Int. Ed.*, 42, 428-431, **2003**.

[17] Yang P., *"The Chemistry of Nanostructured materials"*, World Scientific Publishing Co. Pte. Ldt., Singapore (Singapore), **2003**.

[18] James S. L., *Chem. Soc. Rev.*, 32, 276-288, **2003**.

[19] Rosseinsky M. J., *Microporous Mesoporous Mater.*, 73, 15-30, **2004**.

[20] Rosi N. L., Eddaoudi J., Kim J., O'Keeffe M., Yaghi O. M., *Cryst. Eng. Comm.*, 4, 401, **2002**.

[21] Rowsell J. L. C., Yaghi O. M., *Microporous Mesoporous Mater.*, 73, 3-14, **2004**.

[22] Jung O.-S., Kim Y. J., Lee Y.-A., Park J. K., Chae H. K., *J. Am. Chem. Soc.*, 122, 9921-9925, **2000**.

[23] Kitagawa S., Kondo M., *Bull. Chem. Soc. Jpn.*, 71, 1739-1753, **1998**.

[24] Kitagawa S., Uemura K., *Chem. Soc. Rev.*, 34, 109-119, 2005.

[25] Yaghi O. M., Li H., Groy T. L., *Inorg. Chem.*, 36, 4292-4293, **1997**.

[26] Min K. S., Suh M. P., *Chem. Eur. J.*, 7, 303-313, **2001**.

[27] Chandler B. D., Coté A. P., Cramb D. T., Hill J. M., Shimizu G. K. H., *Chem. Commun.*, 1900-1901, **2002**.

[28] Halder G. J., Kepert C. J., Moubaraki B., Murray K. S., Cashion J. D., *Science*,

298, 1762-1765, **2002**.

[29] Gregg S. J., Sing K. S. W., *"Adsorption, Surface Area and Porosity"*, second edition, Academic Press Inc., London (UK), **1982**.

[30] IUPAC Recommendations, *Pure Appl. Chem.*, 66, 1739, **1994**.

[31] Dubinin M. M., *Q. Rev. Chem. Soc.* 9, 101, **1955**.

[32] Stoeckli F., *Adsorpt. Sci. Technol.*, 10, **1993**.

[33] Polanyi M., *Trans. Faraday Soc.*, 28, 316, **1932**.

[34] Stoeckli F., Lavanchy A., Hugi-Cleary D., *Fundamentals of adsorption,* 6 (1998), 24-28.

[35] Stoeckli F., Hugi-Cleary D., Centeno T. A., *J. Eur. Ceram. Soc.*, 18, 1177-1185, **1998**.

[36] Braga D., Grepioni F., *Angew. Chem. Int. Ed.*, 43, 4002-4011, **2004**.

[37] Tanaka K., Toda F., *Chem. Rev.*, 100, 1025, **2000**.

[38] Cave G. W. V., Raston C. L., Scott J. L., *Chem. Commun.*, 2159, **2001**.

[39] Rothenberg G., Downie A. P., Raston C. L., Scott J. L., *J. Am. Chem. Soc.*, 123, 8701, **2001**.

[40] Tundo P., Anastas P., Black D. StC., Breen J., Collins T., Memoli S., Miyamoto J., Polyakoff M., Tumas W., *Pure Appl. Chem.*, 72, 1207-1228, **2000**.

[41] Anastas P. T., Warner, J. C., *Green Chemistry Theory and Practice*, Oxford University Press, New York, **1998**.

[42] Clark J. H., *Green Chem.*, 1(1), 1-8, **1999**.

[43] Collins T., *Science*, 291, 48-49, **2001**.

2. Complexes with 4,4'-Bipyridine

2. Complexes with 4,4'-Bipyridine

2.1 4,4'-Bipyridine as Bridging Ligand

4,4'-Bipyridine (4,4'-bpy) (Figure 2.1) is an excellent linear bridging ligand with nitrogen donors which show strong coordination behaviour towards a large number of transition metals such as Cu, Ni, Cd, Zn, Co, Mn, etc. The literature is extended and displays all kinds of structural possibilities [1-4]. Mononuclear compounds and 1D, 2D, and 3D polymers can be easily obtained by changing the reaction conditions and the starting materials. Besides the coordination bonds, the 4,4'-bpy is liable to have some weak intermolecular interactions such as hydrogen bonding and π–π stacking effects with other molecules [5]. Indeed, these non-covalent interactions play an important role in the formation of supramolecular structures.

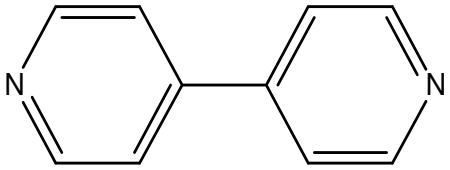

Figure 2.1

2.2 Complexes with Anions Containing Fluorine

2.2.1 $\{[Cu(SiF_6)(4,4'\text{-bpy})_2](H_2O)_8\}_n$: C1

This 3D metal-organic complex (Figure 2.2) was synthesized by Kitagawa et al. in 2000 [6,7]. Violet block-like single crystals of **C1** were obtained by diffusion

experiments. The crystalline powder of **C1** suitable for XRPD analysis was obtained by stirring solutions of the same concentration.

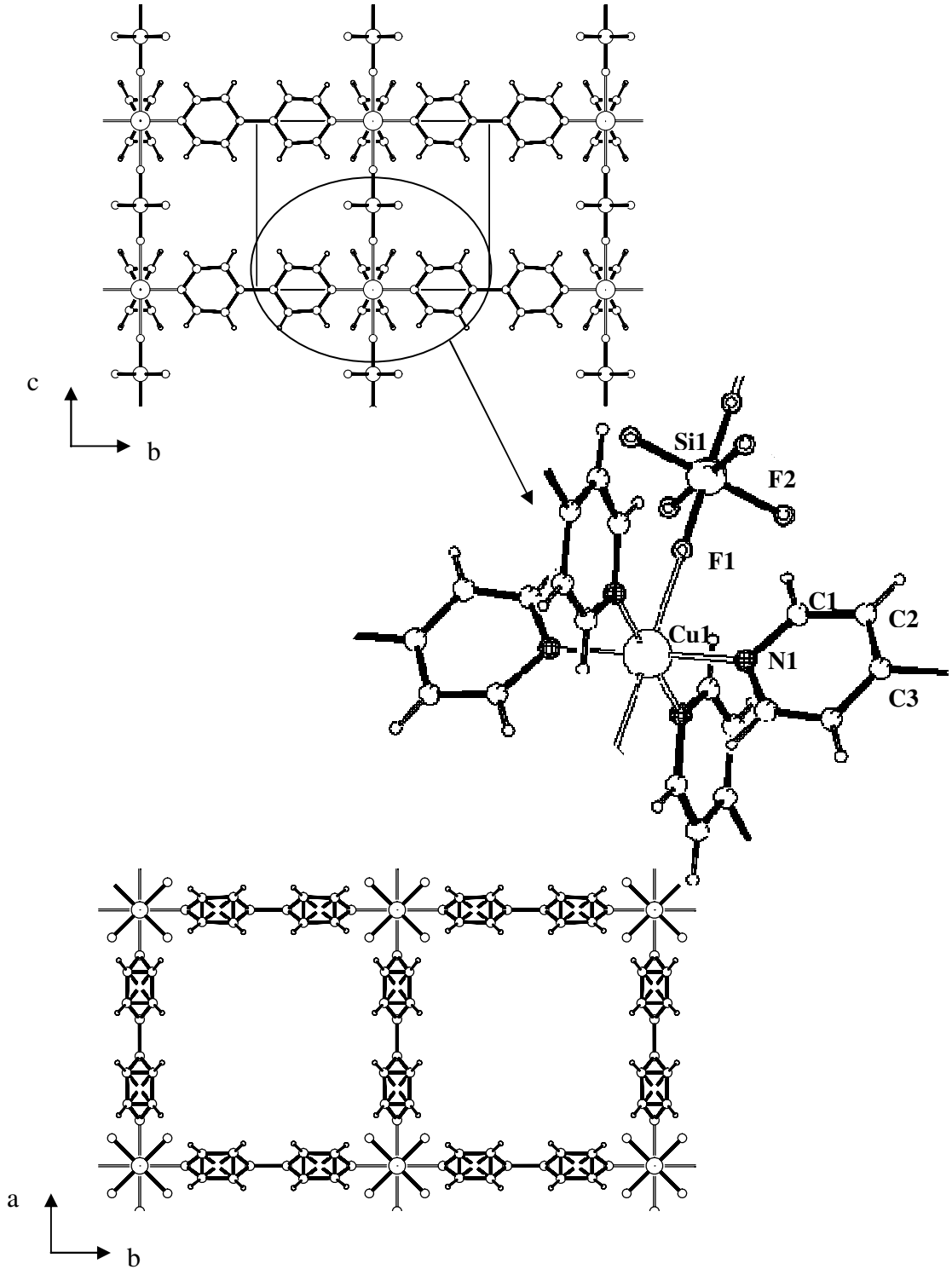

Figure 2.2 Crystal packing diagrams of complex **C1**. The pyridine rings are disordered over two positions, as shown in the bottom figure.

The structure of **C1** was established by X-ray analysis. It crystallizes in the tetragonal crystal system, space group P4/mmm, with a = b = 11.091(2) Å, c = 8.1271(16) Å, Z = 2, V = 999.7(3) $Å^3$, R1 = 0.0758, wR2 = 0.1677. The complex possesses D_{4h} symmetry with the copper atom having site symmetry 4/mmm.

The unit cell contains two molecules of 4,4'-bpy coordinated to a Cu^{II} (d^9) in equatorial positions and a hexafluorosilicate anion in the axial position. The copper ion exhibits a Jahn-Teller distorted octahedral geometry. This results in a 3D regular framework based on square grids of 4,4'-bpy ligands bridging the Cu^{II} metal ions which are pillared by SiF_6^{2-} ions. The pyridine rings of the ligand are disordered over two positions and are connected to the Cu^{II} centres by the nitrogen atoms. The structure provides channels, with dimensions of 7.7×7.7 $Å^2$ along the *c*-axis and 5.8×1.8 $Å^2$ along the *a* and *b*-axes, that are filled with eight water molecules per Cu^{II} ion (Figure 2.2). According to the classification of porous materials reported in the literature [8], **C1** is a second generation compound which has stable rigid porous channels after the removal of the guest molecules.

TG analysis was carried out in order to determine the thermal stability of **C1**. The TG curve shows the loss water molecules of crystallisation from 100 °C to 150 °C, followed by the decomposition of the porous framework. An out-gassed sample was used for the elementary analyses so that the ethylene glycol solvent molecules stuck to the surface of the compound were removed. Since the sample is simultaneously heated while out-gassing, all element percentages were calculated for the molecular weight formula without water molecules of crystallisation. XRPD analysis on the out-gassed sample shows the stability of the 3D porous material.

When **C1** is immersed in water, the 3D framework transforms into a 2D interpenetrated network, which has been denoted as **C2**.

2.2.2 $\{[Cu\ (4,4'\text{-}bpy)_2\ (H_2O)_2]\ (SiF_6)\}_n$: C2

This compound (Figure 2.3) was synthesized by exposing the compound **C1** to water (Reaction 2.1).

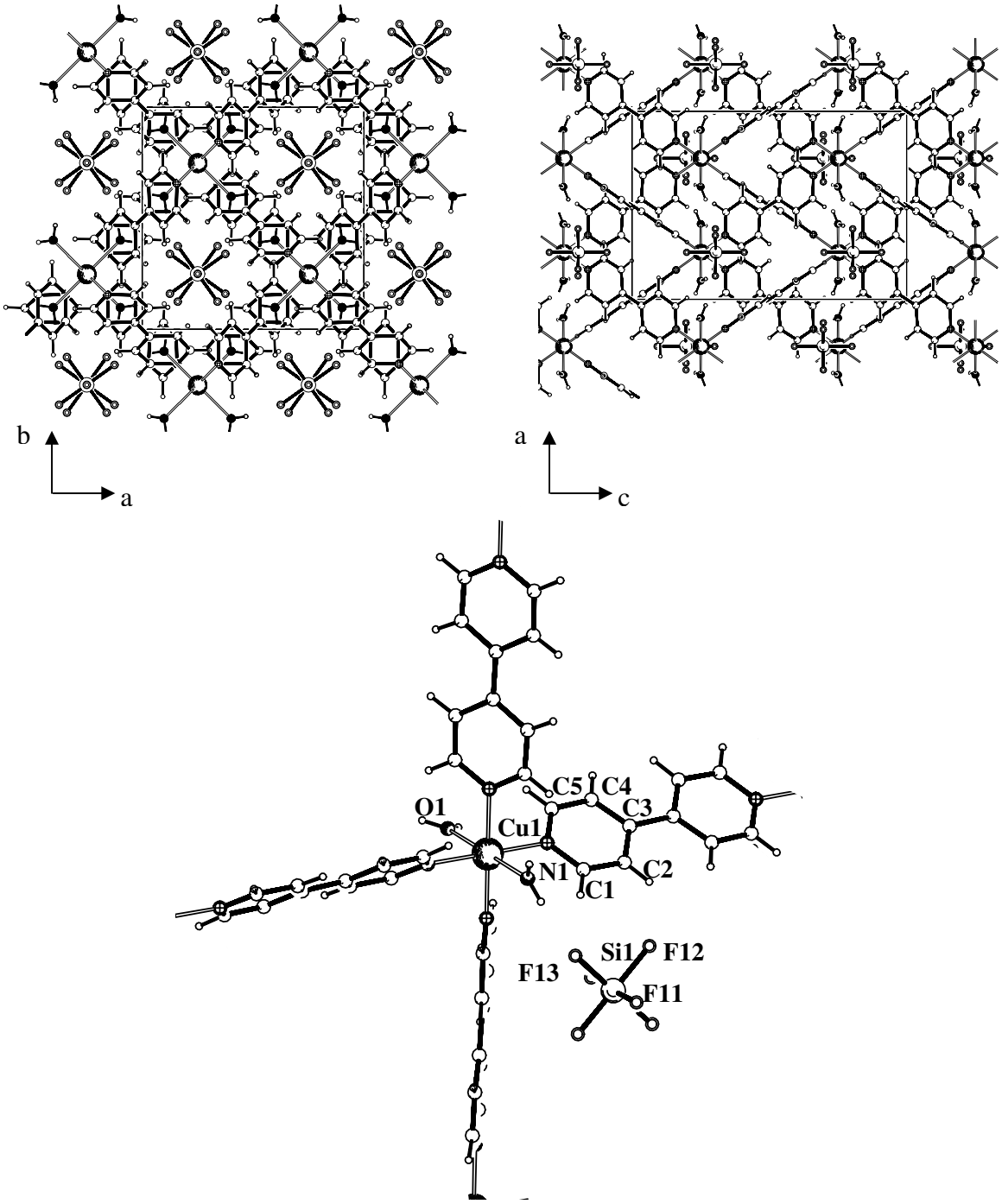

Figure 2.3 Crystal packing diagrams and Cu^{II} coordination sphere of **C2** complex

$$\{[Cu\ (SiF_6)\ (4,4'\text{-}bpy)_2]\ (H_2O)_8\}_n + 2H_2O \rightarrow \{[Cu\ (4,4'\text{-}bpy)_2\ (H_2O)_2]\ (SiF_6)\}_n + 8H_2O$$

Reaction 2.1

The product, blue rod-like crystals, crystallized in the tetragonal crystal system, space group P4/ncc, with a = b =11.0106(10) Å, c = 16.0845(12) Å, Z = 1, V = 1950.0(3) $Å^3$, R1 = 0.0295, wR2 = 0.0853. The symmetry of the complex is D_2, with the copper atom having site symmetry 2.22.

The nitrogen atoms of the 4,4'-bpy are coordinated to Cu^{II} centres in the equatorial plane resulting in the formation of a 2D grid. Two water molecules are coordinated in the axial positions and the anions occupy the cavities of the strucure [7]. This compound presents 2D sheets in the *"diagonal/diagonal"* interpenetration topology [10].

TG analysis shows that **C2** is thermally stable until 180 °C, followed by the decomposition of the metal-organic grid.

2.2.3 $[Cu\ X_2\ (4,4'\text{-}bpy)_2]_n$

When samples of **C1** were prepared with KBr for IR analysis, the colour drastically changed from violet to bright green indicating the possibility of a solid state reaction. Indeed, the bromide anions came into the coordination sphere of the Cu^{II} atom substituting the SiF_6^{2-} anions (Reaction 2.2). This was confirmed by XRPD analysis of solid **C1** after immersion in a saturated KBr solution. The green compound obtained is the already reported metal-organic polymer $[Cu\ Br_2\ (4,4'\text{-}bpy)]_n$ [9]. The vibration bands found for 4,4'-bpy in the KBr pellet of **C1** are quite close to those described in the literature, but different to those found for 4,4'-bpy in a nujol mull of **C1**, where no reaction is observed.

$$\{[Cu\ (SiF_6)\ (4,4'\text{-}bpy)_2]\ (H_2O)_8\}_n + 2KBr \rightarrow [Cu\ Br_2\ (4,4'\text{-}bpy)]_n + 8H_2O + K_2SiF_6 + (4,4'\text{-}bpy)$$

Reaction 2.2

Similarly, the immersion of **C1** in a KCl solution generates the corresponding polymer with Cl^- anions coordinated to Cu^{II}, $[Cu\ Cl_2\ (4,4'\text{-bpy})]_n$, which is also reported in the literature [9] (Reaction 2.3).

$$\{[Cu\ (SiF_6)\ (4,4'\text{-bpy})_2]\ (H_2O)_8\}_n + 2KCl \rightarrow [Cu\ Cl_2\ (4,4'\text{-bpy})]_n + 8H_2O + K_2SiF_6 + (4,4'\text{-bpy})$$

Reaction 2.3

The anion exchange potential of **C1** has already been established by Kitagawa et al. [7]. In fact, it is assumed that the solid state reaction described above in presence of aqueous solutions of halides can occur via the formation of **C2**.

The same solid state reaction has been observed for **C2** in the presence of KBr with the same result (Reaction 2.4), so the IR analysis was also carried out with nujol. The IR analysis carried out as nujol mulls showed that the band which corresponds to the stretching vibrational mode for the Si-F bond was present at 747 cm^{-1} for **C2**. For **C1**, the same band is observed at 738 cm^{-1}. Hence, in **C2** it is concluded that the anion is not coordinated.

$$\{[Cu\ (4,4'\text{-bpy})_2\ (H_2O)_2]\ (SiF_6)\ \}_n + 2KBr \rightarrow [Cu\ Br_2\ (4,4'\text{-bpy})]_n + 2H_2O + K_2SiF_6 + (4,4'\text{-bpy})$$

Reaction 2.4

2.2.4 $[Cu\ F_2\ (4,4'\text{-bpy})]_n$: C3

As stated previously, **C1** and **C2** were thermally stable only in a specific range of temperature. Compound **C3** is the result of the decomposition of these two metal-organic polymers by heating to 300 °C (Figure 2.4).

The samples retain the crystalline state on heating. Both compounds, **C1** and **C2**, present a TG curve with three well defined steps. The first step is the loss of water, the second the loss of the 4,4-bpy ligands and the last step is the loss of a SiF_4 molecule

originated by the decomposition of the hexafluorosilicate anion. **C2** has a higher thermal stability than **C1**, as is shown in Figure 2.4.

Growing single crystals is a difficult task and is not always successful. Moreover, the high insolubility of most metal-organic polymers makes the re-crystallisation process to obtain single crystals impossible. Therefore, an increasing number of crystal structures of such materials are solved from powder X-Ray diffraction data. The samples obtained from the TG experiments of complexes **C1** and **C2** were in both cases a green crystalline powder suitable for analysis by XRPD.

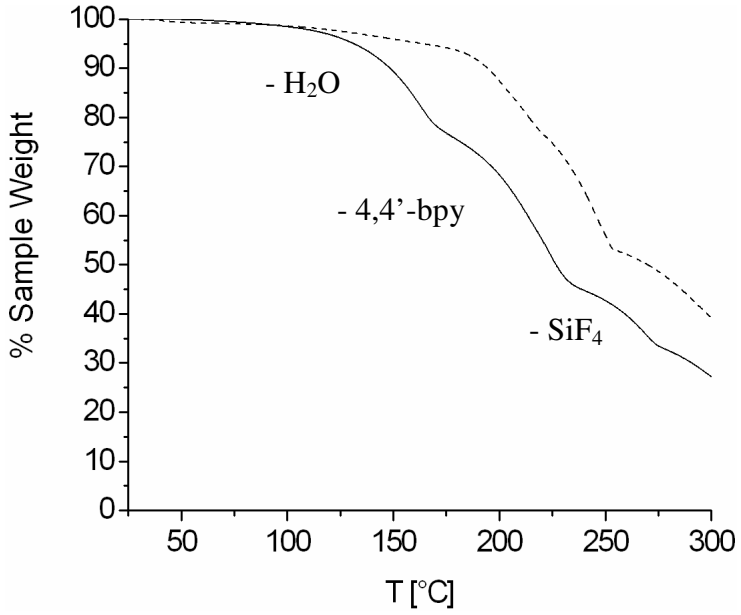

Figure 2.4 TG curves for **C1** (solid line) and **C2** (dash line)

The complex **C3** crystallized in the monoclinic crystal system, space group C2/m, with a = 10.6773(2) Å, b = 11.1566(1) Å, c = 3.5724(1) Å, β = 97.628(2) °, Z = 2, V = 421.79(1) $Å^3$, R_p = 0.0430, R_F = 0.0381. The complex possesses C_{2h} symmetry with the copper atom having site symmetry 2/m.

The Cu^{II} centre has a square planar geometry where two 4,4'-bpy ligands are coordinated in addition to two fluorine anions. The result is a 1D metal-organic polymer (Figure 2.5).

Selected bond lengths and bond angles for this compound are given (Table 2.1). The values found for these parameters in this structure are similar to those reported in the literature [7, 11-14].

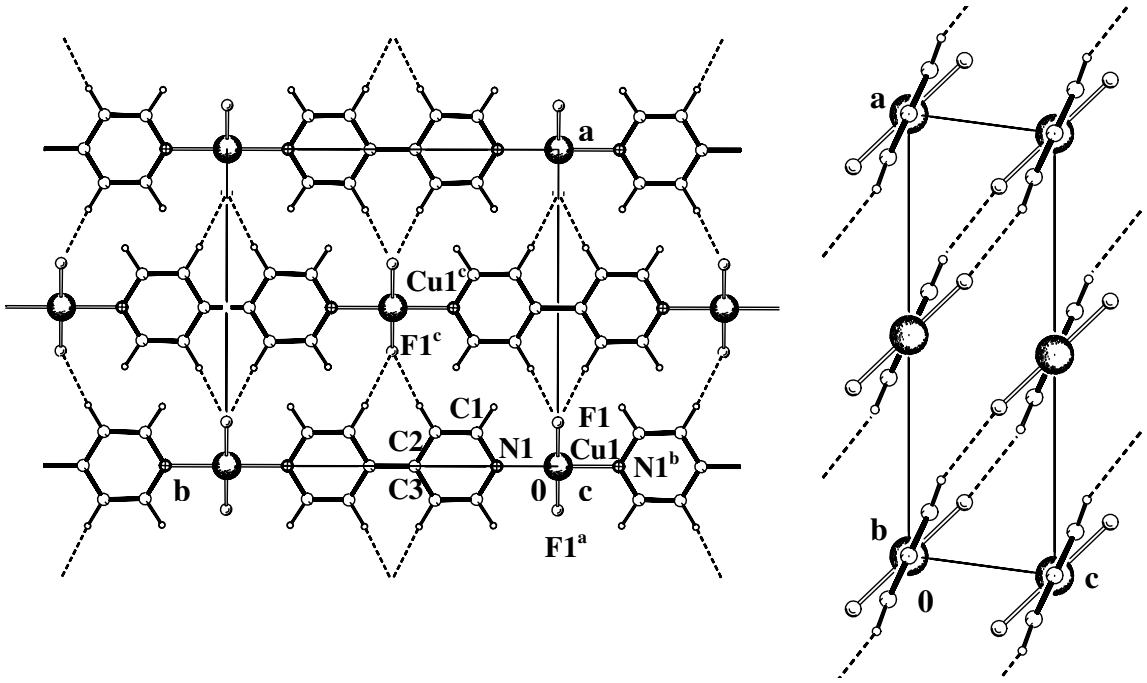

Figure 2.5 Crystal packing diagrams of complex **C3**; [a]) -x,y,-z, [b]) -x,-y,-z

Table 2.1 Selected bond distances (Å) and bond angles (°) for **C3** (C2/m)

Bond	Length (Å)	Angle	Angle (°)
Cu1-F1	1.865(4)	F1-Cu1-N1	90.00(1)
Cu1-N1	2.028(3)	F1-Cu1-F1[a]	180.00
[a]) -x,y,-z			

Complex **C3** has C-H···F type intermolecular interactions and these non-classical hydrogen bonds link the linear chains to form layers. These layers are connected via π–π stacking interactions.

Table 2.2 Hydrogen bonds for **C3** (C2/m)

Hydrogen Bond	D–H (Å)	H···A (Å)	D···A (Å)	D–H···A (°)	Symmetry operation
C1–H1…F1	0.940(6)	2.385(4)	2.832(3)	108.8(3)	
C2–H2…F1[c]	0.923(6)	2.481(8)	3.375(4)	163.3(9)	[c]) 1/2-x,1/2+y,1-z

2.2.5 $[Cu(OCN)_2(4,4'\text{-bpy})]_n$: C4

Compound **C4** (Figure 2.6) was obtained by an anion-exchange reaction with **C1**. An excess amount of KOCN was added to **C1** in an aqueous solution (Reaction 2.5).

$$\{[Cu(SiF_6)(4,4'\text{-bpy})_2](H_2O)_8\}_n + 2KOCN \rightarrow [Cu(OCN)_2(4,4'\text{-bpy})]_n + 8H_2O + (4,4'\text{-bpy}) + K_2SiF_6$$

Reaction 2.5

Complex **C4** is a 2D polymer which crystallized in the orthorhombic crystal system, space group Cmmm, with a = 11.1575(2) Å, b = 15.0236(2) Å, c = 3.5966(1) Å, Z = 2, V = 602.88(2) $Å^3$, R_p = 0.0353, R_F = 0.0798. The symmetry of the complex is D_{2h}, with the copper atom having site symmetry mmm.

The Cu^{II} ion has a *compressed* octahedral geometry (Figure 2.6) where the 4,4'-bpy ligands occupy the axial positions with short Cu···N bonds, and the anions the equatorial plane with long Cu···O coordination bonds. Selected bond lengths and bond angles are given in Table 2.3.

Table 2.3 Selected bond distances (Å) and bond angles (°) for **C4** (Cmmm)

Bond	**Length (Å)**	**Angle**	**Angle (°)**
Cu1-O1	2.427(4)	O1-Cu1-N2	90.00
Cu1-N2	2.065(4)	O1-Cu1-O1[a]	95.62
Cu1-Cu1[a]	3.597(4)	O1-Cu1-O1[c]	84.39
[a]) x,y,-1+z , [b]) -x,-y,1+z , [c]) -x,-y,z , [d]) x,y,1+z		O1-Cu1-O1[b]	180.00
		Cu1-O1-Cu1[d]	95.60

Other anion-exchange properties for **C1** and **C2** have been reported in the literature [7]. In Scheme 2.1, two different solid-state transformations for these compounds are presented, namely, a thermal decomposition of the counter-anion and a complete anion-exchange giving the stable structures denoted previously as **C3** and **C4**. The compounds retain their crystalline state during the process.

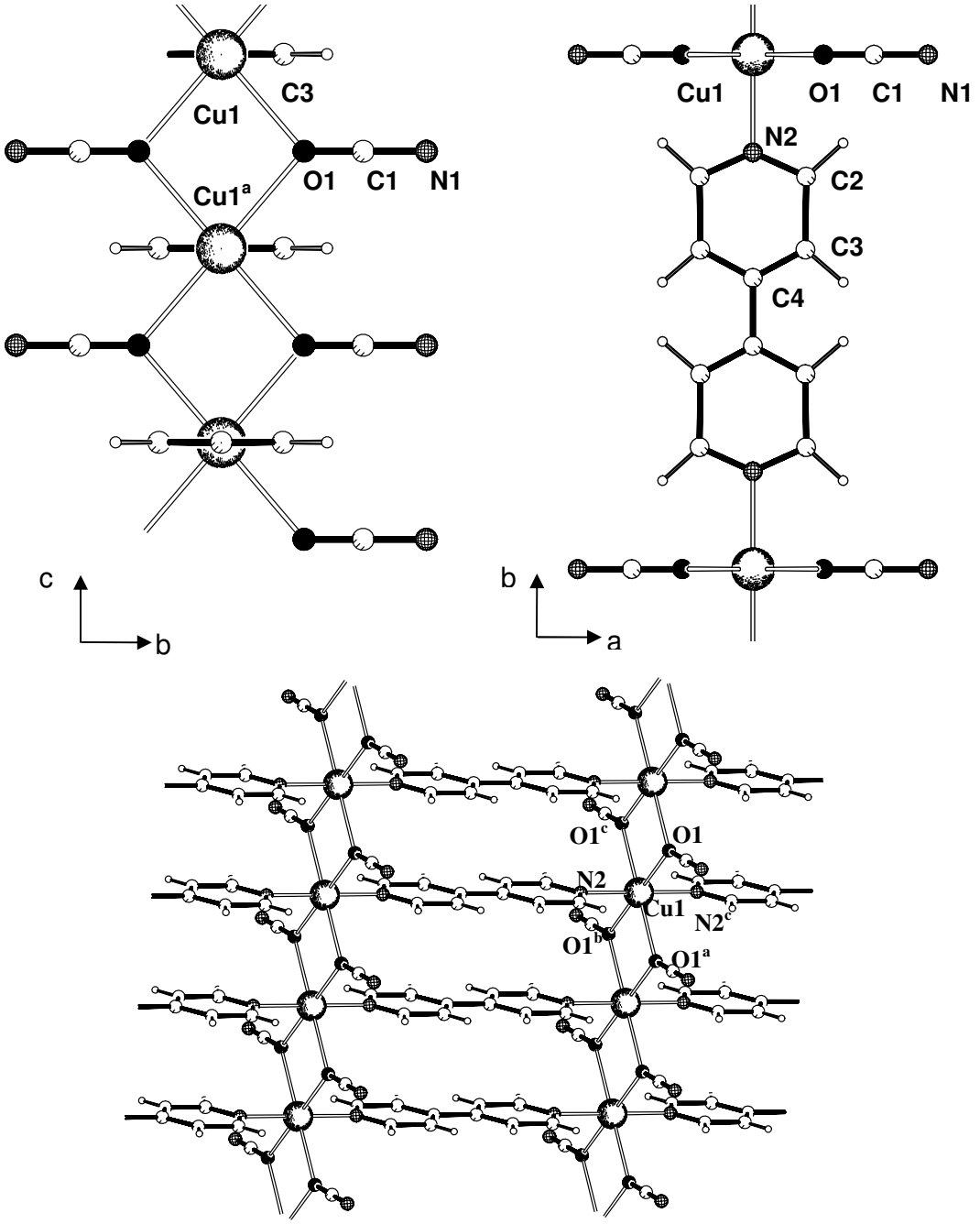

Figure 2.6 Cu^{II} coordination sphere of **C4** and crystal packing diagram; [a]) x,y,-1+z, [b]) -x,-y,-1+z, [c]) -x,-y,z

This compound could be suitable for magnetic coupling experiments.

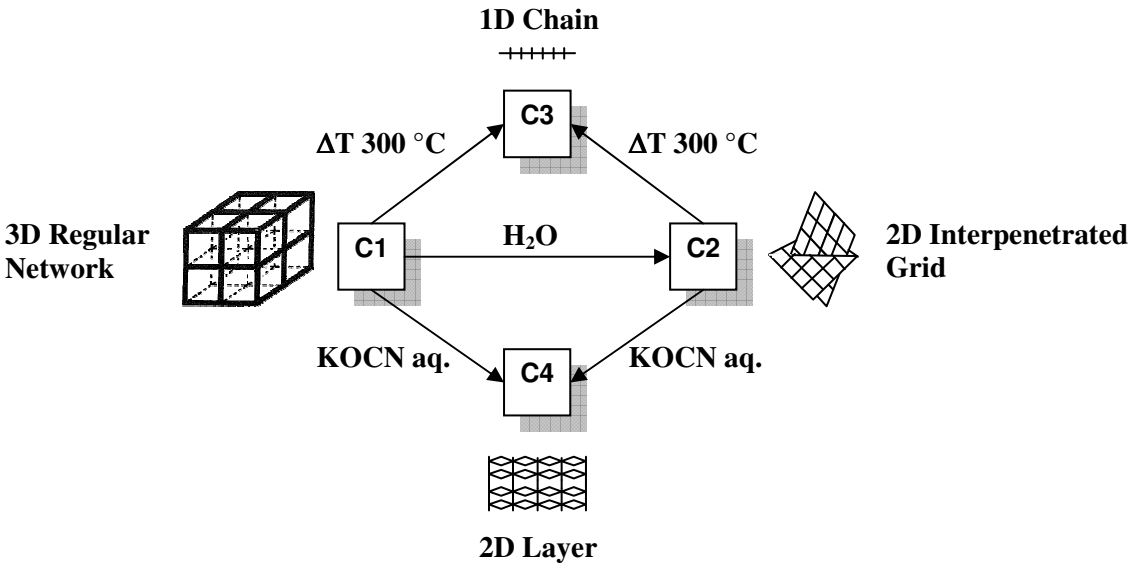

Scheme 2.1 Solid state transformations for **C1** and **C2**

2.2.6 $\{[Ag\ (4,4'\text{-}bpy)]_2\ (SiF_6)\ (HOCH_2CH_2OH)_2\ (H_2O)_2\}_n$: C5

Compound **C5** was prepared by the diffusion of an aqueous ethylene glycol solution containing a mixture of $Ag(BF_4)$ and $(NH_4)_2SiF_6$ into an ethylene glycol solution of 4,4'-bpy. The colourless transparent needle-like crystals were obtained. Monoclinic crystal system, space group Pc (which is a polar space group), with a = 9.8887(8) Å, b = 11.3492(6) Å, c = 14.6304(12) Å, β = 119.701(9) °, Z = 2, V = 1426.2(2) $Å^3$, R1 = 0.0420, wR2 = 0.0878.

The asymmetric unit contains two Ag^I centres (which occupy general positions) coordinated to the nitrogen atoms of the bipyridine that results in the formation of a linear chain (Figure 2.7). Two molecules of water, two molecules of ethylene glycol and one hexafluorosilicate anion are cocrystallised (Figure 2.8). The 4,4'-bipyridine ligands coordinated to the metal ions have the pyridine rings twisted about each other with the dihedral angle between pyridine ring 1 and ring 2 (N1 C1 C2 C3 C4 C5 and N2 C6 C7 C8 C9 C10, respectively) being 36.7(6)° and the dihedral angle between pyridine ring 3 and ring 4 (N3 C11 C12 C13 C14 C15 and N4 C16 C17 C18 C19 C20, respectively) being 39.1(6)°. The distance Ag1···Ag2 is 3.417 Å and hence there is a possibility of a

weak interaction between adjacent chains, since the Van der Waals radius of the silver atom is 1.72 Å, although the distances reported in the literature for Ag···Ag weak coordinative interactions are slightly shorter (3.299 and 3.286 Å) [15, 16].

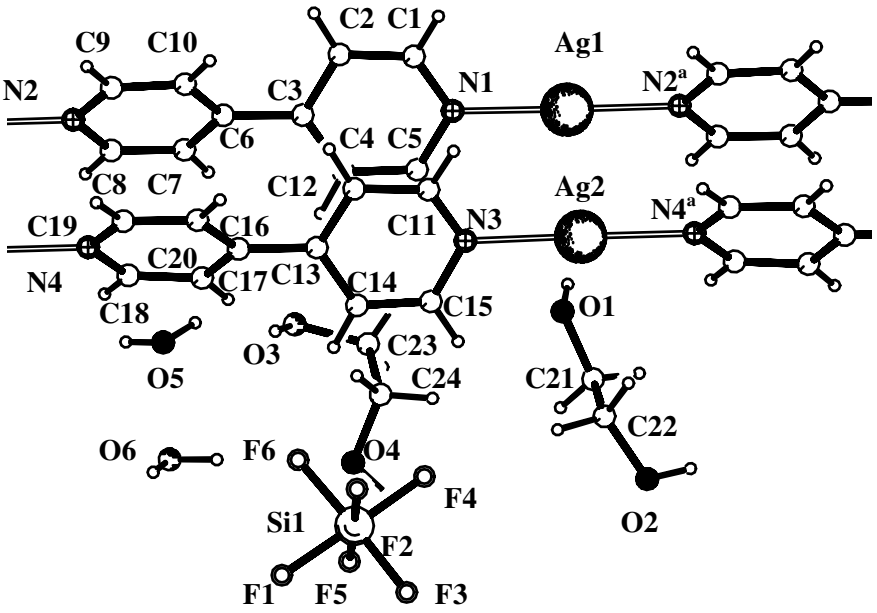

Figure 2.7 Complex **C5**

These double linear chains formed by Ag···Ag interactions (Figure 2.7) are linked with other double chains via aromatic π–π stacking interactions resulting in the formation of layers. The solvent and anion molecules fill the space between the layers (Figure 2.8). The anion and the ethylene glycol and water molecules are involved in hydrogen bond formation with each other. In addition, the hydrogen atoms of the ligand 4,4'-bpy are also involved in hydrogen bond formation with the ethylene glycol and the anion molecules (Table 2.5).

Table 2.4 Selected bond distances (Å) and bond angles (°) for **C5** (Pc)

Bond	**Length (Å)**	**Angle**	**Angle (°)**
Ag1-N1	2.141(8)	N1-Ag1-N2[a]	174.2(7)
Ag1-N2[a]	2.110(7)	N3-Ag2-N4[a]	174.9(7)
Ag2-N4[a]	2.133(8)	[a]) x,1+y,z	
Ag2-N3	2.161(9)		

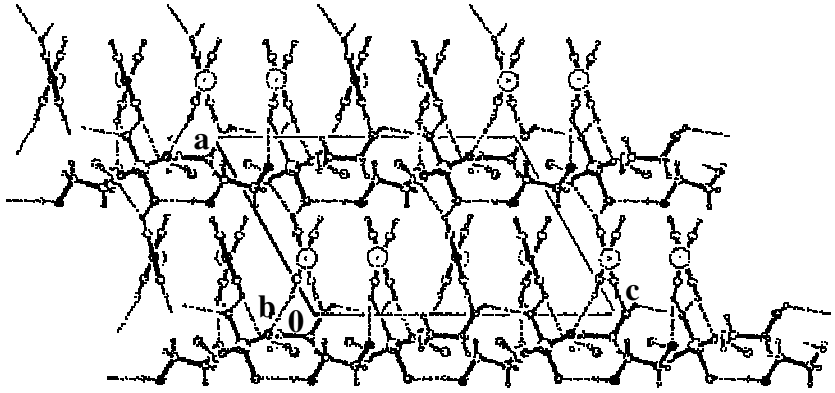

Figure 2.8 Crystal packing of complex **C5**

Table 2.5 Hydrogen bonds for **C5** (Pc)

Hydrogen Bond	D–H (Å)	H···A (Å)	D···A (Å)	D–H···A (°)	Symmetry operation
O1–H1···F2[b]	0.84	1.88	2.72(1)	173	
O5–H1···F1	0.82	1.96	2.76(1)	163	
O2–H2···O6[a]	0.84	1.93	2.64(1)	142	
O5–H2···O3[c]	1.03	1.91	2.74(1)	136	
O3–H3···O5[e]	0.84	2.15	2.74(1)	127	[a]) x,1+y,z
O6–H3···F6	0.95	1.75	2.70(1)	173	[b]) x,1-y,-1/2+z
O4–H4···F5	0.84	2.42	2.72(1)	102	[c]) x,-y,1/2+z
O6–H4···O2[f]	0.78	2.15	2.64(1)	121	[d]) x,1-y,-1/2+z
C1–H1···F3[g]	0.95	2.38	3.05(1)	128	[e]) x,-y,-1/2+z
C8–H8···O4[h]	0.95	2.42	3.21(1)	140	[f]) x,-1+y,z
C9–H9···F2[e]	0.95	2.46	3.20(1)	134	[g]) -1+x,y,-1+z
C9–H9···F6[e]	0.95	2.52	3.43 (2)	162	[h]) -1+x,-y,-1/2+z
C11–H11···F5[i]	0.95	2.54	3.28(1)	135	[i]) -1+x,1-y,-1/2+z
C12–H12···O2[i]	0.95	2.41	3.33(2)	163	
C14–H14···F6	0.95	2.27	3.21(1)	167	
C18–H18···F1[h]	0.95	2.47	3.41(2)	172	
C18–H18···F5[h]	0.95	2.52	3.23(1)	131	
C23–H23···F3[d]	0.99	2.53	3.05(1)	113	

In the TG analysis, the compound shows the loss of the water molecules of crystallization up to 100 °C, and then the loss of ethylene glycol molecules and finally the loss of a SiF_4 molecule, followed by decomposition resulting probably in the formation of $[Ag\ F_2\ (4,4'\text{-bpy})]_n$ (Figure 2.9).

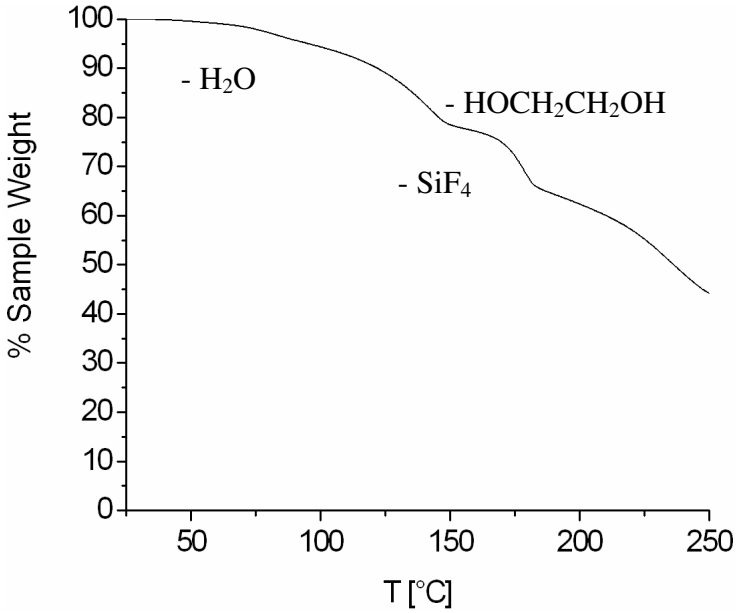

Figure 2.9 TG curve for **C5.**

2.2.7 {[Co (4,4'-bpy)$_3$ (H_2O)$_2$] (BF_4)$_2$ (4,4'-bpy) (H_2O)$_9$}$_n$: C6

This compound was synthesized by adding a water/acetone solution containing a mixture of $Co(BF_4)_2 \cdot 6H_2O$ and $(NH_4)_2SiF_6$ to an acetone solution of 4,4'-bpy (1 mmol). The precipitate was filtered off and the filtrate allowed to stand in air.

Orange block-like crystals were obtained. Monoclinic crystal system, space group C2/c, with a = 17.807(1) Å, b = 11.5037(5) Å, c = 24.592(2) Å, β = 92.446(9) °, Z = 4, V = 5032.9(6) $Å^3$, R1 = 0.0889, wR2 = 0.2514. This compound is isomorphous with another compound already reported in the literature but with a different anion [17]. The complex has C_2 symmetry, with the cobalt atom having site symmetry 2.

The Co^{II} centres have an octahedral geometry where the two 4,4'-bpy ligands are coordinated to the metal ion forming an infinite linear chain. The equatorial plane consists of two 4,4'-bpy ligands and two water molecules (Figure 2.10). The Co^{II} centres are slightly displaced from the equatorial plane and as a consequence, the axial bond distances are not equivalent (Table 2.6).

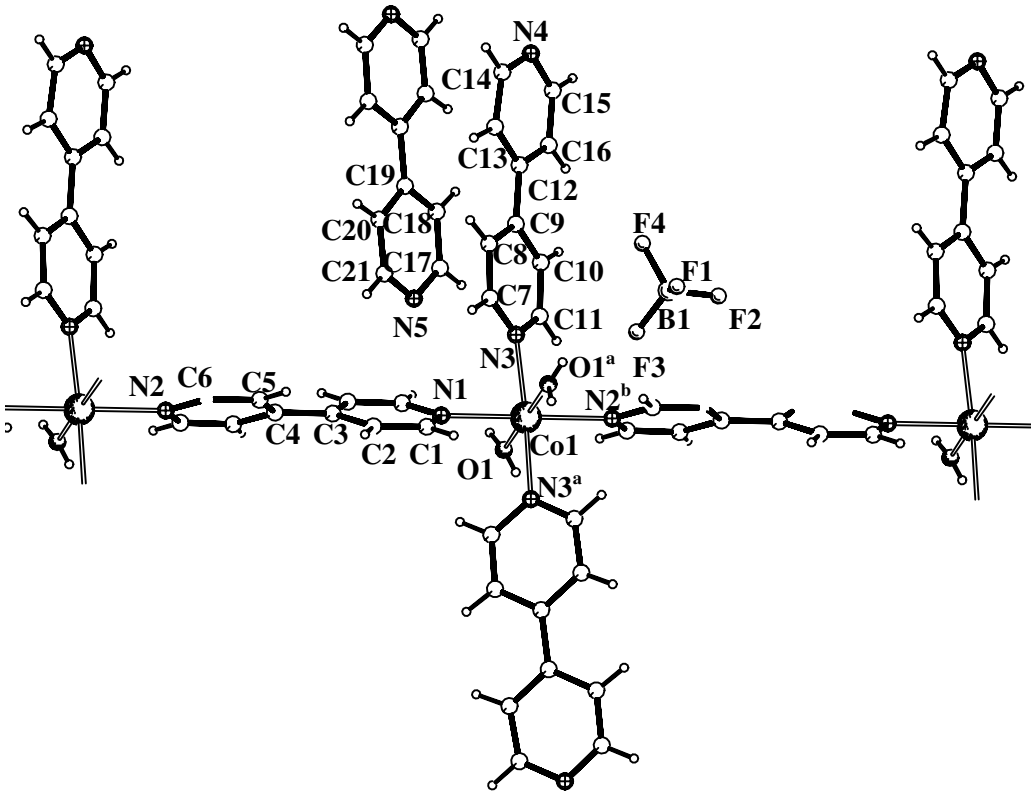

Figure 2.10 Complex **C6**; [a]) -x,y,1/2-z, [b]) x,1+y,z

The 4,4'-bipyridine ligands coordinated to the metal ions have the pyridine rings twisted with respect to one another with the dihedral angle between pyridine ring 1 and ring 2 (N1 C1 C2 C3 $C2^a$ $C1^a$ and N2 C6 C5 C4 $C5^a$ $C6^a$, respectively) being 29.5(2)° [symmetry operation [a]) -x,y,1/2-z], and the dihedral angle between pyridine ring 3 and ring 4 (N3 C7 C8 C9 C10 C11 and N4 C12 C13 C14 C15 C16, respectively) being 7.1(3)°.

The compound presents some hydrogen bonds involving oxygen atoms from the water molecules coordinated to the metal centres and the terminal 4,4'-bpy ligands coordinated to the metal centres of neighbouring chains (Table 2.7). These interactions result in the formation of a 2D polymer (Figure 2.11). The crystal packing is also characterized by π-π stacking interactions between the bipyridine systems of adjacent linear chains and the bipyridine rings crystallized between them.

Table 2.6 Selected bond distances (Å) and bond angles (°) for **C6** (C2/c)

Bond	Length (Å)	Angle	Angle (°)
Co1-O1	2.076(3)	O1-Co1-N1	90.3(1)
Co1-N1	2.176(7)	O1-Co1-N3	92.2(1)
Co1-N3	2.176(4)	O1-Co1-N2[b]	89.7(1)
Co1-N2[b]	2.227(6)	O1-Co1-O1[a]	179.5(2)
		O1-Co1-N3[a]	87.8(1)
[a]) -x,y,1/2-z		N1-Co1-N3	88.5(1)
[b]) x,1+y,z		N1-Co1-N2[b]	180
		N2[b]-Co1-N3	91.5(1)
		N3-Co1-N3[a]	177.0(2)

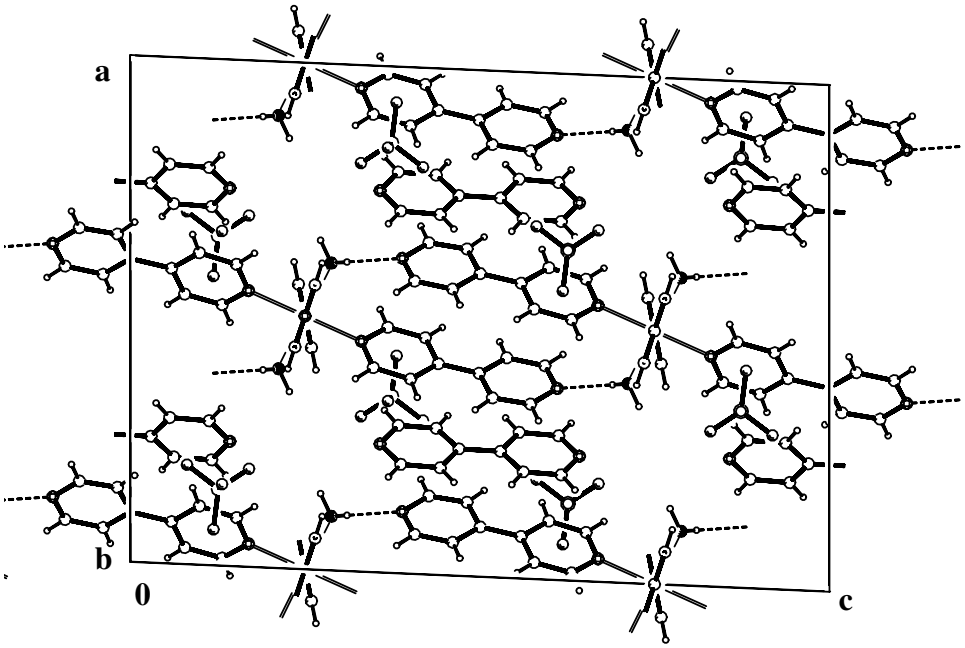

Figure 2.11 Crystal packing diagram of complex **C6**

Table 2.7 Hydrogen bonds for **C6** (C2/c)

Hydrogen Bond	D–H (Å)	H···A (Å)	D···A (Å)	D–H···A (°)	Symmetry operation
O1–H28···N4[c]	0.65	2.11	2.74	171	
C6–H6···O1	0.93	2.48	3.079(7)	122	[c]) x,1-y,1/2+z
C10–H10···F4	0.93	2.53	3.38(2)	152	

The TG curve shows the loss of water molecules of crystallization up to 130 °C, followed by the loss of coordinated water molecules up to 180 °C, and finally the loss of BF_3 molecules accompanied by decomposition (Figure 2.13).

2.2.8 {[Co (4,4'-bpy) $(H_2O)_4$] $(BF_4)_2$ (4,4'-bpy)$_2$ $(H_2O)_2$}$_n$: C7

Compound **C7** was obtained from the same reaction as that of **C6**. Pale orange block-like crystals crystallized in the triclinic crystal system, space group $P\bar{1}$, with a = 8.9726(9) Å, b = 10.760(1) Å, c = 11.401(1) Å, α = 65.27(1) °, β = 70.62(1) °, γ = 66.41(1) °, Z = 1, V = 898.2(2) Å^3, R1 = 0.0357, wR2 = 0.0900. The complex possesses C_i symmetry, with the cobalt atom having site symmetry $\bar{1}$.

The equatorial positions are occupied by water molecules coordinated to the Co^{II} ions (Table 2.8) and the axial positions are occupied by 4,4'-bpy ligands resulting in the formation of a linear polymer (Figure 2.12). This compound is isostructural with that reported in the literature [18]. The water molecules coordinated to the Co^{II} centres form hydrogen bonds with the nitrogen of the non-coordinated ligands and with the fluorine of the anions. There are also some hydrogen bonds between the coordinated bipyridine rings and the anions. The linear chains form layers and the layers in turn form networks via hydrogen bonds (Table 2.9).

Table 2.8 Selected bond distances (Å) and bond angles (°) for **C7** (P-1)

Bond	Length (Å)	Angle	Angle (°)
Co1-O1	2.100(2)	O1-Co1-O2	88.71(7)
Co1-O2	2.098(2)	O1-Co1-N1	90.79(7)
Co1-N1	2.141(2)	O1-Co1-O1^a	180
		O1-Co1-O2^a	91.30(7)
^{a}) -x,1-y,1-z		O1-Co1-N1^a	89.21(7)
		O2-Co1-N1	92.62(7)
		O2-Co1-N1^a	87.39(7)

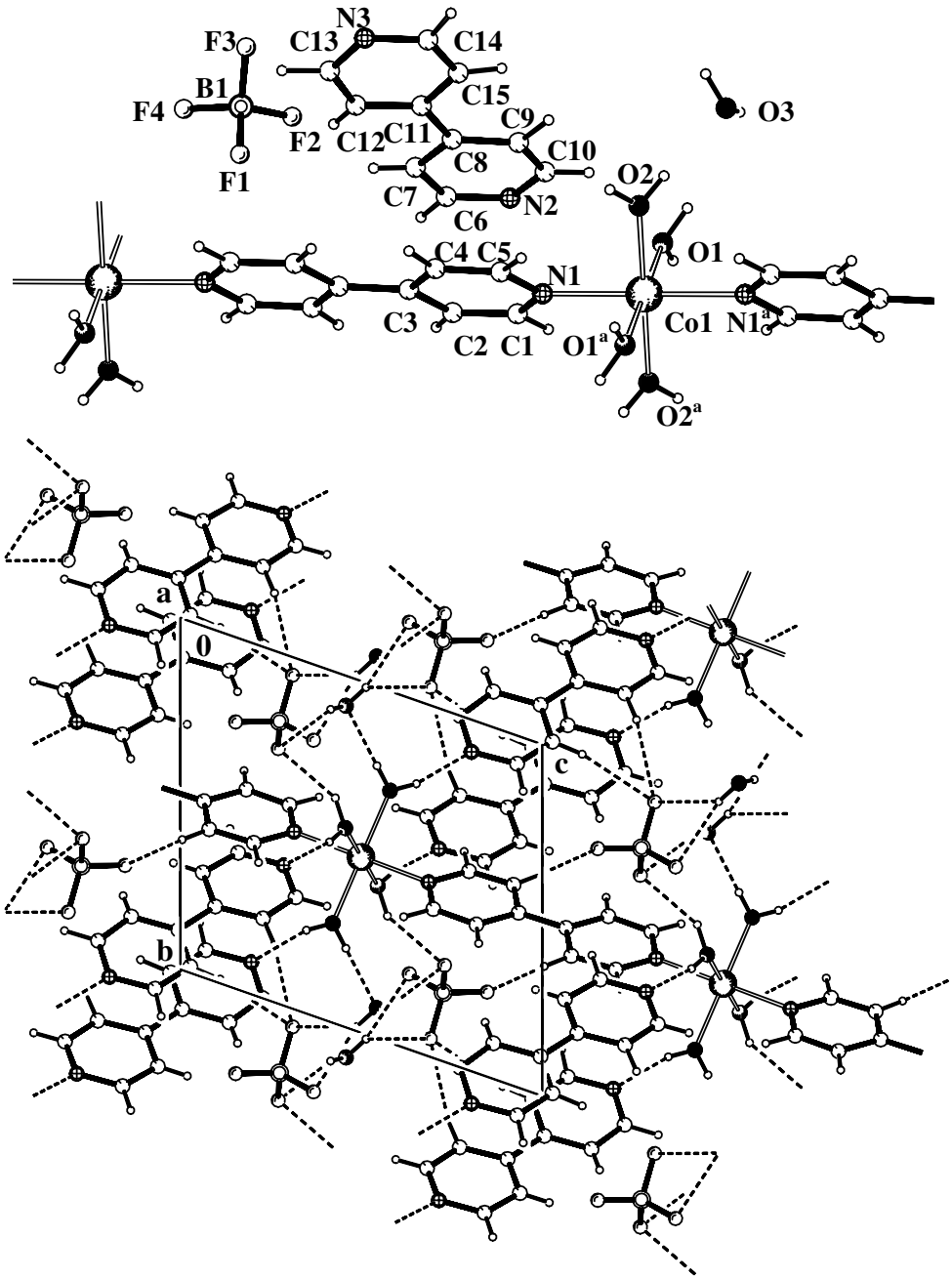

Figure 2.12 Co^{II} coordination sphere for complex **C7** and crystal packing diagram; [a]) -x,1-y,1-z

The TG analysis shows the loss of all water molecules between 75 and 140°C, after that the loss of BF_3 molecules followed by decomposition (Figure 2.13). The thermal decomposition products of **C6** and **C7** were poorly crystalline. Therefore no structure determination was possible using XRPD methods.

Table 2.9 Hydrogen bonds for **C7** (P-1)

Hydrogen Bond	D–H (Å)	H...A (Å)	D...A (Å)	D–H...A (°)	Symmetry operation
O1–H1…N2[b]	0.78(4)	1.94(3)	2.703(3)	169(3)	
O1–H2…F1[c]	0.89(4)	2.12(4)	2.913(3)	149(4)	
O2–H3…O3	0.83(4)	1.92(4)	2.741(3)	170(4)	[b]) 1-x,1-y,1-z
O2–H4…N3[d]	0.80(3)	2.01(3)	2.777(3)	162(3)	[c]) x,y,-1+z
O3–H5…F3[e]	0.83(5)	2.41(5)	3.099(3)	140(4)	[d]) -x,-y,2-z
O3–H5…F4[e]	0.83(5)	2.23(5)	3.033(3)	162(5)	[e]) 1-x,-y,2-z
O3–H6…F1[c]	0.73(4)	2.27(4)	2.950(3)	157(4)	[f]) -1+x,y,z
C4–H4…F2[f]	0.96(3)	2.31(3)	3.265(3)	172(3)	
C9–H9…F3[e]	1.02(3)	2.54(3)	3.523(4)	161(3)	
C15–H15…F3[e]	0.91(4)	2.43(4)	3.326(3)	168(3)	

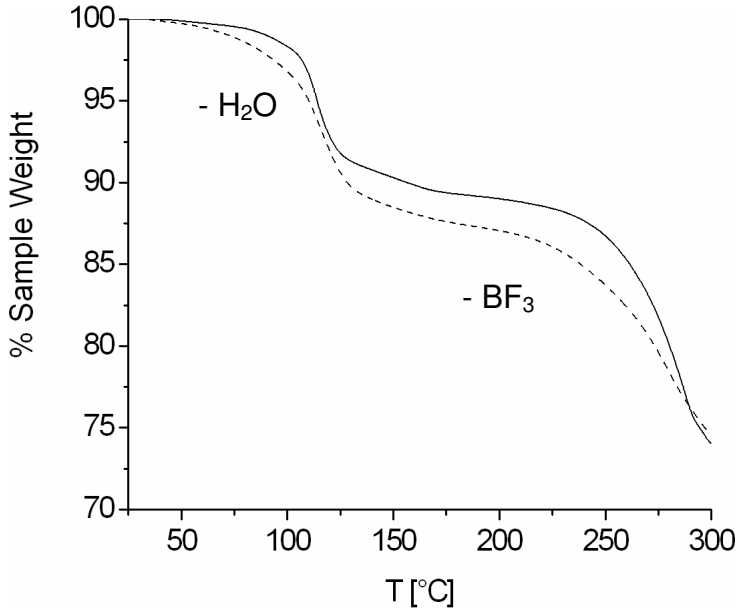

Figure 2.13 TG curve for **C6** (straight line) and **C7** (dash line)

2.3 Complexes with Anions Containing Sulphur

2.3.1 {[Cu (S_2O_6) (4,4'-bpy)$_2$] (H_2O)$_{20}$}$_n$: C8

The reaction of an ethylene glycol solution of 4,4'-bpy and a methanolic solution of $CuS_2O_6 \cdot 6H_2O$ produced light purple needle-like crystals of **C8** (Figure 2.14).

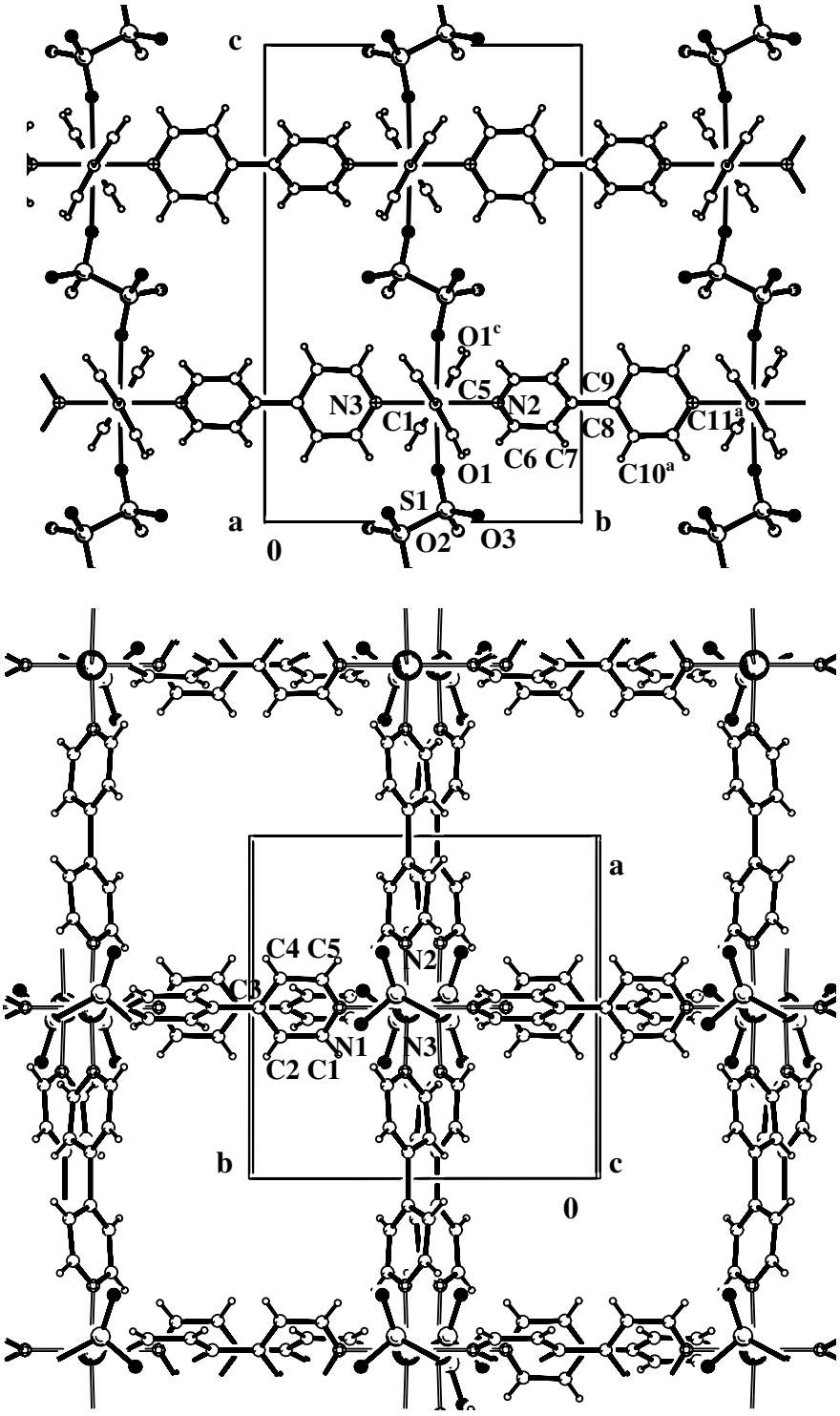

Figure 2.14 Crystal packing diagrams of complex **C8**; [a]) x,-1+y,z [c]) 1-x,y,3/2-z

The compound crystallized in the monoclinic crystal system, space group P2/c, with a = 11.0837(18) Å, b = 11.1496(17) Å, c = 16.937(2) Å, β = 97.534(12) °, Z = 2, V

= 2075.0(5) Å^3, R1 = 0.1396, wR2 = 0.3429. The high R1 value is due to the poor quality of the crystal. The symmetry of the complex is C_2 and the copper atom has site symmetry 2. The selected bond distances and angles are given in Table 2.10.

Dithionate anions occupy the axial positions and 4,4'-bipyridine ligands occupy the equatorial positions around the Cu^{II} centres, which have a Jahn-Teller distorted octahedral geometry (Figure 2.14). The pyridine rings of the ligand are disordered over two positions.

Table 2.10 Selected bond distances (Å) and bond angles (°) for **C8** (P2/c)

Bond	**Length (Å)**	**Angle**	**Angle (°)**
Cu1-O1	2.379(7)	O1-Cu1-N1	89.4(3)
Cu1- N1	2.081(7)	O1-Cu1-N2	88.79(19)
Cu1-N2	2.165(10)	O1-Cu1-N3[b]	91.21(19)
Cu1-N3[b]	2.142(15)	O1-Cu1-O1[c]	177.6(3)
		O1-Cu1-N1[c]	90.5(3)
[b])x,1+y,z		N1-Cu1-N2	88.19(19)
[c])1-x,y,3/2-z		N1-Cu1-N3[b]	91.81(19)
		N1-Cu1-N1[c]	176.4(3)
		N2-Cu1-N3[b]	180.00

The compound presents some hydrogen bonds between the oxygen of the anions and the hydrogens of the bipyridine rings as shown below in Table 2.11.

Table 2.11 Hydrogen bonds for **C8** (P2/c)

Hydrogen Bond	**D–H (Å)**	**H···A (Å)**	**D···A (Å)**	**D–H···A (°)**	**Symmetry operation**
C1–H1···O1	0.95	2.58	3.16(2)	119	
C1A–H1···O1	0.95	2.41	2.99(2)	119	
C5–H5···O1[c]	0.95	2.50	3.06(2)	117	[a]) x,-1+y,z
C5A–H5···O1[c]	0.95	2.51	3.15(2)	124	[c]) 1-x,y,3/2-z
C6A–H6···O3A	0.95	2.60	3.38(2)	139	
C11A–H11···O1[a]	0.95	2.45	3.14(2)	129	

The three-dimensional structure provides channels, with dimensions of *ca.* 8.7×8.7 $Å^2$ along the *c*-axis and *ca.* 5.2×3.1 $Å^2$ along the *a* and *b*-axes, that are filled with solvent molecules [19].

Elementary analysis carried out for **C8** crystalline powder showed five ethylene glycol solvent molecules instead of twenty water molecules crystallized per fundamental unit. This is probably due to differences in the kinetic process during synthesis for powder and single crystal. The XRPD patterns for an out-gassed sample showed that removal of the solvent molecules does not influence the stability of the compound (second generation metal-organic porous material). The TG curve indicated loss of solvent water molecules until 175 °C followed by decomposition (Figure 2.20).

IR studies were carried out as nujol mulls in order to compare the spectra with that obtained for **C1**. 4,4'-bypyridine bands were located at the same wavenumber region as for **C1**. The Cu-O vibrational band was located at 506 cm^{-1}.

C8 exhibits the same anion-exchange properties as **C1** when immersed in a saturated aqueous solution of KOCN (Reaction 2.6). The solid obtained from this reaction was analysed by XRPD and the result is the **C4** polymer already described in section 2.2.5.

$$\{[Cu\ (S_2O_6)\ (4,4'\text{-bpy})_2]\ (H_2O)_{20}\}_n + 2KOCN \rightarrow [Cu\ (OCN)_2\ (4,4'\text{-bpy})]_n + 20H_2O + (4,4'\text{-bpy}) + K_2S_2O_6$$

Reaction 2.6

2.3.2 {[Cu (4,4'-bpy)$_2$ (H$_2$O)$_2$] (S$_2$O$_6$)}$_n$: C9

This compound was synthesized by exposing the compound **C8** to water (Reaction 2.7) [19].

$$\{[Cu\ (S_2O_6)\ (4,4'\text{-bpy})_2]\ (H_2O)_{20}\}_n + 2H_2O \rightarrow [Cu\ (4,4'\text{-bpy})_2\ (H_2O)_2]\ (S_2O_6)\}_n + 20H_2O$$

Reaction 2.7

The product, blue block-like crystals, crystallized in the tetragonal crystal system, space group P4/ncc, with a = b = 11.4395(14) Å, c = 15.471(2) Å, Z = 4, V = 2024.6(4) $Å^3$, R1 = 0.0775, wR2 = 0.1549. This compound possesses D_2 symmetry, with the copper atom having site symmetry 2.22. **C9** is isomorphous with **C2** but with a different anion [7].

During the transformation of **C8** to **C9**, the dithionate anions migrate into the cavities of the structure thereby liberating two copper coordination sites for water molecules (Figure 2.15). This results in the formation of a *"diagonal/diagonal"* interpenetrated 2D network. The nitrogen atoms of the 4,4'-bpy are coordinated to the Cu^{II} centres in the equatorial plane forming a 2D grid (Table 2.12). Two water molecules are coordinated in the axial positions, with elongated Cu···O bonds. The coordinated water molecules form hydrogen bonds with the dithionate anions located in the cavities of the structure (Table 2.13).

Table 2.12 Selected bond distances (Å) and bond angles (°) for **C9** (P4/ncc)

Bond	Length (Å)	Angle	Angle (°)
Cu1-O1	2.373(6)	O1-Cu1-N1	89.48(19)
Cu1-N1	2.037(5)	O1-Cu1-O1[a]	180.00
[a]) 3/2-x,1/2-y,z [b]) 1/2+y,-1/2+x,1/2-z [c]) 1-y,1-x,1/2-z		O1-Cu1-N1[a]	90.52(19)
		N1-Cu1-N1[a]	91.1(2)
		N1-Cu1-N1[b]	88.9(2)
		N1-Cu1-N1[c]	179.0(2)

The TG analysis indicated loss of solvent water molecules until 175 °C followed by decomposition (Figure 2.20).

Table 2.13 Hydrogen bonds for **C9** (P4/ncc)

Hydrogen Bond	D–H (Å)	H···A (Å)	D···A (Å)	D–H···A (°)	Symmetry operation
O1–H6···O3[d]	0.89(9)	1.87(9)	2.749(11)	168(8)	[d]) 1/2+x,-y,1/2-z

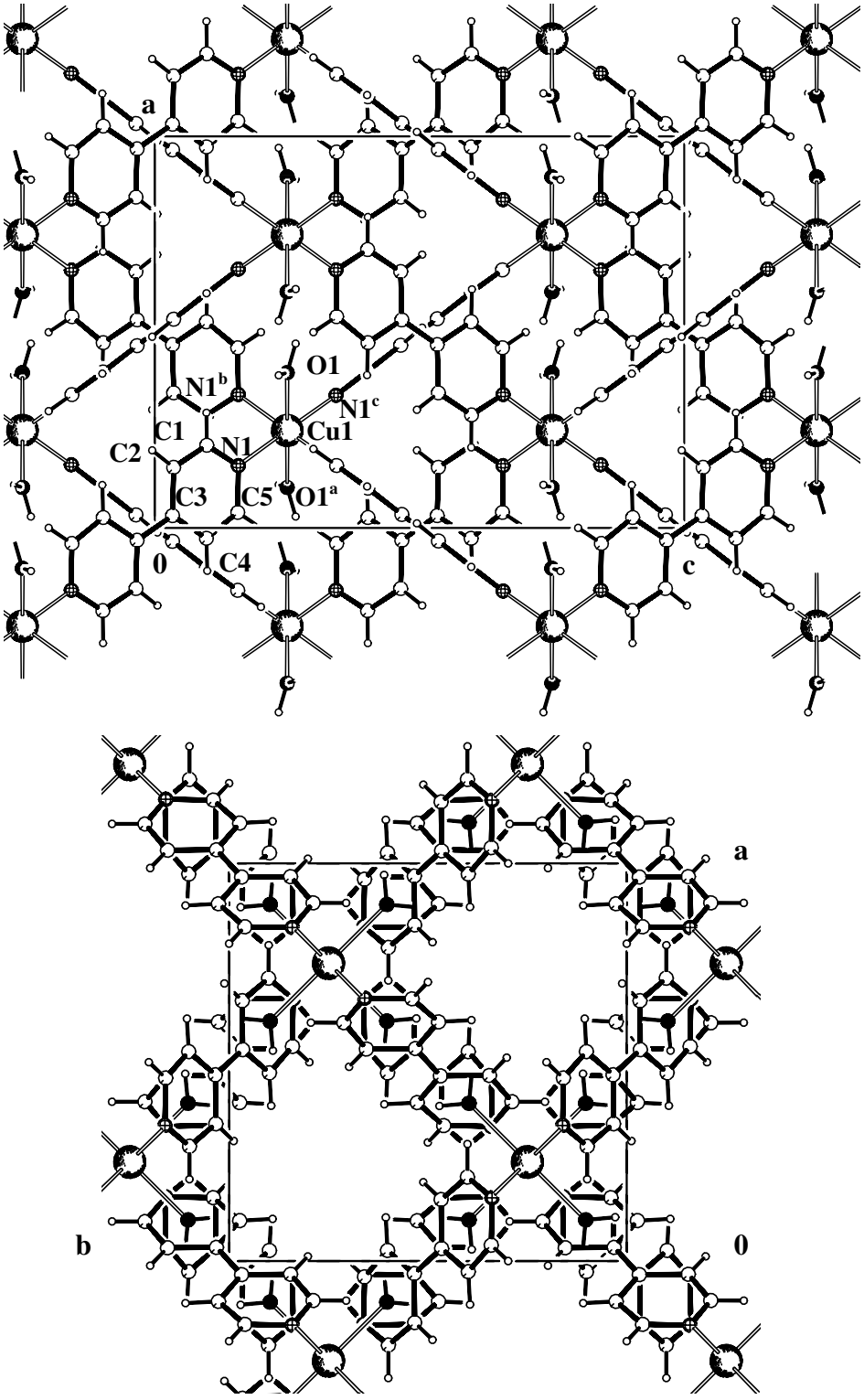

Figure 2.15 Crystal packing diagrams of **C9** (the strongly disordered $S_2O_6^{2-}$ anions are omitted for clarity); [a]) 3/2-x,1/2-y,z, [b]) 1/2+y,-1/2+x,1/2-z, [c]) 1-y,1-x,1/2-z

2.3.3 $\{[Co(4,4'\text{-bpy})_2(H_2O)_2](SO_4)\}_n$: C10

The reaction of an ethylene glycol solution of 4,4'-bpy and a methanolic solution of $CoS_2O_6 \cdot 6H_2O$ produced light orange block-like crystals. This compound crystallized in the tetragonal crystal system, space group P4/ncc, with a = b = 11.319(2) Å, c = 16.400(3) Å, Z = 2, V = 2101.0(6) $Å^3$, R1 = 0.2823, wR2 = 0.5517. The high R1 value is due to the poor quality of the crystal.

This compound is isostructural with **C2** and **C9** [7, 19] but the anion and the metal ion are different. The complex possesses C_4 symmetry, with the cobalt atom having site symmetry 4.

The nitrogen atoms of the 4,4'-bpy are coordinated to the Co^{II} centres (d^7) in the equatorial plane forming a 2D grid. The Co^{II} centre has a distorted octahedral environment. The selected distances and angles are summerized in Table 2.14.

Table 2.14 Selected bond distances (Å) and bond angles (°) for **C10** (P4/ncc)

Bond	Length (Å)	Angle	Angle (°)
Co1-O1	2.100(14)	O1-Co1-N3	89.8(6)
Co1-N3	2.143(17)	O1-Co1-O1[a]	180.00
[a]) 3/2-x,1/2-y,z [b]) 1/2+y,-1/2+x,1/2-z [c]) 1-y,1-x,1/2-z		O1-Co1-N3[a]	90.2(6)
		N3-Co1-N3[a]	91.1(6)
		N3-Co1-N3[b]	179.6(4)
		N3-Co1-N3[c]	88.9(6)

Two water molecules are coordinated in the axial positions. This compound presents 2D sheets which are inclined in the *"diagonal/diagonal"* interpenetration topology (Figure 2.16). This topology of interpenetration of M^{II}-4,4'-bpy layers seems to be strongly assisted when water molecules occupy the axial positions of the sphere of coordination of the metal ions.

The sulphate anions are strongly disordered and they occupy the cavities generated by the interpenetration.

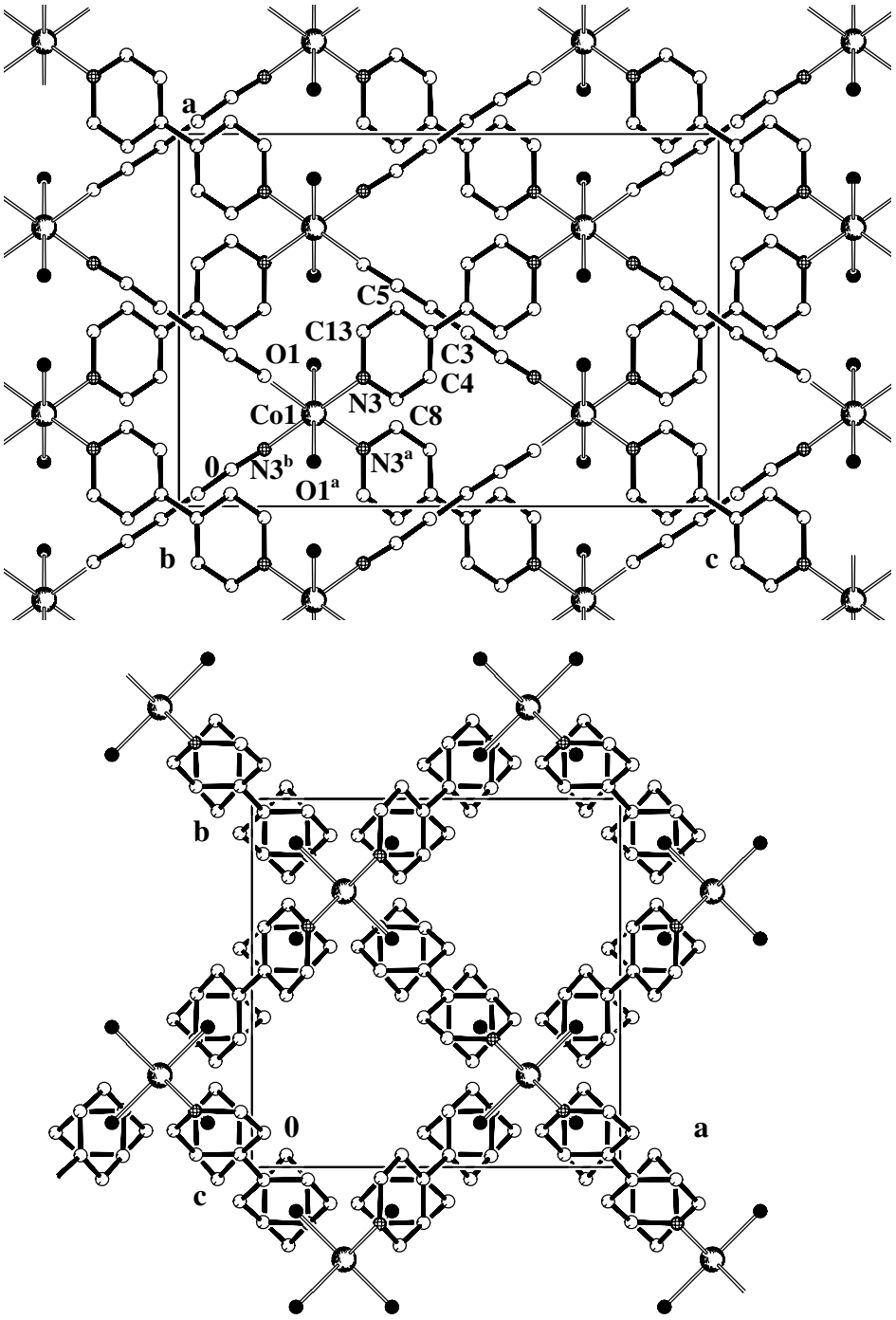

Figure 2.16 Crystal packing diagrams of complex **C10** (the hydrogens, the strongly disordered SO_4^{2-} anions and the solvent molecules are omitted for clarity); [a]) 3/2-x,1/2-y,z, [b]) 1/2+y,-1/2+x,1/2-z

2.3.4 $\{[Cu(SO_4)(4,4'\text{-bpy})_2](H_2O)_3(HOCH_2CH_2OH)_2\}_n$: C11

The reaction of an ethylene glycol solution of 4,4'-bpy and a methanolic solution of $CuSO_4 \cdot 5H_2O$ produced blue block-like crystals of **C11**. This compound crystallized in the monoclinic crystal system, space group I2/m, with a = 15.638(3) Å, b = 15.629(2) Å, c = 15.920(2) Å, β = 90.17(1) °, Z = 4, V = 3890.9(10) $Å^3$, R1 = 0.2444, wR2 = 0.5429. The high R1 value is due to the poor quality of the crystal. The complex possesses C_s symmetry, with the copper atom having site symmetry m.

The Cu^{II} centres have an octahedral geometry where the two sulphate anions are coordinated to the metal ion along the *c*-axis. The equatorial plane consist of four 4,4'-bpy ligands forming a grid pillared by the sulphate anions (Figure 2.17).

The Cu^{II} centres are slightly displaced from the equatorial plane and as a consequence, the axial bond distances Cu···O are not equivalent (Table 2.15). The anions are disordered over two positions.

Table 2.15 Selected bond distances (Å) and bond angles (°) for **C11** (I2/m)

Bond	Length (Å)	Angle	Angle (°)
Cu1-O1	2.09(2)	O1-Cu1-O4	178.5(11)
Cu1-O4	2.73(3)	O1-Cu1-N1	94.3(8)
Cu1-N1	2.01(2)	O1-Cu1-N2	94.5(8)
Cu1-N2	2.02(2)	O4-Cu1-N1	84.7(7)
[a]) x,1-y,z		N1-Cu1-N1[a]	89.4(9)
		N1-Cu1-N2[a]	171.2(7)
		O4-Cu1-N2	86.6(7)
		N1-Cu1-N2	89.9(8)

The structure, a 3D regular framework, provides channels with dimensions of 7.7×7.7 $Å^2$ along the *c*-axis and 5.1×1.4 $Å^2$ along the *a* and *b*-axes that are filled with solvent molecules. According to the classification of porous materials **C11** is a second generation compound which has stable rigid porous channels after the removal of guest molecules.

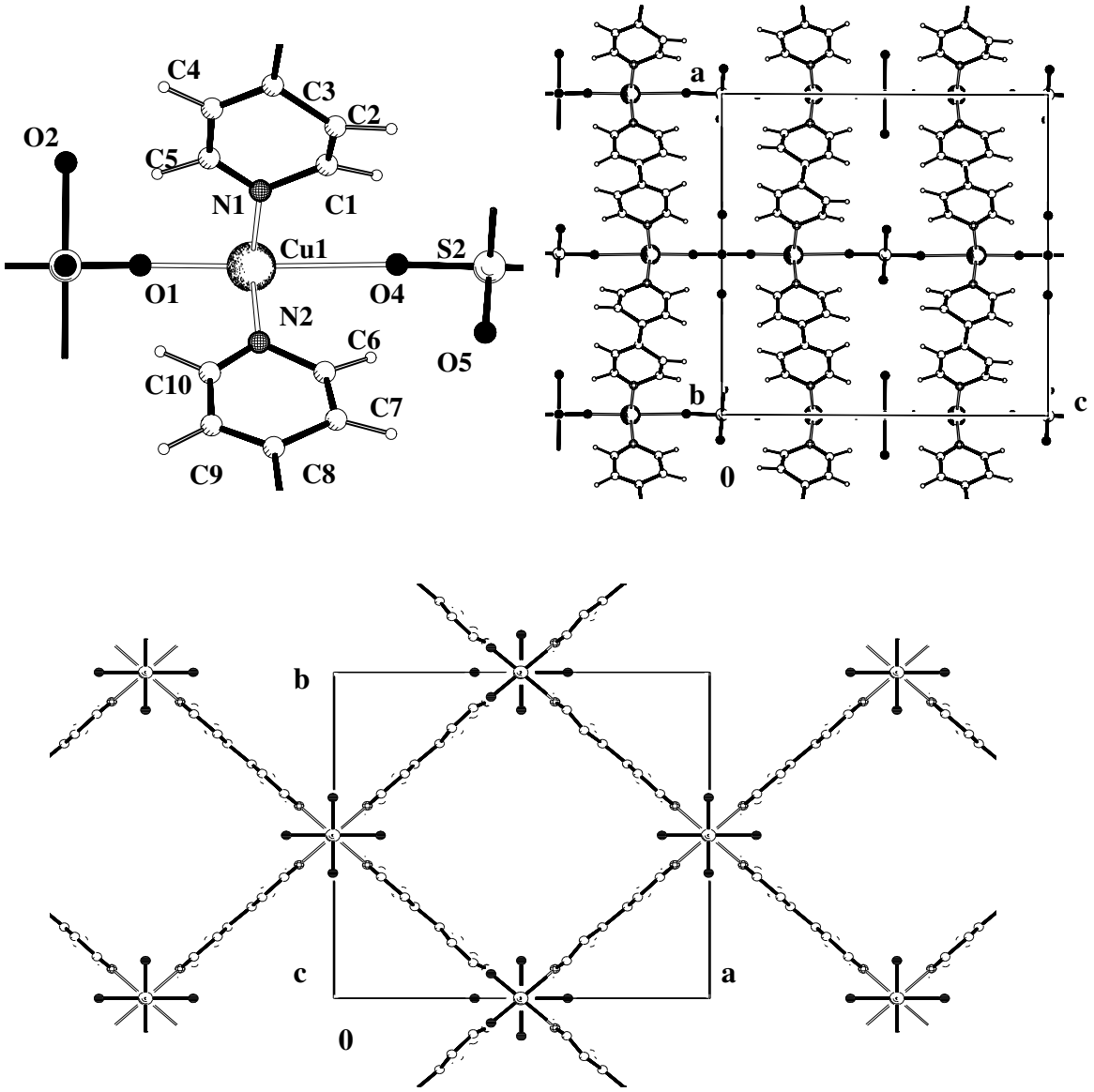

Figure 2.17 Cu^{II} coordination sphere of **C11** and crystal packing diagrams

In the TG analysis, the compound shows the loss of the water molecules of crystallization up to 100 °C and then the loss of ethylene glycol molecules, followed by decomposition (Figure 2.21).

When compound **C11** is immersed in water (Reaction 2.8), a mixture of three polymorphic linear polymers (Figure 2.18) was obtained which are already reported in the literature [20-22].

$$\{[Cu\,(SO_4)\,(4,4'\text{-bpy})_2]\,(H_2O)_3\,(HOCH_2CH_2OH)_2\}_n + 3H_2O \rightarrow [Cu\,(SO_4)\,(H_2O)_3\,(4,4'\text{-bpy})]_n + 3H_2O + (HOCH_2CH_2OH) + (4,4'\text{-bpy})$$

Reaction 2.8

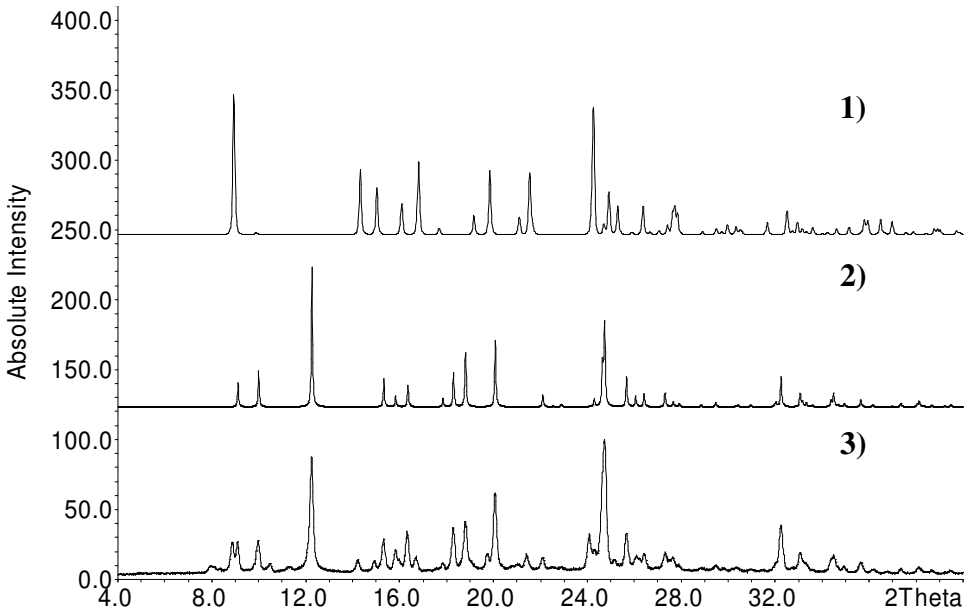

Figure 2.18 XRPD plot; (1) calculated XRD pattern for **C11-1a**, (2) calculated XRD pattern for **C11-1b** and **C11-1c**, (3) measured XRD pattern for **C11** inmersed in water.

The first one, **C11-1a** [20] represents only 10% of the mixture. In this 1D polymer, the Cu^{II} centres have octahedral geometry, with two molecules of 4,4'-bpy and two water molecules coordinated in equatorial positions, while the axial positions are occupied by one sulphate anion and one water molecule (Crystal system monoclinic, space group Cc). The adjacent chains are each arranged by π-π stacking interactions between the pyridine rings and extensive hydrogen bonds between water molecules and the sulphate groups. The others two linear polymers represent 90% of the mixture. The Cu^{II} coordination spheres for **C11-1b** [21] and **C11-1c** [22] are defined by two 4,4'-bpy ligands, three water molecules and one sulphate anion (Crystal system hexagonal, space groups $P6_5$ and $P6_1$, respectively), which indicates that the two compound are enantiomers. The axial positions are occupied by one water molecule and the sulphate anion.

2.3.5 $\{[Cu(SO_4)(H_2O)_2(4,4'\text{-bpy})][Cu(SO_4)(4,4'\text{-bpy})(HOCH_2CH_2OH)_2]\}_n$: C12

When the crystalline powder of **C11** was allowed to stand in solution for a month, a solid state transformation was observed where the dark blue powder changed into light blue cube-like crystals (Reaction 2.9).

$$2\{[Cu(SO_4)(4,4'\text{-bpy})_2](H_2O)_3(HOCH_2CH_2OH)_2\}_n \xrightarrow{\Delta T} \{[Cu(SO_4)(H_2O)_2(4,4'\text{-bpy})][Cu(SO_4)(4,4'\text{-bpy})(HOCH_2CH_2OH)_2]\}_n + 2(4,4'\text{-bpy}) + 4H_2O + 2(HOCH_2CH_2OH)$$

Reaction 2.9

This compound, **C12**, crystallized in the monoclinic crystal system, space group C2/c, with a = 11.0154(17) Å, b = 22.179(3) Å, c = 12.154(2) Å, Z = 8, V = 2952.7(8) $Å^3$, β = 96.070(13), R1 = 0.0393, wR2 = 0.1006. The complex possesses C_2 symmetry, with the copper atoms having site symmetry 2.

There are two kinds of Cu^{II} centres both showing octahedral geometry. The Cu1 centre has two water molecules in the axial positions, two 4,4'-bpy ligands coordinated in equatorial positions, forming a chain along the *b*-axis, and two sulphate anions also in equatorial positions and linking the metal centres (Table 2.16). The Cu2 centre has a similar environment but the axial positions are occupied by two ethylene glycol molecules. The result is a 2D metal-organic polymer (Figure2.19). The Cu···O and Cu···N distances are coherent with those found in the literature [23].

The 4,4'-bipyridine ligands coordinated to the metal ions have the pyridine rings twisted with the dihedral angle between pyridine ring 1 and ring 4 (N1 C1 C2 C3 $C2^b$ $C1^b$ and N4 C10 C11 C12 $C11^a$ $C10^a$, respectively) being 17.55(13)° and the dihedral angle between pyridine ring 2 and ring 3 (N2 C4 C5 C6 $C5^b$ $C4^b$ and N3 C7 C8 C9 $C8^a$ $C7^a$, respectively) being 10.35(12)° [symmetry operation $^{a)}$ -x,y,1/2-z; $^{b)}$ 1-x,y,1/2-z].

Compound **C12** presents some hydrogen bonds involving oxygen atoms from the solvent molecules coordinated to the metal centres, sulphate anions and 4,4'-bpy ligands

(Table 2.17). The hydrogen bonds formed between the different layers result in the formation of a 3D network.

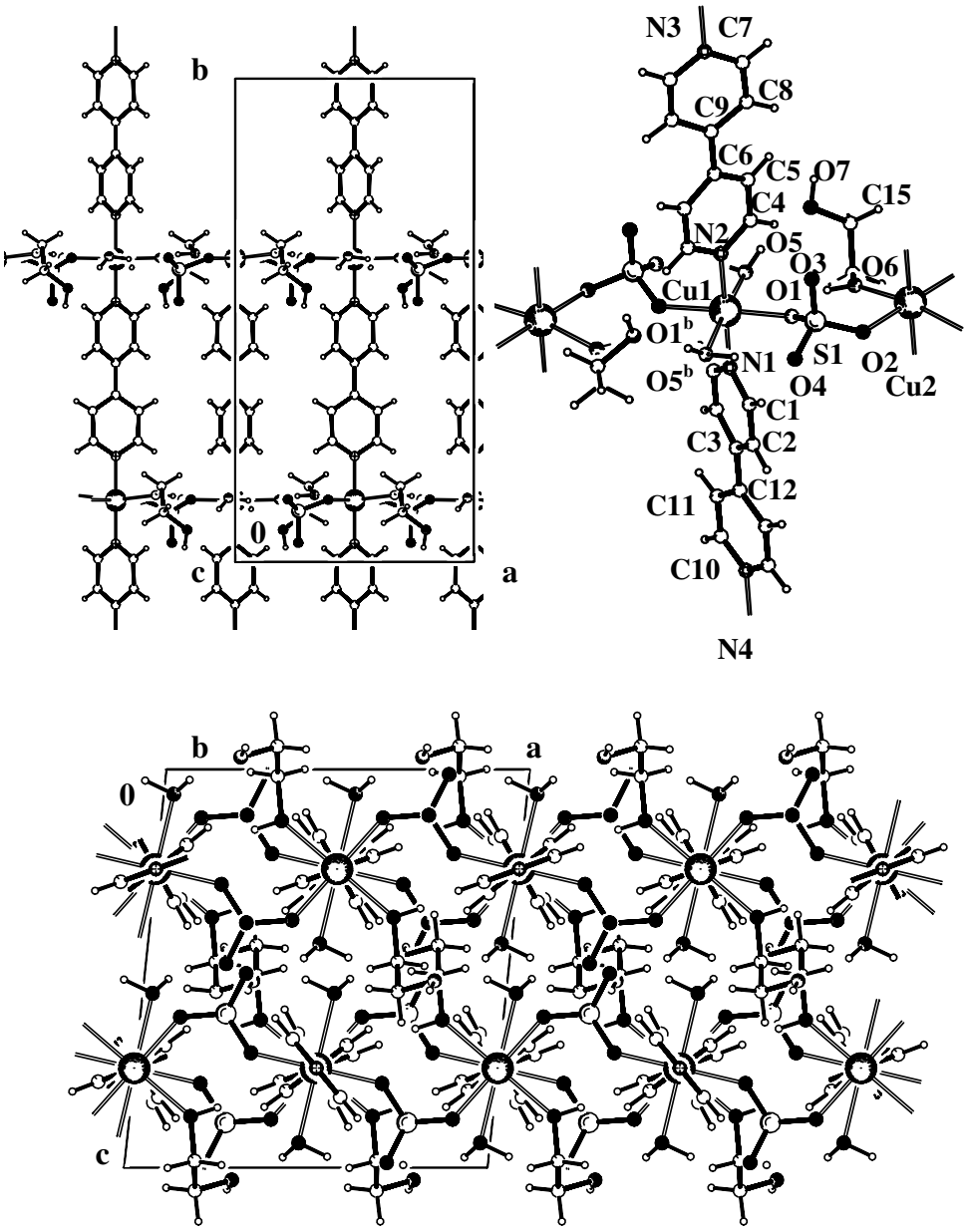

Figure 2.19 Crystal packing diagrams of **C12;** [b]) 1-x,y,1/2-z

Table 2.16 Selected bond distances (Å) and bond angles (°) for **C12** (C2/c)

Bond	Length (Å)	Angle	Angle (°)
Cu1-O1	2.042(2)	O1-Cu1-O5	89.68(8)
Cu1-O5	2.337(2)	O1-Cu1-N1	91.03(5)
Cu1-N1	1.980(3)	O1-Cu1-N2	88.97(5)
Cu1-N2	2.006(4)	O1-Cu1-O1[b]	177.95(8)
Cu2-O2	2.078(2)	O1-Cu1-O5[b]	90.23(8)
Cu2-O6	2.251(2)	O5-Cu1-N1	92.64(5)
Cu2-N3	2.001(3)	O5-Cu1-N2	87.36(5)
Cu2-N4	2.018(4)	O1[b]-Cu1-O5	90.23(8)
[a]) -x,y,1/2-z [b]) 1-x,y,1/2-z		O5-Cu1-O5[b]	174.72(7)
		N1-Cu1-N2	180.00(2)
Angle	**Angle (°)**	O2-Cu2-O6	89.13(8)
O6-Cu2-N3	95.79(6)	O2-Cu2-N3	90.33(5)
O6-Cu2-N4	84.22(6)	O2-Cu2-N4	89.67(5)
O6-Cu2-O6[a]	168.43(9)	O2-Cu2-O2[a]	179.34(8)
N3-Cu2-N4	180.00(1)	O2-Cu2-O6[a]	90.81(8)

Table 2.17 Hydrogen bonds for **C12** (C2/c)

Hydrogen Bond	D–H (Å)	H···A (Å)	D···A (Å)	D–H···A (°)	Symmetry operation
O5–H1···O7	0.82(4)	1.94(4)	2.742(3)	163(4)	
O5–H2···O3[b]	0.96(4)	1.82(4)	2.739(3)	159(3)	
O6–H3···O1	0.85(4)	1.95(5)	2.663(3)	140(4)	
O7 –H4···O4[c]	0.86(3)	1.84(4)	2.687(3)	167(4)	[a]) -x,y,1/2-z [b]) 1-x,y,1/2-z
C1–H1···O7	0.95	2.57	3.432(4)	151	[c]) x,1-y,1/2+z
C2–H2···O3[c]	0.95	2.55	3.467(4)	163	[d]) 1/2-x,1/2-y,-z
C5–H5···O3[d]	0.95	2.42	3.313(4)	157	[e]) -x,1-y,-z
C7–H7···O6[a]	0.95	2.49	3.136(4)	125	
C8–H8···O3[e]	0.95	2.47	3.424(4)	176	
C10–H10···O2	0.95	2.44	2.956(4)	114	

The TG curve shows the loss of water molecules and then thermal stability until 210 °C (Figure 2.21).

2.3.6 $[Cu(SO_4)(4,4'\text{-bpy})]_n$: C13

As stated previously, **C8**, **C9**, **C11**, and **C12** were thermally stable only in a specific range of temperature (Figures 2.20 and 2.21). **C13** is the result of the

decomposition of this kind of copper-4,4'-bpy polymer containing anions with sulphur [coordinated or non-coordinated to the metallic centres: such as $S_2O_6^{2-}$ and SO_4^{2-}] on heating to 210-225 °C (Scheme 2.3).

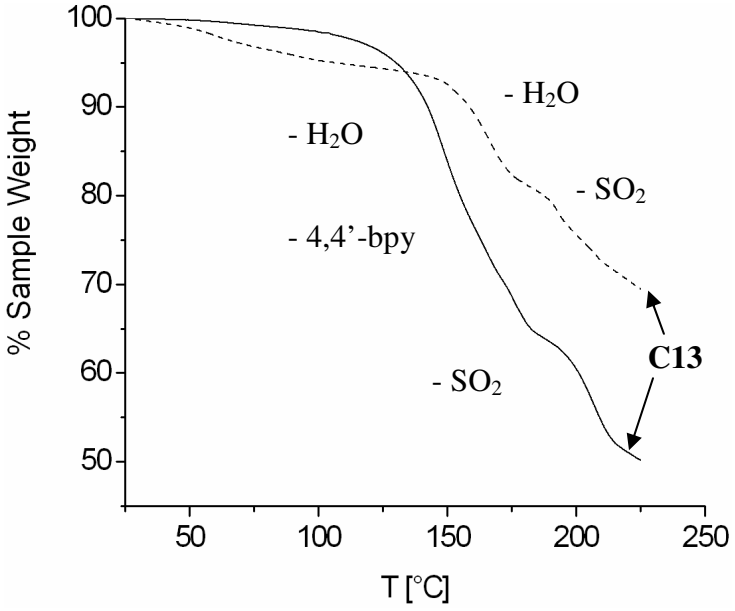

Figure 2.20 TG curve for **C8** (straight line) and **C9** (dash line)

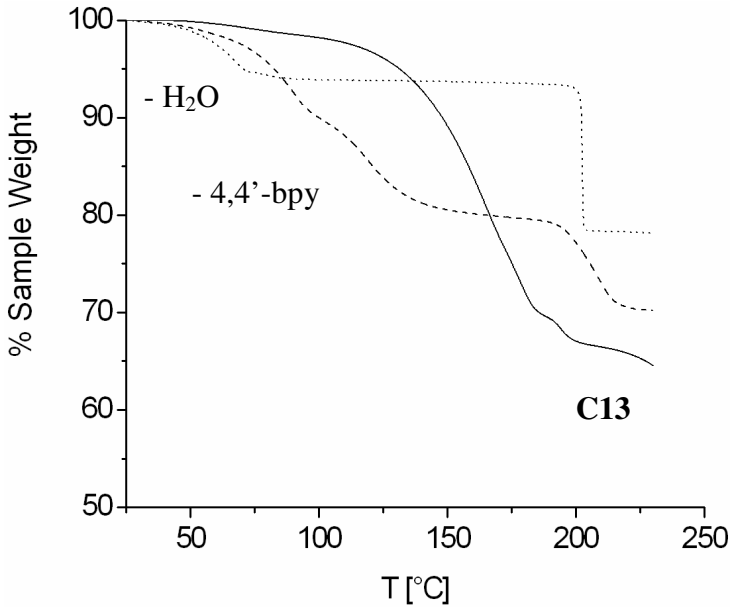

Figure 2.21 TG curve for **C11** (solid line), **C11** immersed in water (dash line) and **C12** (dot line).

The compounds retained their crystalline state while heating and the green powder obtained after the thermogravimetric analysis was suitable for XRPD studies. The compound **C13** crystallized in the monoclinic crystal system, space group C2/c, with a = 20.3330(5) Å, b = 11.4237(3) Å, c = 3.3270(3) Å, Z = 8, V = 2103.60(11) $Å^3$, β = 103.836(3), R_p = 0.0555, R_F = 0.0683.

The coordination sphere around the copper atom is intermediate between trigonal bipyramidal and square pyramidal geometry (Table 2.18). The Cu centres occupy general positions.

Table 2.18 Selected bond distances (Å) and bond angles (°) for **C13** (C2/c)

Bond	**Length (Å)**	**Angle**	**Angle (°)**
Cu1-O1	2.018(14)	O1-Cu1-N1	92.7(4)
Cu1-N1	1.944(10)	O1-Cu1-N2	88.4(5)
Cu1-N2	2.095(7)	O1-Cu1-O2[a]	105.1(6)
Cu1-O2[a]	2.142(10)	O1-Cu1-O3[b]	139.1(6)
Cu1-O3[b]	1.998(11)	N1-Cu1-N2	171.5(5)
		O2[a]-Cu1-N1	85.9(6)
[a]) x,-y,-1/2+z		O3[b]-Cu1-N1	89.9(5)
[b]) 3/2-x,-1/2+y,1/2-z		O2[a]-Cu1-N2	85.7(5)
		O3[b] -Cu1-N2	94.8(5)
		O2[a]-Cu1-O3[b]	115.8(6)

The angular structural parameter τ is defined as an index of trigonality and as a general descriptor of five-coordinate centric molecules (Equation 2.1). The equation is given by

$$\tau = (\beta - \alpha)/60 \qquad (2.1)$$

Ideally, square planar geometry is associated with α = β = 180°, for A as the axial ligand β is the greater of the basal angles (BMC) (Scheme2.2). For bipyramidal geometry, α becomes 120° and BMC the principal axis [24]. Therefore, the extreme

forms of geometry namely, square planar and trigonal bipyramidal, show $\tau = 0.00$ and $\tau = 1.00$, respectively.

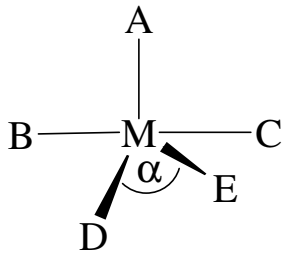

Scheme2.2

By this criterion, the irregular coordination geometry of **C13** in the solid state is best described as being in between trigonal bipyramidal and square pyramidal geometry with a slightly higher trigonal bipyramidal component (Figure 2.22) as revealed by the trigonal index τ of 0.54 where α = O1-Cu1-O3^{b} = 139.1(6)° and β = N1-Cu1-N2 = 171.5(5)°.

Each Cu^{II} ion is coordinated to two 4,4'-bpy ligands and to three SO_4^{2-} anions resulting in the formation of a 3D framework. For **C8** and **C9,** the sulphate anions came from the thermal decomposition of the dithionate anions (Figure 2.20). The Cu···O and Cu···N distances are comparable with those found in the literature [25, 26]. One oxygen atom from each sulphate anion is not coordinated to a Cu^{II} center.

Oxygen atoms from the sulphate anions are involved in hydrogen bonds with the ligands (Table 2.19).

Table 2.19 Hydrogen bonds for **C13** (C2/c)

Hydrogen Bond	**D–H (Å)**	**H···A (Å)**	**D···A (Å)**	**D–H···A (°)**	**Symmetry operation**
C1–H1···O2^{a}	0.931(15)	2.42(2)	2.916(17)	113.2(13)	^{a}) x,-y,-1/2+z
C4–H4···O4^{c}	0.929(11)	2.308(15)	3.217(15)	165.9(11)	^{b}) 3/2-x,-1/2+y,1/2-z
C5–H5···O3^{b}	0.931(16)	2.517(16)	2.929(14)	107.1(12)	^{c}) x,-y,1/2+z
C6–H6···O3^{b}	0.935(15)	2.458(17)	3.010(15)	117.8(10)	

The Scheme 2.3 is a representation of diverse solid state transformations carried out with different compounds, formed with anions containing sulphur like **C8**, **C9**, **C11** and **C12**. These solid state transformations are based on anion-exchange or thermal decomposition experiments.

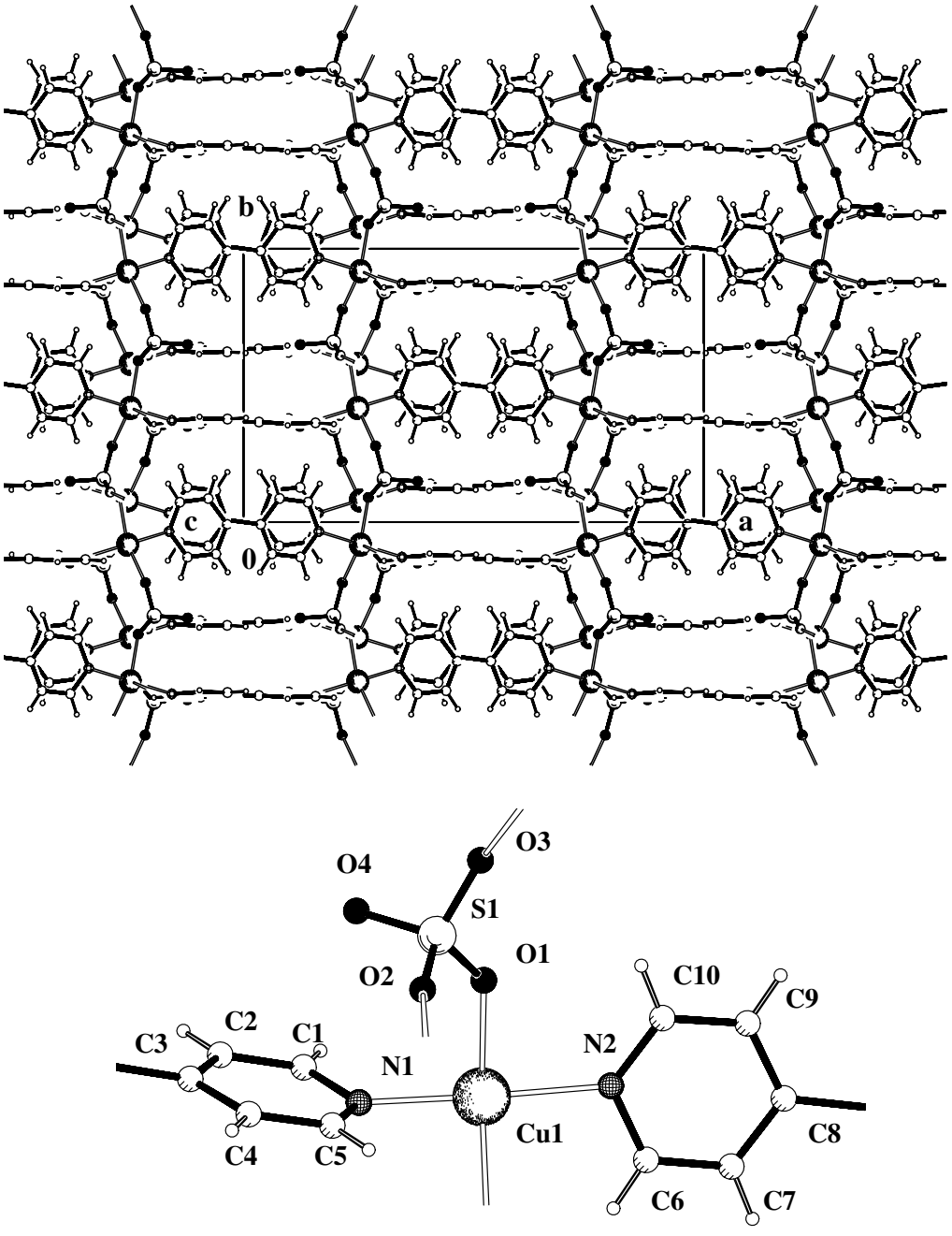

Figure 2.22 Asymmetric unit and crystal packing diagram for compound **C13**

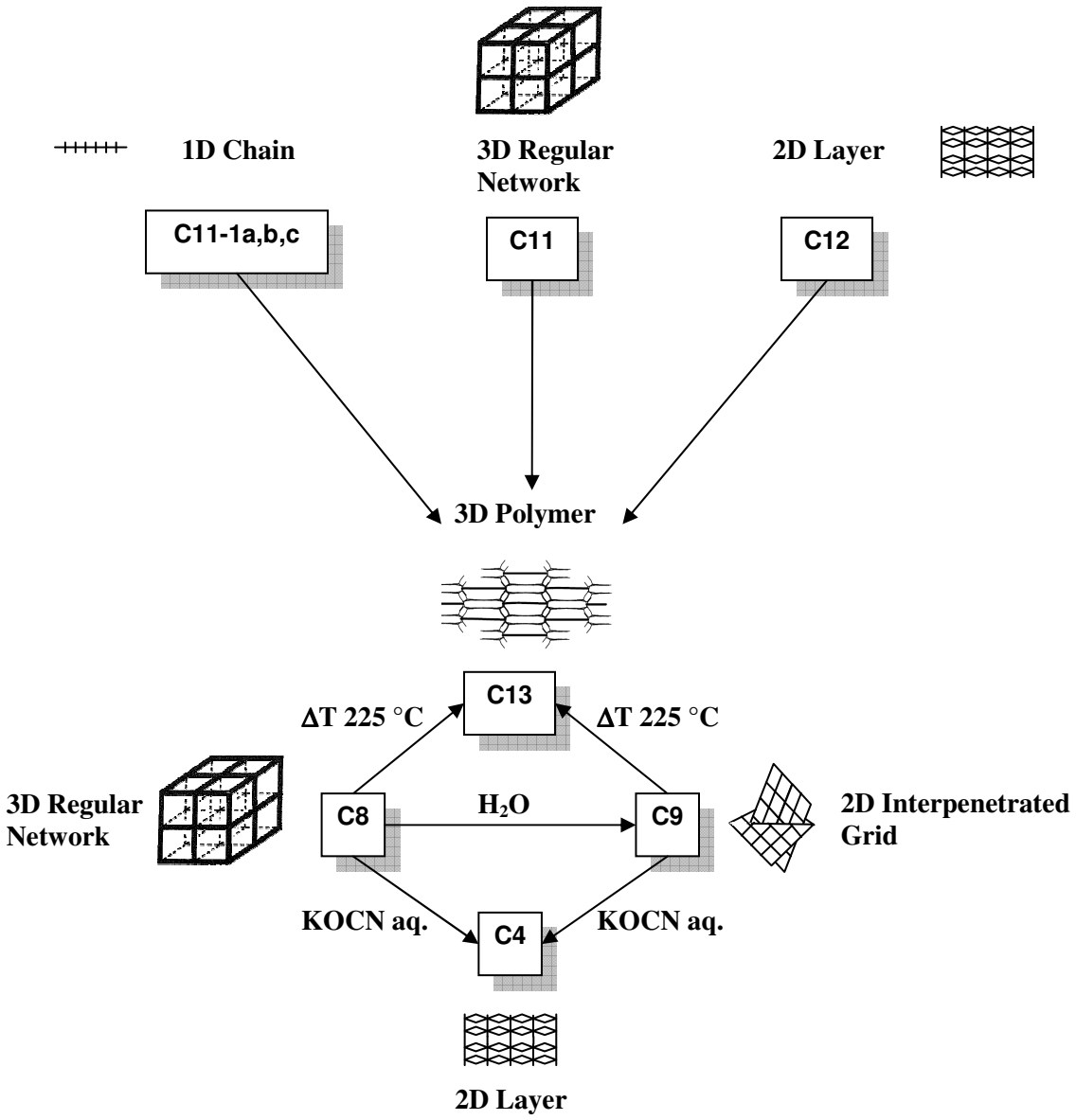

Scheme 2.3 Solid state transformations for **C8**, **C9**, **C11** and **C12**

2.3.7 $\{[Co_2(SO_4)(S_2O_6)(4,4'\text{-bpy})_4](H_2O)_5\}_n$: C14

This compound was synthesized like that of **C10** but using anhydrous CoS_2O_6 and dry solvents in N_2 atmosphere. Two weeks later, light orange block-like crystals appeared in the solution. The compound crystallized in the orthorhombic crystal system, space group Cmca, with a = 22.6372(15) Å, b = 28.960(3) Å, c = 22.6702(13) Å, Z = 8, V =

14862(2) $Å^3$, R1 = 0.1276, wR2 = 0.3458. The high R1 value is due to the poor quality of the crystal.The Co centres occupy general positions.

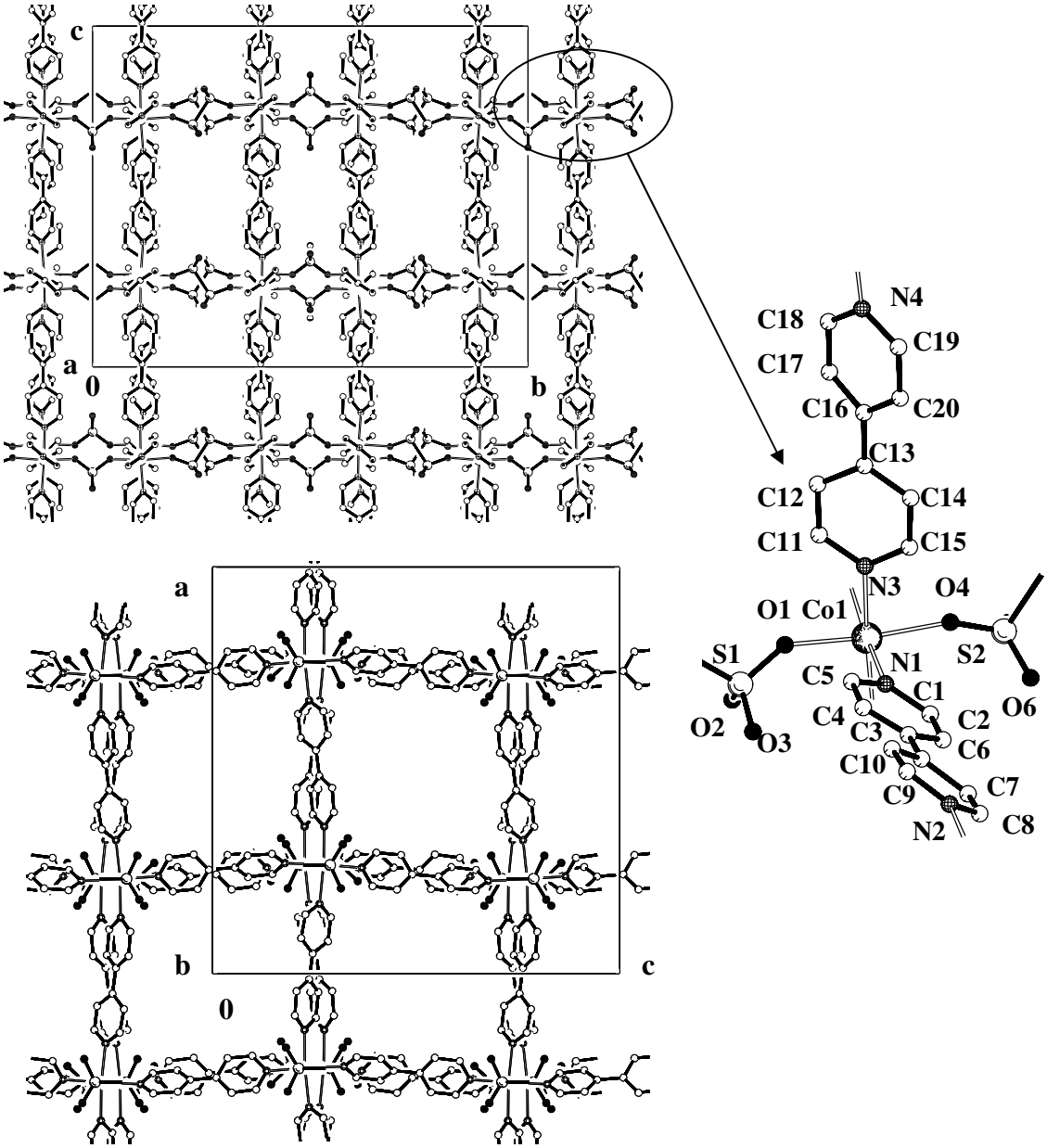

Figure 2.23 Crystal packing diagrams of compound **C14**

The structure, a 3D framework, provides channels with dimensions of 9.3×8.7 $Å^2$ along the *b*-axis, 6.8×4.2 $Å^2$ and 5.7×5.3 $Å^2$ along the *a* and 6.9×3.4 $Å^2$ and 5.7×5.8 $Å^2$ along the *c*-axis that are filled with solvent molecules (Figure 2.23). These channels are made up of layers of Co_4-(4,4'-bpy)$_4$ pillared by alternate sulphate and dithionate anions.

The Co^{II} centres present a distorted octahedral geometry where the axial positions are occupied by one sulphate anion and one dithionate anion and the equatorial positions are occupied by the 4,4'-bpy ligands. The Co^{II} centres are in a general position and are slightly displaced from the equatorial plane and as a consequence, the axial bond distances Co···O are not equivalent (Table 2.20).

Table 2.20 Selected bond distances (Å) and bond angles (°) for **C14** (Cmca)

Bond	**Length (Å)**	**Angle**	**Angle (°)**
Co1-O1	2.047(5)	O1-Co1-O4	174.4(2)
Co1-O4	2.107(5)	O1-Co1-N1	91.9(2)
Co1-N1	2.130(7)	O1-Co1-N3	87.6(2)
Co1-N3	2.159(7)	O1-Co1-N2[a]	89.4(2)
Co1-N2[a]	2.177(5)	O1-Co1-N4_d	95.6(2)
Co1-N4_d	2.140(7)	O4-Co1-N1	89.5(2)
		O4-Co1-N3	87.0(2)
		O4-Co1-N2[a]	88.7(2)
		O4-Co1-N4_d	89.8(2)
[a]) -1/2+x,y,1/2-z		N1-Co1-N3	88.3(2)
[b]) 1/2-x,y,-1/2+z		N1-Co1-N2[a]	174.7(2)
		N1-Co1-N4_d	93.5(2)
		N2[a]-Co1-N3	86.6(2)
		N3-Co1-N4_d	176.3(2)
		N2[a]-Co1-N4_d	91.5(2)

The 4,4'-bipyridine ligands coordinated to the metal ions have the pyridine rings twisted with the dihedral angle between pyridine rings, plane n° 1 and plane n° 2 (Co1 N1 C1 C2 C3 C4 C5 and N2 C6 C7 C8 C9 C10 C3, respectively) being 9.2(3)° and the dihedral angle between pyridine rings, plane n° 3 and plane n° 4 (N3 C11 C12 C13 C14 C15 C16 and N4 C16 C17 C18 C19 C20 C13, respectively) being 25.4(3)° .

Dithionate salts are not stable upon heating and in solution easily decompose with loss of SO_2 producing the metal sulphate. The fact that only 50 % of dithionate decomposed to form the structure could be explained by synthetic conditions and stability.

2.4 Adsorption by Metal-Organic Frameworks

The ability to control the functionality and dimensions of pores and channels of a metal-organic framework produces possibilities for separation and storage of gases, especially in the area of fuel gases where there are actual technological needs [27-29]. As stated previously, a rational modification of the starting material to build-up the metal-organic network modifies also the physical properties of the new material [30-32]. In this section three compounds have been studied and characterized using their property of adsorption capacity. These compounds are **C8**, **C11** and the already known **C1**. Even if there are some other porous materials in the previous sections, these three present layers formed by 4,4'-bpy and Cu^{II} ions along the equatorial plane bridged by dithionate, sulphate and hexafluorosilicate anions respectively enabling comparisons. Since the structural differences are minimal and all of them present square channels along an axis with a similar size, it could be possible to analyze the influence of the nature of the anions during the adsorption process.

2.4.1 Adsorption Properties of Compound C1

In order to determine the best conditions to out-gas the compound **C1** before the adsorption experiments, several samples were prepared at different temperatures and in different time periods in vacuum (10^{-4} Torr). Four sets of samples were selected. The first set was out-gassed at room temperature for 24 h where the weight loss was about 16 %, the second set was out-gassed at 50 °C for 24 h where the weight loss was about 20 %, the third set was out-gassed at 100 °C for 24 h where the weight loss was about 40 %, and the fourth set was out-gassed at 100 °C for 72 h where the weight loss was about 50 %. Once the samples were prepared, benzene immersion calorimetric studies were performed in order to establish the influence of the weight loss in the enthalpy of immersion value (Figure 2.24). At the same time XRPD analyses were also carried out in order to evaluate the stability of the sample after various conditions of out-gassing.

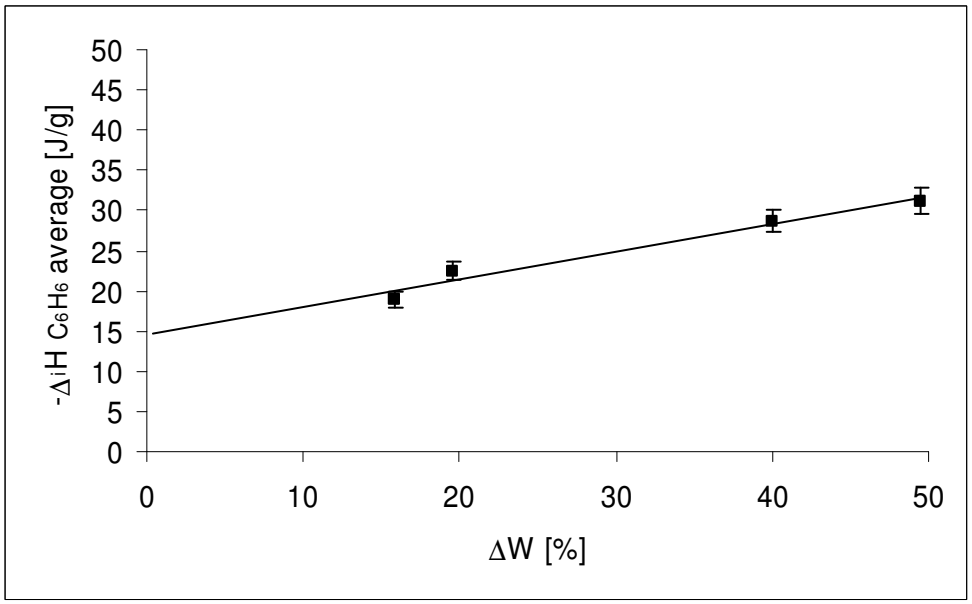

Figure 2.24 Influence of weight loss on the heat of immersion of compound **C1** into benzene. The samples were prepared at different temperatures while out-gassing.

Figure 2.24 shows that the heat of immersion of **C1** into benzene increases linearly with the weight loss, giving $\overline{\Delta_i H}(C_6H_6)$ = -31.2 J/g for a 50 % of weight loss. Compound **C1** retained its crystalline state while out-gassing. The samples which belong to the fourth set present a green coloration after the out-gassing process but the XRPD patterns do not exhibit any significant change. Using these conditions, solvent molecules stuck to the surface of the compound and into the pores can be eliminated and the pores are more accessible to the benzene molecules.

As stated previously, this network provides channels with dimensions of ca. 7.7×7.7 $Å^2$ along the *c*-axis and ca. 5.8×1.8 $Å^2$ along the *a* and *b*-axes (Figure 2.25) and are accessible for small guest molecules.

Compound **C1** is capable of the reversible adsorption of benzene, as was found from vapour adsorption (Figure 2.26) and calorimetry studies (Figure 2.24) [33-34]. The benzene vapour adsorption/desorption isotherms were carried out at two temperatures 293 K and 308 K and in the range of relative pressures $10^{-4} < p/ps < 0.9$.

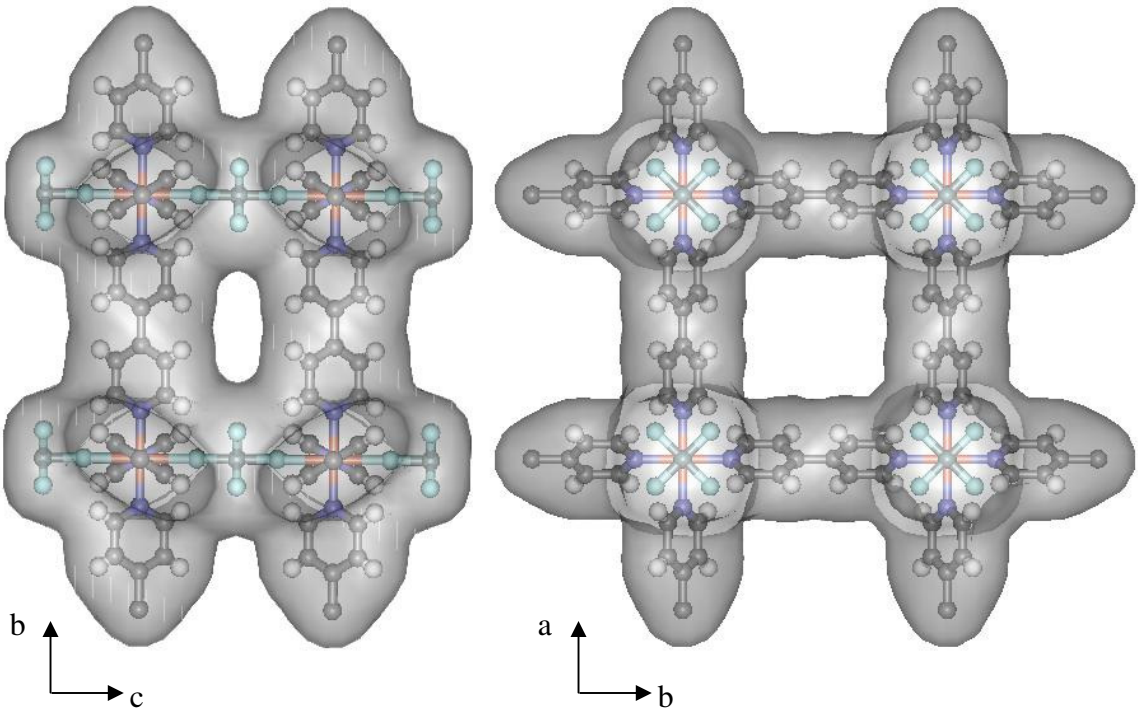

Figure 2.25

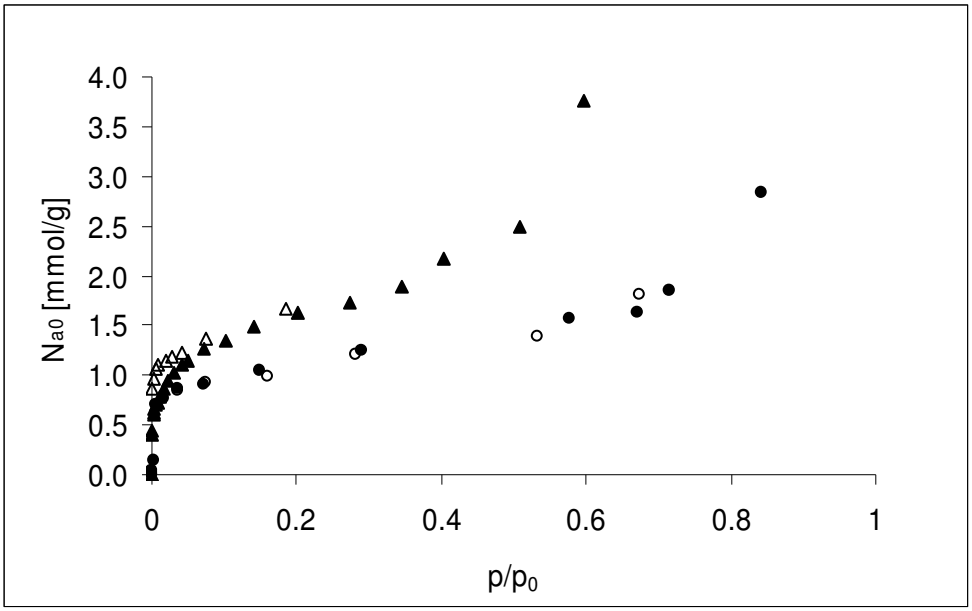

Figure 2.26 Gravimetric isotherms for benzene adsorbed by compound **C1** after 50% outgassing: Adsorption at 293 K (●) and 308 K (▲), Desorption at 293 K (○) and 308 K (△).

Dichloromethane, methane and nitrogen adsorption experiments were also carried out on **C1** samples. The different isotherms showed type I behaviour and were analyzed by Dubinin's theory [35-36]. The logarithmic plots of the DR equation (Equation 2.2), ln (N_a/N_{a0}) *versus* $(A/\beta)^n$, where $\beta = E/E_{C_6H_6}$ with n = 2, shows a good overlap for the different adsorbates (Figure 2.27).

$$N_a = N_{a0} \exp\left[-(A/E)^n\right] \tag{2.2}$$

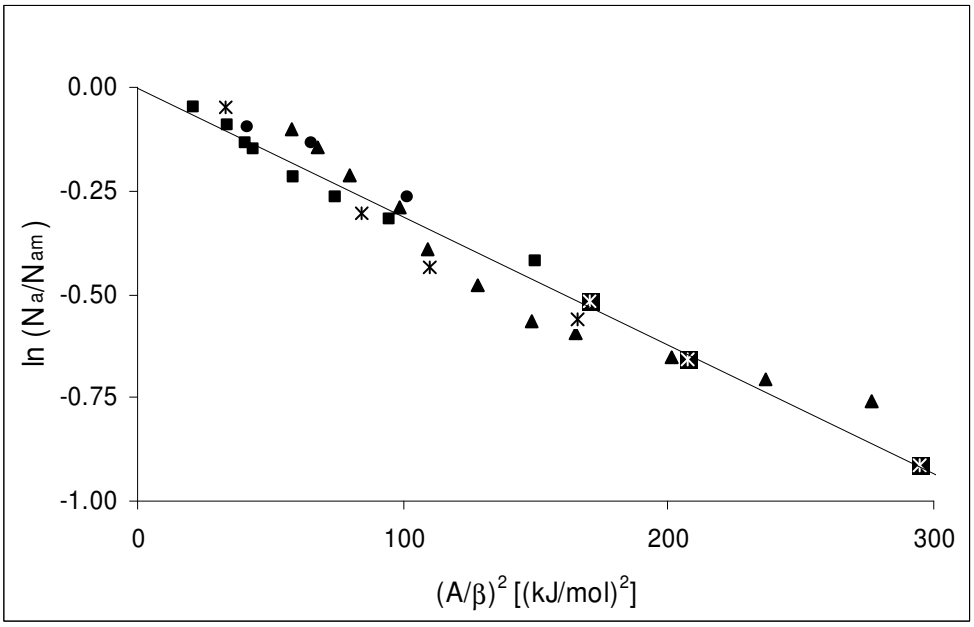

Figure 2.27 General DR plot for adsorption on solid **C1** after 50% out-gassing ($E_{C_6H_6}$ = 20 kJ/mol with n=2): Benzene isotherm at 293 K (●) and 308 K (▲), dichloromethane isotherm at 293 K (■), methane isotherm at 85 K (∗), nitrogen isotherm at 80 K (⊠).

Adsorption experiments on **C1** were already reported in the literature [6, 7]. The methane adsorption experiments were carried out in the range between 1 and 36 atm at 298 K. The methane adsorption at high pressure was much larger than that on *zeolite 5A*, which has the highest methane adsorption capacity in zeolites. Comparison with the previously reported experiments is not possible as the present experiments were carried out at low pressure (p < 1 atm).

2.4.2 Adsorption Properties of Compound C8

Similar studies to determine the best out-gassing conditions were performed on **C8**. The samples were out-gassed at different temperatures and for different times in vacuum (10^{-4} Torr). It was possible to observe that even if all the samples presented a similar weight loss, about 20 %, the heat of immersion of **C8** into benzene decreases linearly with the temperature and the exposure time to these conditions (Figure 2.28).

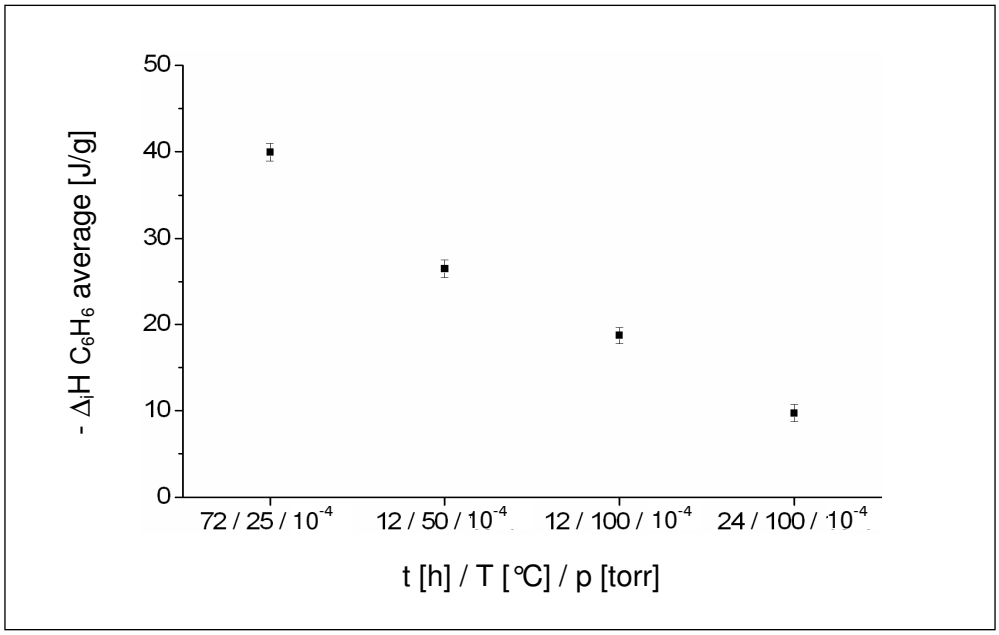

Figure 2.28 Influence of out-gas conditions for **C8** carried out with 20% out-gassed samples.

XRPD studies were performed on several samples in order to study these results (Figure 2.29). In the samples where the heat of immersion of **C8** into benzene was the lowest (hard out-gas conditions), it was possible to observe differences in crystallinity regarding their XRPD patterns compared to the XRPD pattern of the initially form. One of the diffraction peaks is located at about $2\theta = 8°$. When the samples are out-gassed at 100 °C, this peak shifts to the right of the scale (towards higher 2θ values). From this observation it is evident that the parameters of the unit cell have become smaller i.e., the unit cell has become smaller. Moreover the peak half-width (in degrees) became large after heating the samples. In general, a decrease in the crystalline state of the compound was observed. All these changes in the XRD pattern manifest a decomposition of the 3D

network. It is difficult to verify if this decomposition process is due to the already stated thermal decomposition of dithionate anions upon heating or the collapse of the 3D network. Nevertheless, thermally stable complexes containing coordinated dithionate anions are known [37], but their stability depends on the thermal stability of the whole network.

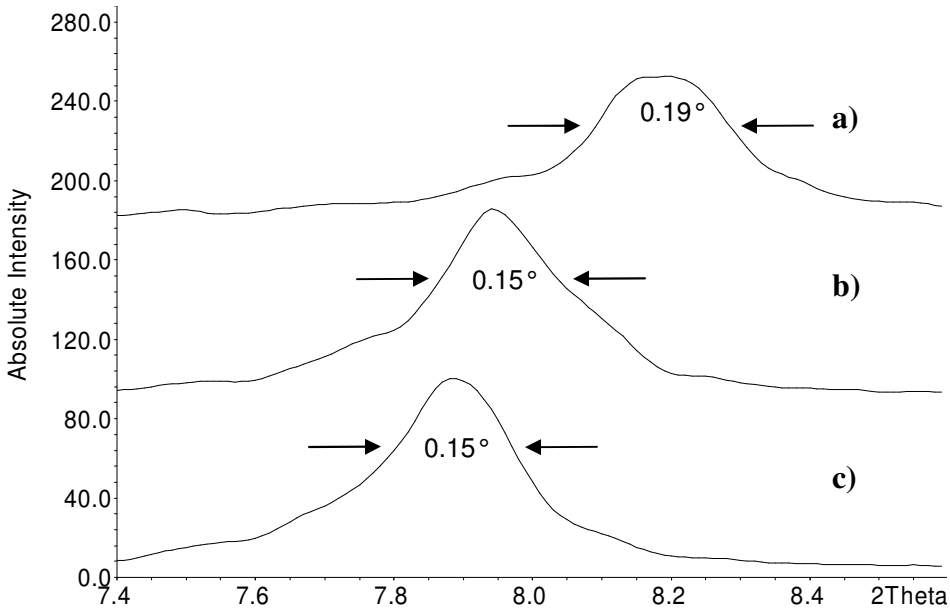

Figure 2.29 XRPD plot; measured XRD pattern for **C8** samples out-gassed (100 °C / 24 h / 10^{-4} torr) (a), measured XRD pattern for **C8** samples out-gassed (25 °C / 72 h / 10^{-4} torr) (b), measured XRD pattern for **C8** (c).

The three-dimensional structure provides channels with dimensions of *ca.* 8.7×8.7 $Å^2$ along the *c*-axis and *ca.* 5.2×3.1 $Å^2$ along the *a* and *b*-axes that are filled with solvent molecules (Figure 2.30). These molecules must be out-gassed from the pores for subsequent small molecule adsorption experiments. Using the first conditions related previously in this section, a heat of immersion of **C8** into benzene, $\overline{\Delta_i H}(C_6H_6)$ = -39.2 J/g was obtained for a 20 % weight loss and they were selected as protocol for out-gas samples before the adsorption experiments.

Like compound **C1**, **C8** is also capable of the reversible adsorption of benzene, as was found from vapour adsorption (Figure 2.31) and by calorimetry studies (Figure 2.28).

The benzene vapour adsorption/desorption isotherms were carried out at two temperatures 293 K and 308 K and in the range of relative pressures $10^{-4} < p/ps < 0.8$.

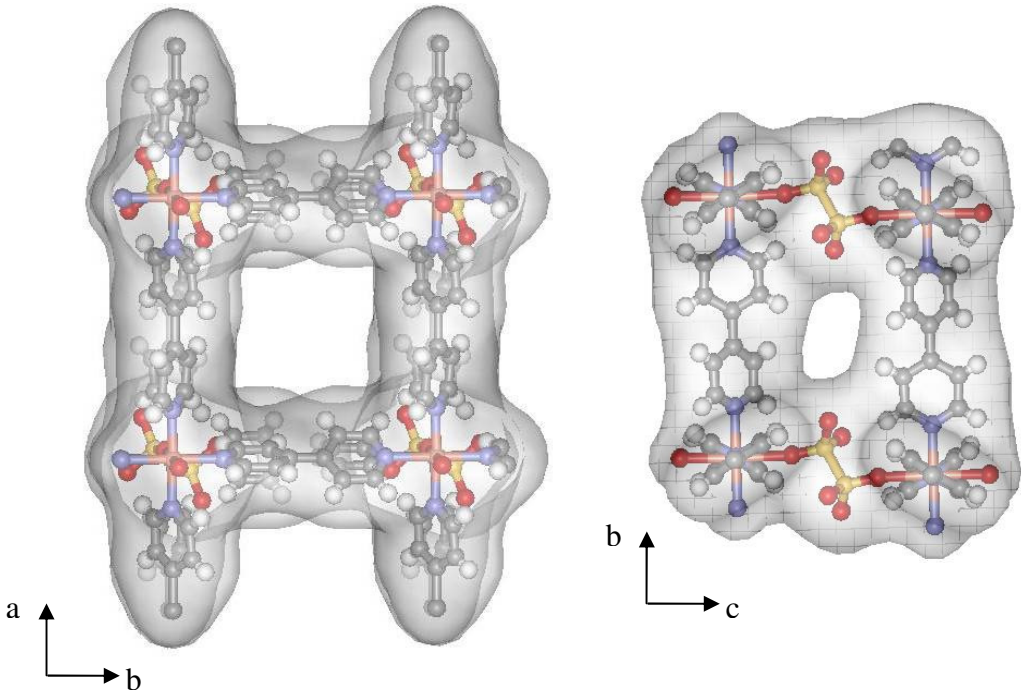

Figure 2.30

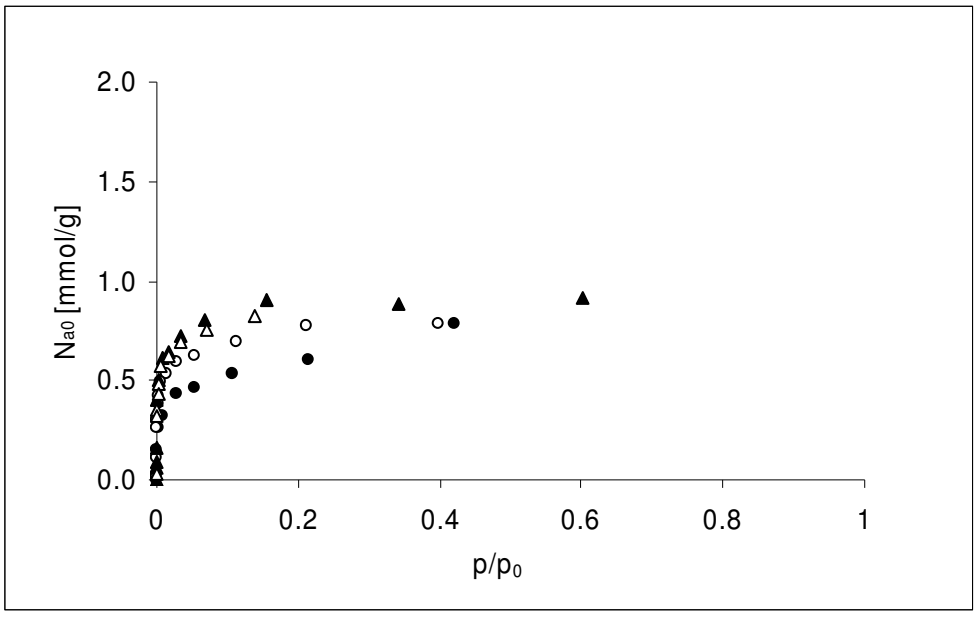

Figure 2.31 Gravimetric isotherm for benzene adsorbed by compound **C8** after 20% out-gassing: Adsorption at 293 K (●) and 308 K (▲), Desorption at 293 K (○) and 308 K (△).

The benzene adsorption capacity for **C8** shows that an amount of 0.57 mmol/g at 293K was adsorbed which is slightly lower to that observed for **C1** (0.99 mmol/g in the same conditions).

The desorption isotherms showed that the rigid framework can maintain its porosity in the absence of guests. When the benzene guest molecules were removed no additional weight loss was observed under the same out-gassing conditions used previously.

Dichloromethane, methane and nitrogen adsorption experiments were also carried out on compound **C8**. The different vapour adsorption isotherms on **C8** showed type I behaviour and they were analyzed by Dubinin's theory. In the case of vapours adsorbed on **C8**, the logarithmic plot of the DR equation (Equation 2.2), ln (N_a/N_{a0}) *versus* $(A/\beta)^n$, where $\beta = E/E_{C_6H_6}$ with n = 2, shows a good overlap for the different adsorbates (Figure 2.32).

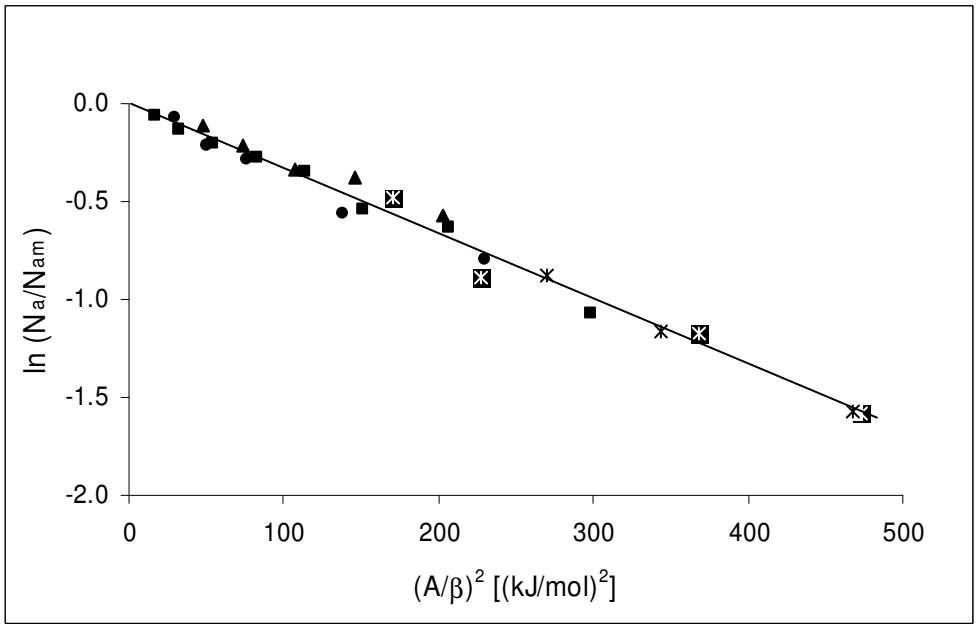

Figure 2.32 General DR plot for adsorption on solid **C8** after 20% out-gassing ($E_{C_6H_6}$ = 18 kJ/mol with n=2): Benzene isotherm at 293 K (●) and 308 K (▲), dichloromethane isotherm at 293 K (■), methane isotherm at 85 K (∗), nitrogen isotherm at 80 K (⊠).

This plot indicates coherence for the adsorption of the different vapours, within the framework of Dubinin's theory.

2.4.3 Adsorption Properties of Compound C11

In order to determine the best out-gassing conditions for **C11** the samples were prepared at several temperatures and out-gassed for different times in vacuum (10^{-4} Torr). All the samples presented a similar weight loss, about 20 %, and similar values for the heat of immersion of **C11** into benzene (Figure 2.33).

The structure provides channels, with dimensions of 7.7×7.7 $Å^2$ along the *c*-axis and 5.1×1.4 $Å^2$ along the *a* and *b*-axes, that are initially filled with solvent molecules (Figure 2.34).

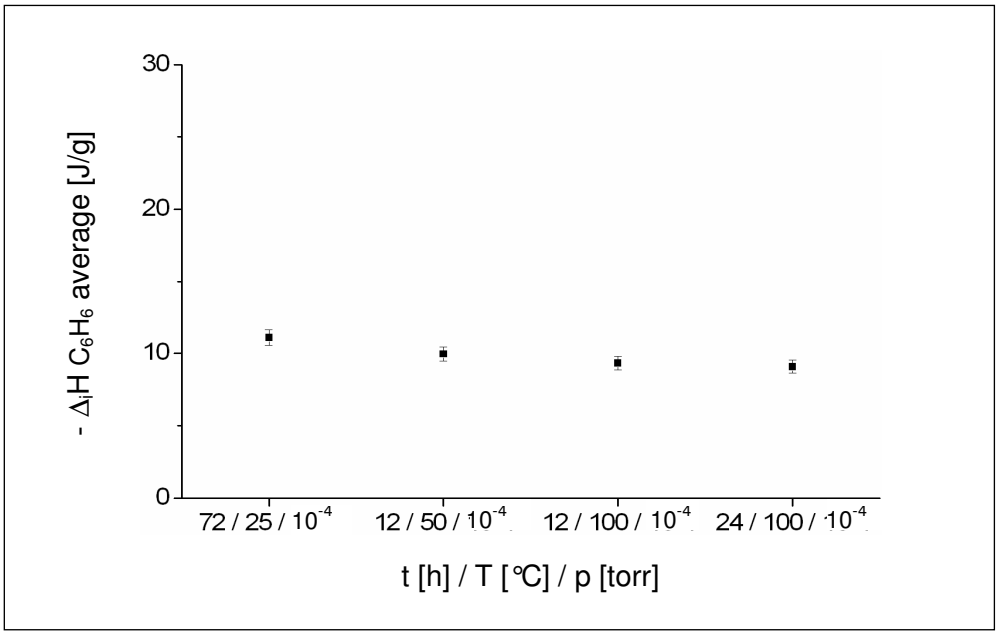

Figure 2.33 Influence of out-gassing conditions for **C11** carried out after weight losses of 20%.

The heat of immersion of **C11** into benzene obtained for samples out-gassed at room temperature for 72 h in vacuum was $\overline{\Delta_i H}(C_6H_6)$ = -11.1 J/g for 20 % weight loss.

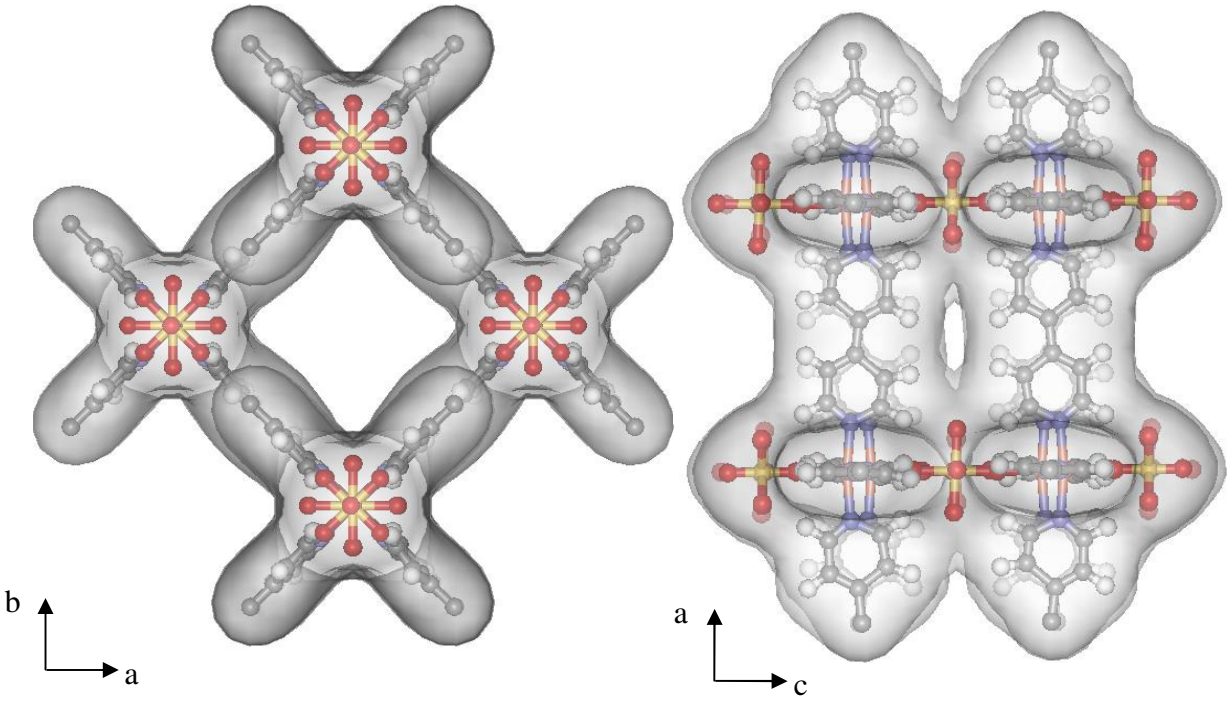

Figure 2.34

The reversible benzene vapour adsorption/desorption isotherms were determined at two temperatures 293 K and 308 K and in the range of relative pressures $10^{-4} < p/ps <$ 0.8 (Figure 2.35). The total amount of benzene adsorbed by **C11** at 293 K was 0.35 mmol/g.

As found for compounds **C1** and **C8**, the initial porosity is maintained after the removal of the guest molecules. The dichloromethane, methane and nitrogen adsorption experiments were also performed on **C11** samples to allow comparison. The adsorption of these adsorbates on **C11** can be also fitted, with a good approximation, to Equation 2.2. The single representation of the DR equation (Equation 2.2), ln (N_a/N_{a0}) *versus* $(A/\beta)^n$, where $\beta = E/E_{C_6H_6}$ with n = 2, is shown in Figure 2.36.

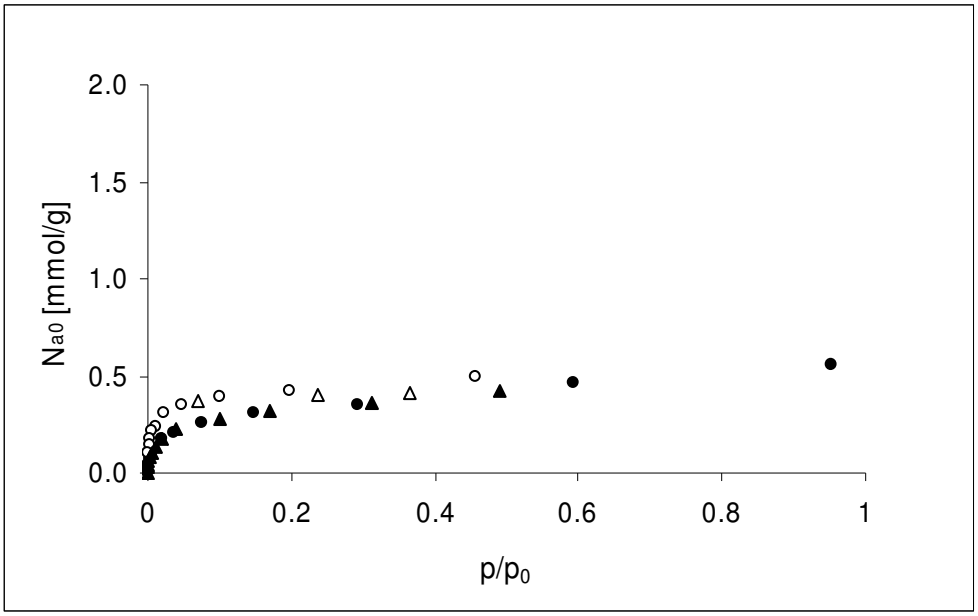

Figure 2.35 Gravimetric isotherms for benzene adsorbed by compound **C11** after 20% out-gassing: Adsorption at 293 K (●) and 308 K (▲), Desorption at 293 K (○) and 308 K (△).

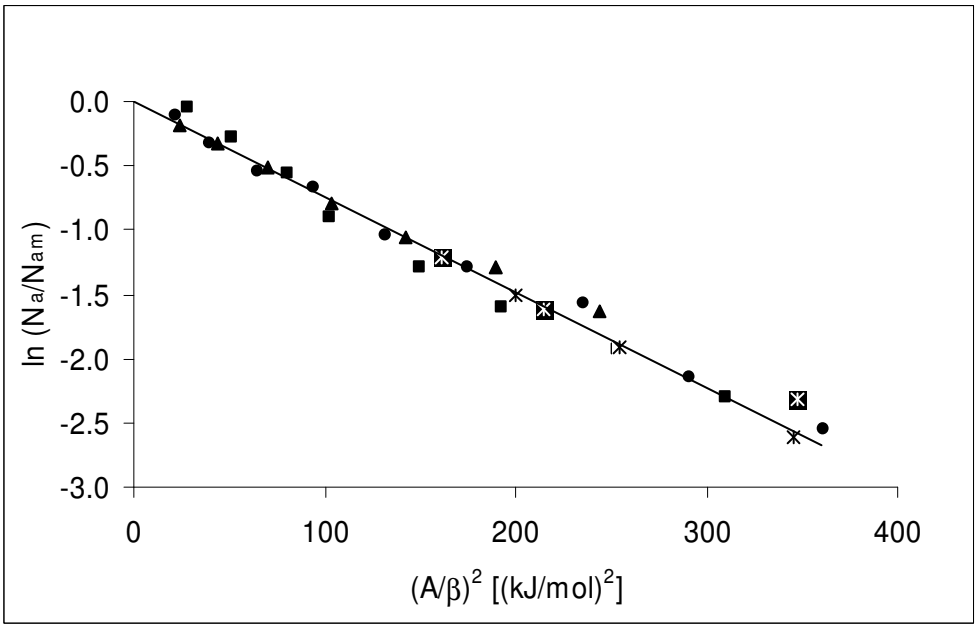

Figure 2.36 General DR plot for adsorption on solid **C11** after 20% out-gassing (**E**C_6H_6 = 12 kJ/mol with n=2): Benzene isotherm at 293 K (●) and 308 K (▲), dichloromethane isotherm at 293 K (■), methane isotherm at 85 K (∗), nitrogen isotherm at 80 K (⊠).

2.4.4 General Results from Adsorption Studies

The three compounds showed a similar behaviour for the adsorption of small molecules. The data obtained from vapour adsorption isotherms and from immersion calorimetry studies are given in Table 2.21.

Table 2.21 Summary of the adsorption and calorimetric experiments performed on solids **C1**, **C8** and **C11**.

			C1	C8	C11
Adsorption Isotherms	C_6H_6	E [kJ/mol]	20.85 (293K) 19.97 (308K)	16.01 (293K) 18.90 (308K)	11.47 (293K) 11.54 (308K)
		N_{a0} [mmol/g]	0.99 (293K) 1.27 (308K)	0.57 (293K) 0.89 (308K)	0.35 (293K) 0.38 (308K)
		$W_{0\ theoretic}$ [cm^3/g]	0.09 (293K) 0.11 (308K)	0.05 (293K) 0.08 (308K)	0.03 (293K) 0.03 (308K)
		$\Delta_i H_{calc}$ [J/g]	-24.86 (293K) -27.86 (308K)	-11.07 (293K) -20.66 (308K)	-4.83 (293K) -5.42 (308K)
	CH_2Cl_2	E [kJ/mol]	19.61 (293K)	17.15 (293K)	10.78 (293K)
		N_{a0} [mmol/g]	2.70 (293K)	1.49 (293K)	0.46 (293K)
		$W_{0\ theoretic}$ [cm^3/g]	0.17 (293K)	0.10 (293K)	0.03 (293K)
		$\Delta_i H_{calc}$ [J/g]	-65.45 (293K)	-31.58 (293K)	-6.16 (293K)
	CH_4	E [kJ/mol]	3.60 (85K)	3.10 (85K)	2.36 (85K)
		N_{a0} [mmol/g]	1.93 (85K)	0.33 (85K)	0.30 (85K)
		$W_{0\ theoretic}$ [cm^3/g]	0.09 (85K)	0.02 (85K)	0.01 (85K)
	N_2	E [kJ/mol]	3.58 (80K)	3.72 (80K)	2.51 (80K)
		N_{a0} [mmol/g]	0.94 (80K)	0.19 (80K)	0.13 (80K)
		$W_{0\ theoretic}$ [cm^3/g]	0.03 (80K)	0.01 (80K)	0.005 (80K)
Immersion Calorimetry Experimental values at 293K		$\overline{\Delta_i H}_{C_6H_6}$ [J/g]	-31.17	-39.24	-11.08
		$\overline{\Delta_i H}_{CH_2Cl_2}$ [J/g]	-45.73	-28.91	-25.61
		$\overline{\Delta_i H}_{H_2O}$ [J/g]	-98.94*	-85.06*	-111.44*
		$\overline{\Delta_i H}_{CCl_4}$ [J/g]	------**	------**	------**

* Enthalpy of transformation / decomposition

** Size of the molecule is too large (L_c = 0.63 nm)

First of all, it can be observed that CCl_4, with a width L = 0.63 nm, reveals a size limit for adsorption experiments for the three compounds. The molecule is too large to enter the pore system and no signal was detected in the calorimeter.

It is interesting to note that in the case of water immersion, the heat measured is not the heat of immersion but the heat of transformation of the 3D network into the 2D grid structure. It is follows that the decomposition process can be quantified and the values are close to 100 J/g. These values are much higher than that obtained on immersion into C_6H_6 and CH_2Cl_2.

As mentioned previously, Dubinin's theory can be applied to immersion calorimetry studies based on Equation 2.3.

$$\Delta_i H = -EN_{a0}\sqrt{\pi}\frac{(1+\alpha T)}{2} \qquad (2.3)$$

The experimental values obtained for immersion calorimetric studies on **C8** and **C11** are higher than those calculated from the adsorption data. This could be due to slight kinetic differences between the vapour and the liquid adsorption.

The highest overall amount of gas adsorbed has been observed for CH_2Cl_2 vapour adsorption isotherms. The comparisons with the C_6H_6 vapour adsorption isotherms (performed under the same conditions) indicate several inferences which could explain this fact. First, the width of the CH_2Cl_2 molecule is smaller than that of C_6H_6 (Table 2.22) and consequently a larger amount of CH_2Cl_2 will be adsorbed. Secondly, the CH_2Cl_2 molecule has a dipole moment which can influence the adsorption, as established by Currit [38]. Finally, hydrogen bonds between the pyridine rings and the CH_2Cl_2 molecules and between the CH_2Cl_2 molecules and the anions can be formed behaving as attractive forces to help the adsorption process. In the case of the C_6H_6 molecule, depending on the orientation of the planar molecules in the pore and the available volume, the amount of benzene adsorbed could change. The disposition of these

molecules could be forced by increasing the pressure of the system. Several researchers have carried out this kind of experiment at high pressure with methane between 1 and 36 atm at room temperature obtaining satisfactory results [7, 32, 41].

Table 2.22 Characteristics of the adsorbates

Adsorbate	MW [g/mol]	p_0 [mmHg]	V_m [cm^3/mol]	L [nm]	Moment*
C_6H_6	78.11	75.6 (293K)	88.91	0.41	(μ) 0.00
CH_2Cl_2	84.93	348.9 (293K)	64.02	0.33	(μ) 1.60
CH_4	16.00	36.75 (85K)	48.00	0.38	(μ) 0.00
N_2	28.01	1028 (80K)	34.67	0.33	(Q) $1.60 \cdot 10^{-2}$
Ar	39.95	305.3 (80K)	28.53	0.19	(Q) 0.00
H_2O	18.02	17.5 (293K)	18.05	0.30	(μ) 1.85
CCl_4	153.82	95.5 (293K)	96.5	0.63	(μ) 0.00

*molecular dipole moment (μ) [D]or electric quadrupole moment (Q) in multiples of barns [$\cdot 10^{-24}$ cm^2]. Data obtained from [39].

The literature also shows several examples where metal-organic networks exhibited a similar behaviour for the CH_2Cl_2 and C_6H_6 adsorption isotherms [32, 40-41]. However, the vapour adsorption of other molecules like N_2 is also reported in the literature but the behaviour is different from that expected, considering the fact that the size is smaller. This is the case for CH_4 and N_2 gas adsorption experiments carried out on **C1**, **C8** and **C11** nanoporous materials. The results in Table 2.21 show a constriction at low temperature for gas adsorption. This effect is more perceptible for the N_2 adsorption and so it is assumed that the electric quadrupole moment of the molecule is not involved. A kinetic study was carried out as a consequence of this effect (Figure 2.37).

From the representation of $\ln[1-N_a/N_{a0}]$ *versus* t, three rate constant were obtained: $k_{293K}\left[s^{-1}\right] = 2.1 \cdot 10^{-4}$, $k_{301K}\left[s^{-1}\right] = 2.4 \cdot 10^{-4}$, $k_{308K}\left[s^{-1}\right] = 3.3 \cdot 10^{-4}$.

The kinetic experiments show the increase of the kinetic constant k with the temperature even if the range of temperature is not wide. This effect will be stronger if it is taken into account that the adsorption of CH_2Cl_2 is performed at 293 K and the adsorption of CH_4 and N_2 is performed at 85 K and 80 K, respectively.

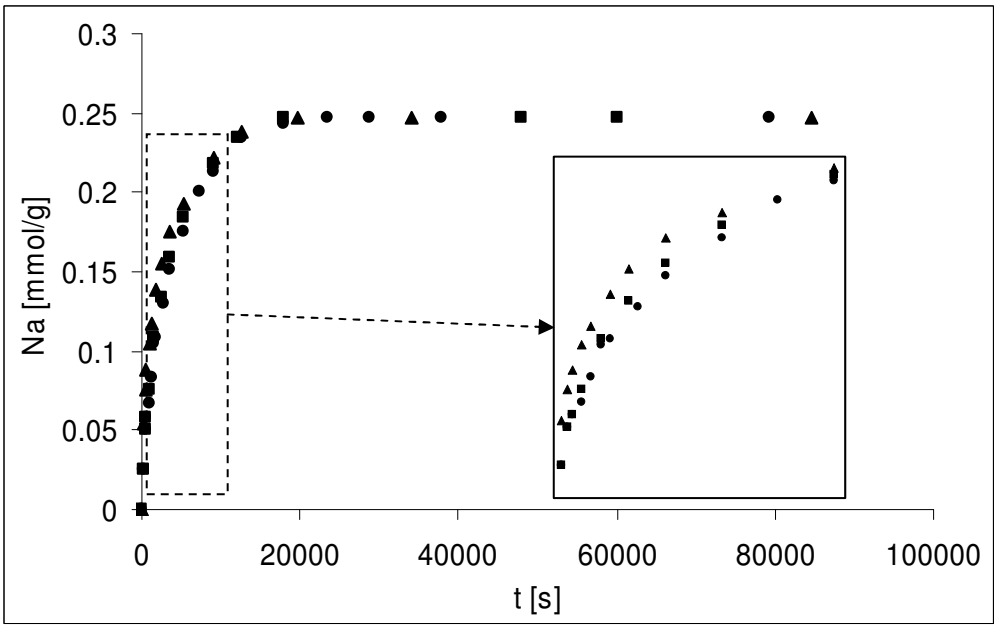

Figure 2.37 Kinetic studies for CH_2Cl_2 adsorption on **C11** at 293 K (●),301 K (■) and 308 K (▲).

Quantitatively the relationship between the rate a reaction proceeds and its temperature is determined by the Arrhenius Equation (Equation 2.4).

$$k = A \cdot e^{\left(-E_a/RT\right)} \tag{2.4}$$

where k is the rate coefficient, A is a constant, E_a is the activation energy, R is the universal gas constant, and T is the temperature (in degrees Kelvin).

Taking the natural logarithm of the Arrhenius equation yields

$$\ln(k) = -\frac{E_a}{R}\frac{1}{T} + \ln(A) \tag{2.5}$$

When the rate constants obeys the Arrhenius equation, the plot of ln(k) versus T^{-1} gives a straight line. If it is assumed that A and the activation energy E_a do not vary with temperature, the slope can be used to determine E_a [42]. The energy of activation

calculated for CH_2Cl_2 vapeur adsorption on **C11** using Equation 2.5 was E_a = 22 kJ/mol. This is a typical energy for entry into pores [43-45].

The scaling factors β relative to the benzene were obtained from the overall adsorption isotherms for the relevant adsorbates (Table 2.23).

The $\beta_{CH_2Cl_2}$ are in all the cases higher than that observed in the case of carbon ($\beta_{CH_2Cl_2}$ = 0.66) [46] which suggests the presence of specific interactions. The difference of approximately 0.3 visibly reflects additional interaction from the dipole of CH_2Cl_2, which are absent in the case of carbons. The literature reports some other similar cases like *Cabosil* with $\beta_{CH_2Cl_2}$ = 0.85 [47] and *zeolite 13X* with $\beta_{CH_2Cl_2}$ = 0.98 [38]. The β_{CH_4} and β_{N_2} obtained are smaller than those observed for various carbons. The reason is probably the nature of the interactions between the anions present in the structure and the molecules adsorbed.

Table 1.2 Comparison of β values for **C1**, **C8** and **C11**

	C1		**C8**		**C11**		**Carbon**
	E [kJ/mol]	**β**	**E [kJ/mol]**	**β**	**E [kJ/mol]**	**β**	**β**
C_6H_6	20.41	1.00	17.62	1.00	11.51	1.00	1.00**
CH_2Cl_2	19.61	0.96	17.15	0.97	10.78	0.94	0.66**
CH_4	3.60	0.18	3.10	0.18	2.36	0.21	0.35**
N_2	3.58	0.18	3.72	0.21	2.51	0.22	0.33**
Ar	10.30*	0.50*	------	------	------	------	0.32**

*Adsorption data obtained from [7]
** Adsorption data obtained from [46]

Due to the different nature of the adsorbent materials, it is always a difficult task to define the kind of interactions which influence or control the adsorption process. For the 3D metal-organic framework the situation is similar and adsorption capacities have already been reported in the literature [32, 40-41]. However, there are not many explanations concerning the interactions involved in the process itself.

In earlier sections, we pointed out the relevance of *Crystal Engineering* for the design of new materials based on the rational selection of the starting materials to construct the building-block. Ideally, this selection will be easier if we know the direct influence of every component on the physical property derived for the whole structure.

For the three structures characterised here, the significant difference is the nature of the counteranion; SiF_6^{2-} for **C1**, $S_2O_6^{2-}$ for **C8** and SO_4^{2-} for **C11**. An observed general behaviour for these three compounds is summarized in Scheme 2.4

$$N_{a0}(CH_2Cl_2) > N_{a0}(C_6H_6) > N_{a0}(CH_4) > N_{a0}(N_2)$$

Scheme 2.4

If it is considered that the first two adsorptions were carried out at 293 K and the last two at about 80 K, it is possible to separate them into two groups since it is already known that there is a constriction at low temperature. For the first group some ideas could be taken into account:

1. The size of the dichloromethane molecule is smaller so its adsorption is enhanced with regard to that of benzene.
2. The dichloromethane molecule presents a dipolar moment that could assist its adsorption.
3. The dichloromethane molecules could be involved in hydrogen bonds with the pyridine rings and also with the anions.
4. The benzene molecules could be involved in hydrogen bonds with the anions and form π–π stacking interactions with the pyridine rings. Due to its molecule shape and size, the adsorption process is probably highly influenced by steric interactions.

Regarding the second group:

1. The methane molecules could be involved in hydrogen bonds with the anions but not the nitrogen molecules.

For a given gas, the amount adsorbed for the three compounds can be classified as follows (Scheme 2.5).

$$N_{a0}(C1) > N_{a0}(C8) > N_{a0}(C11)$$

Scheme 2.5

If the small differences in the size of the pores for the three compounds are insignificant, a direct influence could be ascribed to the different number of atoms not coordinated to the metal centres present in the anion and to their electronegativity. Electronegativity is a measure of the tendency of an atom to attract a bonding pair of electrons. Fluorine is the most electronegative element with a value of 4.0 in the Pauling's scale followed by oxygen with a value of 3.4. For **C1**, the anion presents four fluorines which are not coordinated to the metal centres that could exercise an attractive interaction force with the gas molecules. For **C8**, the anion presents four oxygens which are not coordinated to the metal centres and for **C11**, the anion presents only two and hence the force of attraction could be lower resulting in lower adsorption.

The adsorption process is very complex and is not governed by a single kind of interaction. In the literature [48] the adsorption of a gas by a solid is defined as, "The outcome of the forces of attraction between the individual molecules of the gas and the atoms or ions composing the solid". Indeed, comparatives studies between metal-organic adsorbents with similar structures could help to understand the kind of factors involved in this process.

2.5 References

[44] Kondo M., Shimamura M., Noro S., Yoshitomi T., Minakoshi S., Kitagawa S., *Chem. Lett.*, 9, 285-286, **1999**.

[45] Subramanian S., Zaworotko M. J., *Angew. Chem. Int. Ed.*, 34, 2127-2129, **1995**.

[46] Yaghi O. M., Li H., Groy T. L., *Inorg. Chem.*, 36, 4292-4293, **1997**.

[47] Fu A., Huang X., Li J., Yuen T., Lin C. L., *Chem. Eur. J.*, 8, 2239-2247, **2002**.

[48] Roesky H. w., Andruh M., *Coord. Chem. Rev.*, 236, 91-119, **2003**.

[49] Noro S., Kitagawa S., Kondo M., Seki K., *Angew. Chem. Int. Ed.*, 39, 2081-2084, **2000**.

[50] Noro S., Kitaura R., Kondo M., Kitagawa S., Ishii T., Matsuzaka H, Yamashita M., *J. Am. Chem. Soc.*, 124, 2568-2583, **2002**.

[51] Kitagawa S., Kondo M., *Bull. Chem. Soc. Jpn.*, 71, 1739-1753, **1998**.

[52] Masciocchi N., Cairati P., Carlucci L., Mezza G., Ciani G., Sironi A., *J. Chem. Soc., Dalton Trans.*, 13, 2739-2746, **1996**.

[53] Batten S. R., *Cryst. Eng. Comm.*, 18, 1-7, **1998**.

[54] Blake J. A., Hill S. J., Hubberstey P., Li W.-S., *J. Chem. Soc., Dalton Trans.*, 6, 913-914, **1997**.

[55] Arii H., Funahashi Y., Jitsukawa K., Masuda H., *J. Chem. Soc., Dalton Trans.*, 11, 2115-2116, **2003**.

[56] Rijn J., Reedijk J., Dartmann M., Krebs B., *J. Chem. Soc., Dalton Trans.*, 11, 2579-2593, **1987**.

[57] Emsley J., Reza N. M., Dawes H. M., Hursthouse M. B., *J. Chem. Soc., Dalton Trans.*, 2, 313-316, **1996**.

[58] Sun D., Cao R., Sun Y., Bi W., Li X., Wang Y., Shi Q., Li X., *Inorg. Chem.*, 42, 7512-7518, **2003**.

[59] Tong M.-L., Chen X.-M., Weng Ng S., *Inorg. Chem. Commun.*, 3, 436-441, **2000**.

[60] Woodward J. D., Backov R., Abboud K. A., Ohnuki H., Meisel M. W., Talham D. R., *Polyhedron*, 22, 2821, **2003**.

[61] Tong M.-L., Cai J.-W., Yu X.-L., Chen X.-M., Ng S. W., Mak T. C. W., *Aust. J. Chem.*, 51, 637, **1998**.

[62] Neels A., Alfonso M., González Mantero D., Stoeckli-Evans H, *Chimia*, 57, 619-622, **2003**.

[63] Tong M.-L., Chen X.-M., *Cryst. Eng. Comm.*, 1, 1-5, **2000**.

[64] Hagrman D., Hammond R. P., Haushalter R., Zubieta J., *Chem. Mater.*, 10, 2091-

2100, **1998**.

[65] Lin B.-Z-, Liu P.-D., *Chinese J. Struct. Chem.*, 22, 673, **2003**.

[66] Lah N., Cigic I. K., Leban I., *Inorg. Chem. Commun.*, 6, 1441, **2003**.

[67] Addison A. W., Rao T. N., Reedijk J., Rijn J. van, Verschoor G. C., *J.Chem.Soc.Dalton Trans.*, 7, 1349-1356, **1984**.

[68] Lah N., Cigic I. K., Leban I., *Inorg. Chem. Commun.*, 6, 1441-1444, **2003**.

[69] Du M., Guo Y.-M., Chen S.-T., Bu X.-H., Batten S. R., Ribas J., Kitagawa S., *Inorg. Chem.*, 43, 1287-1293, **2004**.

[70] James S. L., *Chem. Soc. Rev.*, 32, 276-288, **2003**.

[71] Rosseinsky M. J., *Microporous Mesoporous Mater.*, 73, 15-30, **2004**.

[72] Barton T. J., Bull L. M., Klemperer W. G., Loy D. A., McEnaney B., Misono M., Monson P. A., Pez G., Scherer G. W., Vartuli J. C., Yaghi O. M., *Chem Mater.*, 11, 2633-2656, **1999**.

[73] Kitaura R., Seki K., Akiyama G., Kitagawa S., Angew. Chem. Int. Ed., 42, 428-431, 2003.

[74] Kitaura R., Iwahori F., Matsuda R., Kitagawa S., Kubota Y., Takata M., Kobayashi T. C., *Inorg. Chem.*, 43, 6522-6524, **2004**.

[75] Sudik A. C., Millward A. R., Ockwig N. W., Côté A. P., Kim J., Yaghi O. M., *J. Am. Chem. Soc.*, 127, 7110-7118, **2005**.

[76] Bansal R. C., Donnet J. B., Stoeckli F., *Active Carbon*, Marcel Dekker, New York, 119-162, **1988**.

[77] Stoeckli F., *Porosity in Carbons*, Ed. J. Patrick, Arnold, London, 67-92, **1995**.

[78] Stoeckli F., *Russ. Chem. Bull. Int. Ed.*, 50, 2265-2272, **2001**.

[79] Dubinin M. M., *Progress in Surface and Membrane Science*, Ed. D. A. Cadenhead, Academis Press, London, 19, 1-69, **1975**.

[80] Rusanov E. B., Ponomarova V. V., Komarchuk V. V., Stoeckli-Evans H., Fernandez-Ibañez E., Stoeckli F., Sieler J., Domasevitch K. V., *Angew. Chem. Int. Ed.*, 42, 2499-2501, **2003**.

[81] Currit L., *Développement et application d'une méthode généralisée pour l'adsorption solide-liquide et solide-gas*, Thèse de Doctorat, Université de Neuchâtel, Neuchâtel, **1995**.

[82] CRC Handbook of Chemistry and Physics, 71st edition, CRC Press, Inc., **1990-1991**.

[83] Eddaoudi M., Li H., Yaghi O. M., *J. Am. Chem. Soc.*, 122, 1391-1397, **2000**.

[84] Eddaoudi M., Kim J., Rosi N., Vodak D., Wachter J., O'keeffe M., Yaghi O. M., *Science*, 295, 469-472, **2002**.

[85] Fiani E., Perier-Cambry L., Thomas G., *J. Therm. Anal. Cal.*, 60, 557-570, **2000**.

[86] Fletcher A. J., Cussen E. j., Bradshaw D., Rosseinsky M. J., Thomas K. M., *J. Am. Chem. Soc.*, 129, 9750-9759, **2004**.

[87] Kuznetsova A., Mawhinney D. B., Naumenko V., Yates J. T. Jr., Smalley R. E., *Chem. Phys. Lett.*, 321, 292-296, **2000**.

[88] Reid C. R., Thomas K. M., *J. Phys. Chem. B*, 105, 10619-10629, **2001**.

[89] Wood G.O., *Carbon*, 39, 343-356, **2001**.

[90] Hugi-Cleary D., Wermeille S., Stoeckli F., *Chimia*, 57, 611-615, **2003**.

[91] Gregg S. J., Sing K. S. W., *"Adsorption, Surface Area and Porosity"*, second edition, Academic Press Inc., London (UK), **1982**.

3. Complexes with 4,4'-Dipyridyl-N,N'-dioxide

3. Complexes with 4,4'-Dipyridyl-N,N'-dioxide

3.1 4,4′-Dipyridyl-N,N′-dioxide as Bridging Ligand

It has been found that 4,4'-Dipyridyl-N,N′-dioxide (dpdo) (Figure 3.1) is also an excellent rigid bridging ligand, and that it can coordinate to a large number of transition metals [1-10].

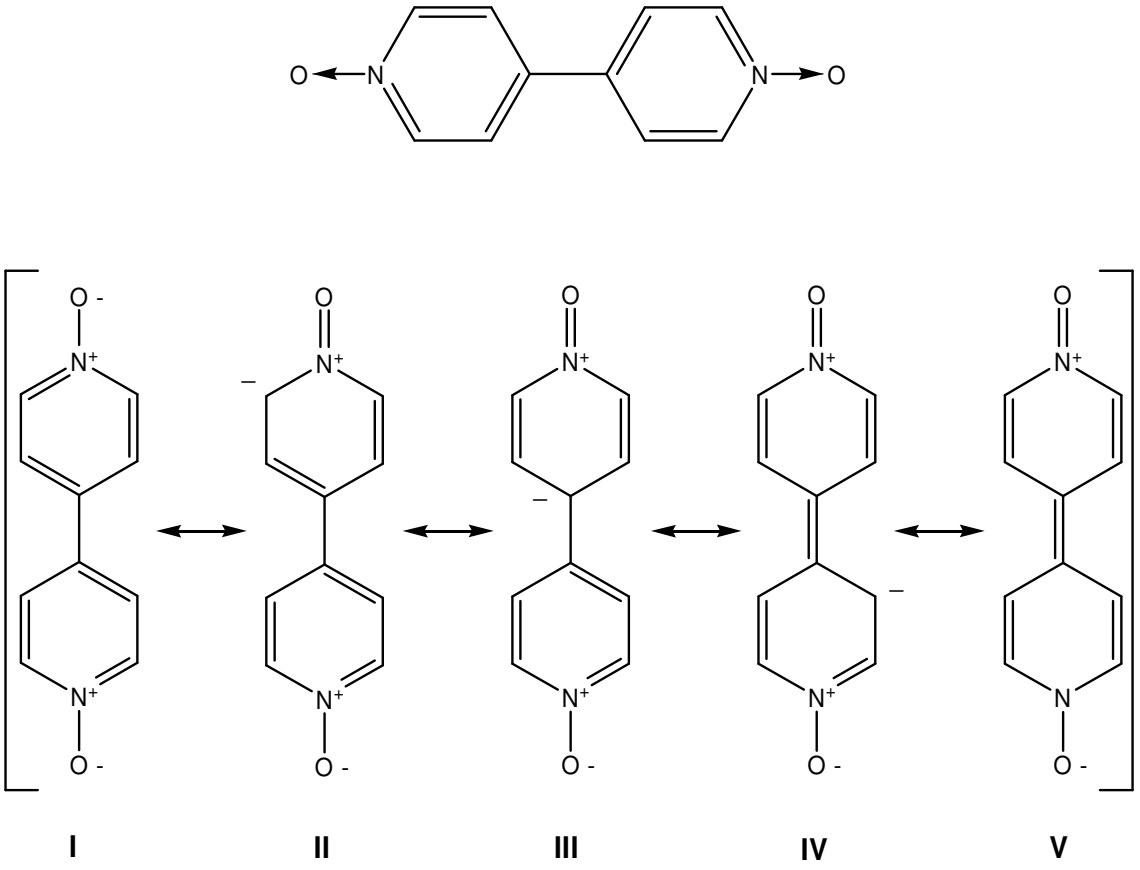

Figure 3.1 Resonance of dpdo ligand

In contrast with 4,4'-bpy, the potentialities of dpdo have not been extensively exploited. Its aromatic rings can also be involved in π–π aromatic interactions and it is a good hydrogen bond acceptor [11]. Another interesting aspect of this ligand is that it can form coordination bonds with different geometries, either *cis* or *trans* (Scheme 3.1).

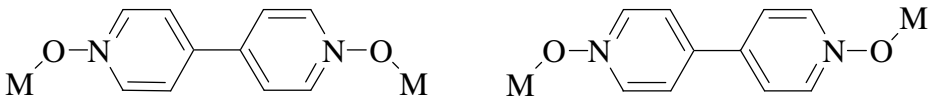

cis *trans*

Scheme 3.1 *cis* and *trans* coordination modes

3.2 Complexes with 4,4′-Dipyridyl-N,N′-dioxide

3.2.1 {[Cu (H_2O) ($dpdo)_2$] (S_2O_6) (H_2O)}$_n$: C15

This compound was synthesized by diffusion of ethanolic solutions of the starting materials, CuS_2O_6 and dpdo (1:2) (Reaction 3.1). This compound crystallized in the monoclinic crystal system, space group P2/n, with a = 9.7716(9) Å, b = 9.8378(7) Å, c = 11.9907(12) Å, β = 90.770(8), Z = 2, V = 1152.57(18) Å^3, R1 = 0.0271, wR2 = 0.0659. The symmetry of the complex is C_2, the copper atom having site symmetry 2.

$$CuS_2O_6 + 2\ dpdo \xrightarrow{EtOH} \{[Cu(H_2O)(dpdo)_2](S_2O_6)(H_2O)\}_n$$

Reaction 3.1

The Cu^{II} coordination sphere is formed by four dpdo ligands and one water molecule, which occupy equatorial and axial positions, respectively (Figure 3.2). The water comes either from the ethanol which was analytical grade or the atmosphere. The dpdo ligands adopt a *trans* geometry to coordinate to the metal centres. One water molecule and a dithionate anion are co-crystallised per molecule of complex.

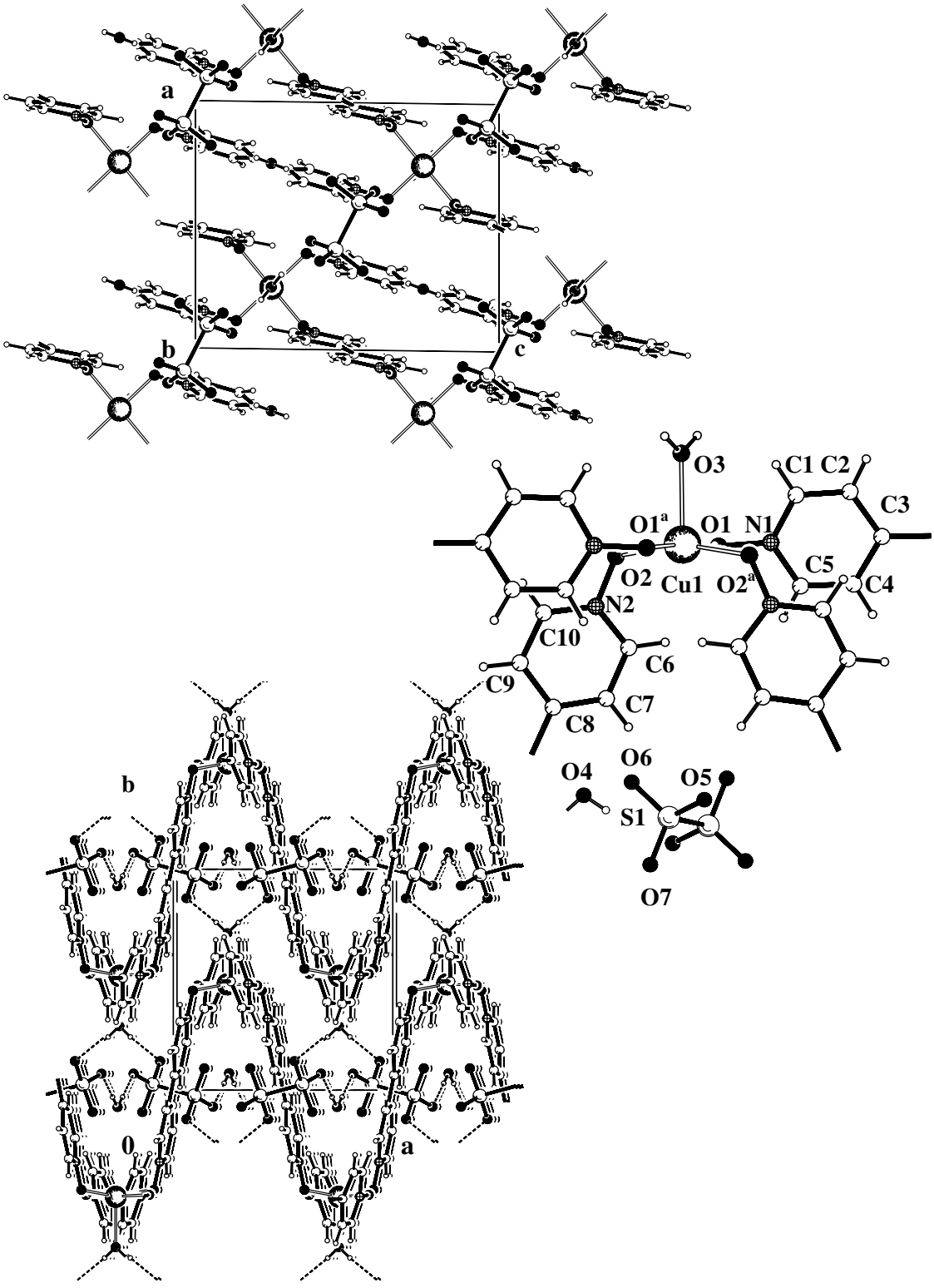

Figure 3.2 Crystal packing diagrams and Cu^{II} coordination sphere for complex **C15**; [a]) 1/2-x, y, 1/2-z

The coordination around the copper is intermediate between trigonal bipyramidal and square pyramidal geometry, and is best described as distorted square pyramidal [12], based on the angular structural parameter τ of 0.22 where β = O1-Cu1-O1[a] = 175.96(7)° and α = O2-Cu1-O2[a] = 163.03(6)° (Table 3.1). The coordination bond distances Cu···O for dpdo are comparable with those described in the literature [2,13].

Table 3.1 Selected bond distances (Å) and bond angles (°) for **C15** (P2/n)

Bond	Length (Å)	Angle	Angle (°)
Cu1-O1	1.9178(14)	O1-Cu1-O2	85.46(6)
Cu1-O2	2.0045(14)	O1-Cu1-O3	92.02(5)
Cu1-O3	2.262(2)	O1-Cu1-O1[a]	175.96(7)
[a]) 1/2-x,y,1/2-z		O1-Cu1-O2[a]	93.95(6)
		O2-Cu1-O3	98.48(4)
		O2-Cu1-O2[a]	163.03(6)

The dpdo ligands connected to the metal centres form a sinusoidal wave-like structure. In the crystal hydrogen bonded water and dithionate chains are threaded through the sinusoidal polymer chain (Figure 3.2). The dithionate anions are also involved in hydrogen bonds with the water molecule coordinated to the metal centre (Table 3.2, Figure 3.2).

Table 3.2 Hydrogen bonds for **C15** (P2/n)

Hydrogen Bond	D–H (Å)	H···A (Å)	D···A (Å)	D–H···A (°)	Symmetry operation
O3–H11···O6	0.79(3)	2.07(4)	2.8558(19)	174(4)	
O4–H12···O5	0.77(3)	2.14(3)	2.901(2)	172(3)	
C1–H1···O5	0.95	2.60	3.217(3)	123	
C1–H1···O6	0.95	2.50	3.344(2)	147	[b]) x,-1+y,z
C4–H4···O4[b]	0.95	2.39	3.257(3)	152	[c]) -x,1-y,1-z
C5–H5···O7[b]	0.95	2.19	3.060(3)	151	
C6–H6···O7[b]	0.95	2.35	3.129(3)	139	
C10–H10···O2[c]	0.95	2.38	3.215(2)	147	

3.2.2 {[Co (dpdo)$_3$] (S_2O_6) (C_2H_5OH)$_7$}$_n$: C16

The diffusion of an ethanolic solution of dpdo into an ethanolic solution of CoS_2O_6 produced orange block-like crystals of **C16** (Reaction 3.2, Figure 3.3).

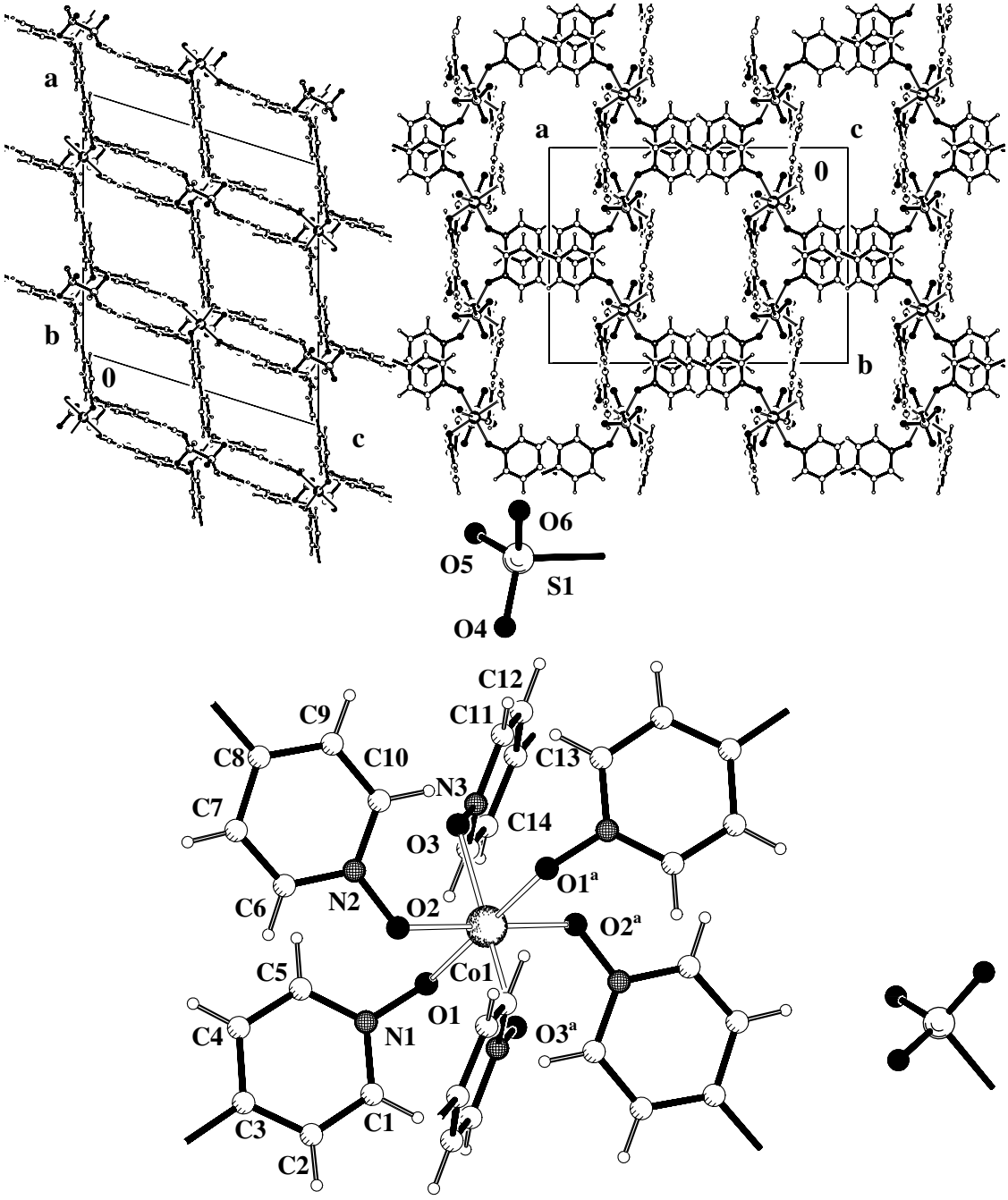

Figure 3.3 Crystal packing diagrams and Co^{II} coordination sphere for complex **C16**; [a]) 1/2-x, 1/2-y, 1-z

$$CoS_2O_6 + 3\ dpdo \xrightarrow{EtOH} \{[Co(dpdo)_3](S_2O_6)(EtOH)_7\}_n$$

Reaction 3.2

This compound crystallized in the monoclinic crystal system, space group C2/c, with a = 20.681(4) Å, b = 14.1352(17) Å, c = 19.564(4) Å, β = 107.482(15), Z = 4, V = 5455.0(17) Å^3, R1 = 0.0561, wR2 = 0.1200. The complex is centrosymmetric C_i, the cobalt atom having site symmetry $\bar{1}$.

The coordination around the Co^{II} centres is octahedral. The coordination positions are occupied by dpdo ligands resulting in the formation of a 3D network (Figure 3.3). The coordination bond distances, Co···O, for the dpdo ligand, are comparable with those described in the literature [1-2, 14-15] (Table 3.3). The dpdo ligands coordinated to the metal centres display both *cis* and *trans* coordination modes; four *cis* and two *trans*.

Table 3.3 Selected bond distances (Å) and bond angles (°) for **C16** (C2/c)

Bond	**Length (Å)**	**Angle**	**Angle (°)**
Co1-O1	2.065(3)	O1-Co1-O2	91.78(10)
Co1-O2	2.088(3)	O1-Co1-O3	91.82(10)
Co1-O3	2.073(2)	O1-Co1-O1[a]	180.00
[a]) 1/2-x,1/2-y,1-z		O1-Co1-O2[a]	88.22(10)
		O1-Co1-O3[a]	88.18(10)
		O2-Co1-O3	94.75(10)
		O2-Co1-O3[a]	85.25(10)

The TG curve shows the loss of solvent molecules in two steps until 190 °C followed by the loss of a dpdo and a SO_2 molecule and finally decomposition at 300 °C (Figure 3.4).

The 3D coordination polymer has pores of dimensions ca. 8.3×8.5 Å^2 along the *c*-axis, and 6.0×0.8 Å^2 and ca. 6.7×4.8 Å^2 along the *b*-axis. The pores were initially filled with solvent molecules (Figure 3.3) and the free pore volume calculated was 50%.

The hydrogen bonds formed between the dpdo ligands and the anions are presented in Table 3.4.

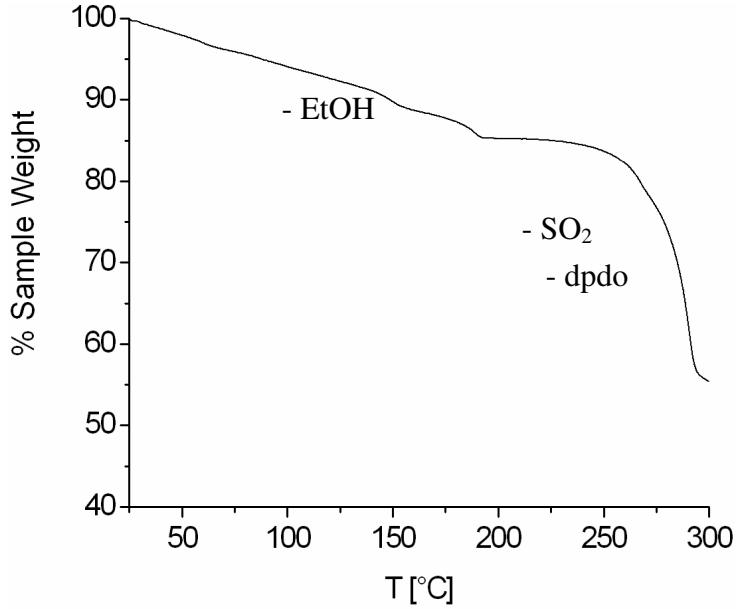

Figure 3.4 TG curve for **C16**

Table 3.4 Hydrogen bonds for **C16** (C2/c)

Hydrogen Bond	D–H (Å)	H···A (Å)	D···A (Å)	D–H···A (°)	Symmetry operation
C1–H1···O4[a]	0.93	2.28	3.087(5)	144	
C7–H7···O5[b]	0.93	2.52	3.444(6)	173	
C10–H10···O3	0.93	2.49	2.951(5)	111	[a]) 1/2-x,1/2-y,1-z
C10–H10···O1[a]	0.93	2.55	3.269(4)	135	[b]) 1/2-x,1/2+y,3/2-z
C11–H11···O4	0.93	2.58	3.494(7)	167	
C15–H15···O1	0.93	2.27	3.066(5)	143	

3.2.3 $\{[Ni(dpdo)_3](S_2O_6)(C_2H_5OH)_7\}_n$: C17

Compound **C17** was synthesized in a similar way to **C16** but using NiS_2O_6 as the metal salt (Reaction 3.3). The orange needle-like crystals were obtained, having crystallized in the monoclinic crystal system, space group C2/c, with a = 20.828(5) Å, b = 13.499(4) Å, c = 20.020(5) Å, β = 106.179(19), Z = 4, V = 5406(3) $Å^3$, R1 = 0.1496,

wR2 = 0.3140. The high R1 value is due to the poor quality of the crystal. The complex is centrosymmetric C_i, the cobalt atom having site symmetry $\bar{1}$.

$$NiS_2O_6 + 3\ dpdo \xrightarrow{EtOH} \{[Ni(dpdo)_3](S_2O_6)(EtOH)_7\}_n$$

Reaction 3.3

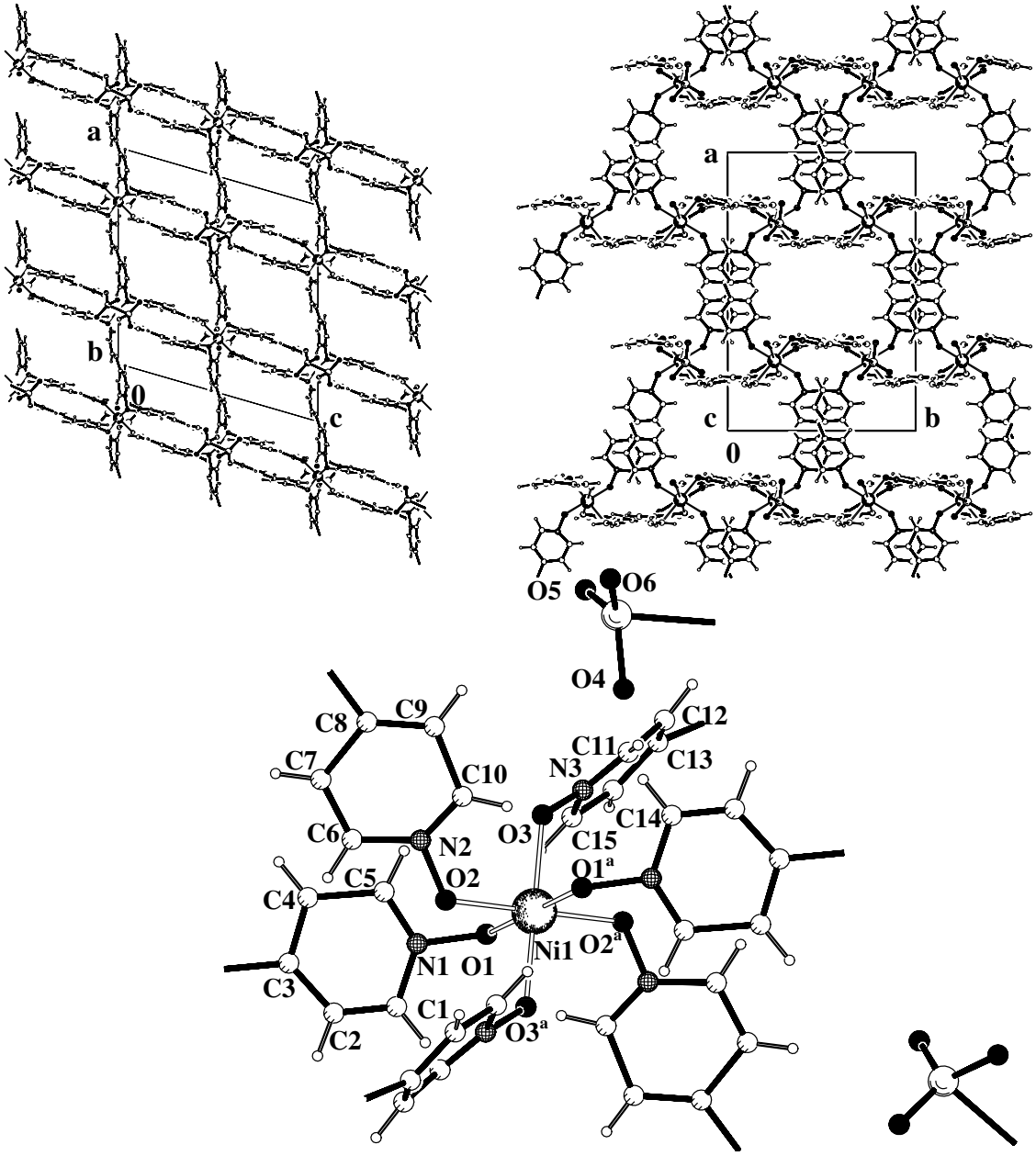

Figure 3.5 Crystal packing diagrams and Ni^{II} coordination sphere for complex **C17**; [a]) 1/2-x, 1/2-y, 1-z

The coordination around the Ni^{II} centre is octahedral and all the coordination positions are occupied by dpdo ligands (Figure 3.5). Dithionate anions and solvent molecules have cocrystalized in the structure. The Ni···O (dpdo) distances (Table 3.5) are comparable with those reported in the literature [1]. For every Ni^{II} ion, four dpdo ligands present a *cis* coordination mode and the other two a *trans* coordination mode.

Table 3.5 Selected bond distances (Å) and bond angles (°) for **C17** (C2/c)

Bond	**Length (Å)**	**Angle**	**Angle (°)**
Ni1-O1	2.107(14)	O1-Ni1-O2	91.6(5)
Ni1-O2	2.038(11)	O1-Ni1-O3	92.2(5)
Ni1-O3	2.009(13)	O1-Ni1-O1[a]	180.00
[a]) 1/2-x,1/2-y,1-z		O1-Ni1-O2[a]	88.4(5)
		O1-Ni1-O3[a]	87.8(5)
		O2-Ni1-O3	94.9(5)
		O2-Ni1-O3[a]	85.1(5)

The TG curve shows the loss of solvent molecules until 120 °C followed by the loss of SO_2 molecules and finally decomposition (Figure 3.6).

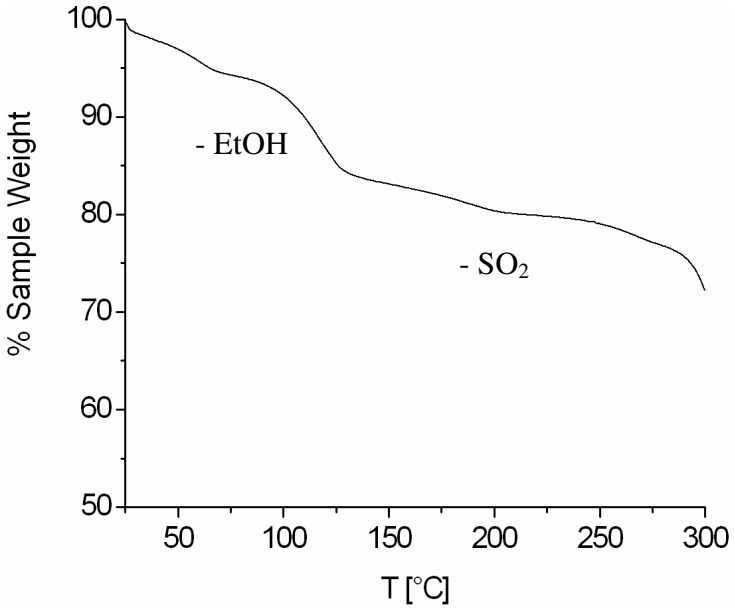

Figure 3.6 TG curve for **C17**

Compounds **C17** and **C16** are isostructural and they have pores with similar sizes and shapes. In **C17** the channels, with dimension of ca. 8.3×8.5 $Å^2$ along the *c*-axis, and ca. 6.0×0.8 $Å^2$ and 6.7×4.8 $Å^2$ along the *b*-axis, were initially filled with solvent molecules (Figure 3.5). The free pore volume calculated is 51%.

The crystalline cohesion is assured by non-classical hydrogen bonds between the dpdo ligands and the dithionate anions (Table 3.6).

Table 3.6 Hydrogen bonds for **C17** (C2/c)

Hydrogen Bond	D–H (Å)	H···A (Å)	D···A (Å)	D–H···A (°)	Symmetry operation
C1–H1···O4[a]	0.93	1.90	2.75(4)	150	
C2–H2···O5[b]	0.93	2.55	3.42(4)	157	[a]) 1/2-x,1/2-y,1-z
C7–H7···O5[c]	0.93	2.56	3.47(4)	167	[b]) x,1+y,z
C10–H10···O1[a]	0.93	2.24	3.04(2)	144	[c]) 1/2-x,1/2+y,3/2-z
C15–H15···O1	0.93	2.26	3.06(3)	143	

The XRPD studies on compounds **C15**, **C16** and **C17** samples demonstrate that these compounds loose the solvent molecules when exposed to the air and their structures collapse, hence they are not suitable for adsorption experiments.

3.2.4 {[Co (dpdo) (H_2O)$_5$] (SO_4) (H_2O)$_2$}: C18

When the synthesis of **C16** was performed with CoS_2O_6 in aqueous solution (Reaction 3.4), a mononuclear compound was formed, which has been denoted as **C18**.

$$CoS_2O_6 + \text{dpdo} \xrightarrow{EtOH/H_2O} \{[Co(H_2O)_5(dpdo)](SO_4)(H_2O)_2\} + SO_2$$

Reaction 3.4

The dithionate anions decompose in the presence of water giving sulphate anions and SO_2. Crystals of **C18** (Figure 3.7) can also be obtained directly by using the metal sulphate in ethanolic or aqueous solution. Orange needle-like crystals were obtained after slow evaporation of the solvent. This compound crystallized in the monoclinic crystal

system, space group $P2_1/n$, with a = 7.137(1) Å, b = 25.432(2) Å, c = 10.226(1) Å, β = 92.59(1), Z = 4, V = 1854.2(3) $Å^3$, R1 = 0.0332, wR2 = 0.0782.

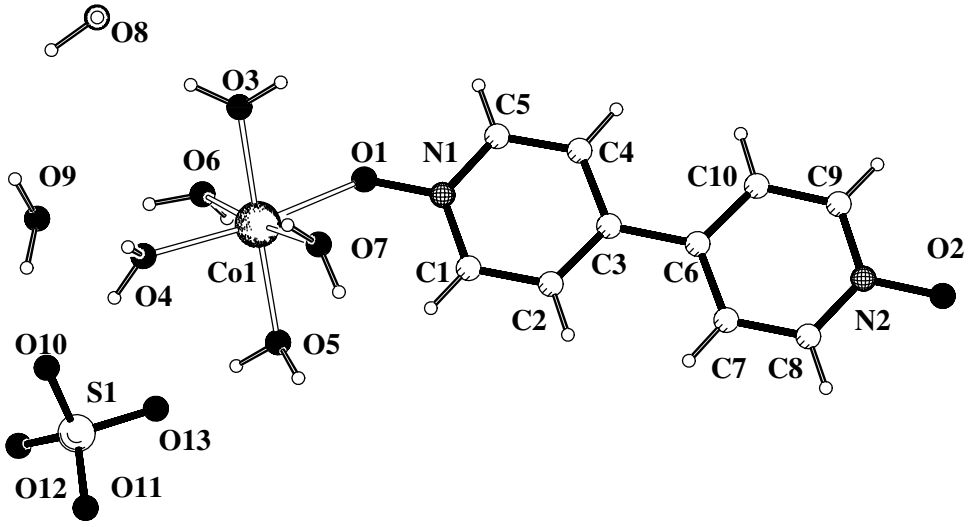

Figure 3.7 Co^{II} coordination sphere for complex **C18**

The octahedral coordination sphere of the Co^{II} ions is defined by five water molecules and one dpdo ligand (Table 3.7).

Table 3.7 Selected bond distances (Å) and bond angles (°) for **C18** ($P2_1/n$)

Bond	**Length (Å)**	**Angle**	**Angle (°)**
Co1-O1	2.119(2)	O1-Co1-O3	87.23(8)
Co1-O3	2.053(2)	O1-Co1-O4	171.74(8)
Co1-O4	2.092(2)	O1-Co1-O5	92.59(8)
Co1-O5	2.072(2)	O1-Co1-O6	83.14(7)
Co1-O6	2.080(2)	O1-Co1-O7	93.21(7)
Co1-O7	2.089(2)	O3-Co1-O4	88.75(8)
Angle	**Angle (°)**	O3-Co1-O5	178.75(7)
O4-Co1-O7	93.69(8)	O3-Co1-O6	90.54(7)
O5-Co1-O6	90.67(7)	O3-Co1-O7	85.97(7)
O5-Co1-O7	92.80(7)	O4-Co1-O5	91.59(8)
O6-Co1-O7	175.08(7)	O4-Co1-O6	89.70(8)

The dpdo ligand coordinated to the metal ion has the pyridine rings very slightly twisted, with a dihedral angle (N1 C1 C2 C3 C4 C5 and N2 C6 C7 C8 C9 C10) of

2.13(12)°. Compound **C18** is isomorph with a mononuclear compound of Fe^{II} reported in the literature [16].

The mononuclear units are connected via hydrogen bonds formed by the dpdo ligands, the SO_4^{2-} anions and the water molecules (Table 3.8). As a consequence of these weak interactions, a 3D structure is obtained (Figure 3.8). Furthermore, adjacent dpdo ligands are involved in weak π–π stacking interactions (distance ca. 3.72 Å).

Table 3.8 Hydrogen bonds for **C18** ($P2_1/n$)

Hydrogen Bond	D–H (Å)	H···A (Å)	D···A (Å)	D–H···A (°)	Symmetry operation
O3–H11···O8	0.90(2)	1.90(2)	2.781(3)	167(3)	
O3–H12···O2[a]	0.90(3)	1.82(2)	2.715(2)	175(3)	
O4–H13···O10	0.87(3)	1.95(3)	2.792(3)	161(3)	
O4–H14···O12[b]	0.88(2)	1.87(2)	2.750(3)	176(2)	
O5–H15···O12[c]	0.87(2)	1.83(2)	2.688(3)	169(2)	
O5–H16···O13	0.91(3)	1.76(3)	2.668(2)	178(3)	[a]) 1-x,-y,1-z
O6–H17···O9	0.89(2)	1.87(2)	2.754(3)	175(2)	[b]) -1+x,y,z
O6–H18···O2[d]	0.88(3)	1.82(2)	2.689(2)	168(3)	[c]) -1/2+x,-1/2-y, 1/2+z
O7–H19···O10[c]	0.89(2)	1.79(2)	2.682(3)	174(3)	[d]) 2-x,-y,1-z
O7–H20···O13[b]	0.90(3)	1.76(3)	2.661(2)	172(2)	[e]) -1/2+x,-1/2-y,1/2+z
O8–H21···O9[b]	0.96	1.86	2.794(3)	164	[f]) 1-x,-y,-z
O8–H22···O11[e]	0.94	1.98	2.842(3)	152	[g]) x,y,-1+z
O9–H23···O11[e]	0.92	1.88	2.790(3)	175	[h]) x,y,1+z
O9–H24···O10	0.92	2.01	2.887(3)	159	
C2–H2···O11[c]	0.93	2.55	3.216(3)	129	
C4–H4···O8[f]	0.93	2.59	3.489(3)	163	
C5–H5···O2[g]	0.93	2.32	3.250(3)	176	
C8–H8···O1[h]	0.93	2.34	3.269(3)	175	
C9–H9···O7[a]	0.93	2.42	3.241(3)	147	

The presence of water during the synthesis has a direct influence not only on the decomposition of the dithionate anions but also on the loss of dimensionality since the water molecules are involved in the coordination sphere of the metal ions.

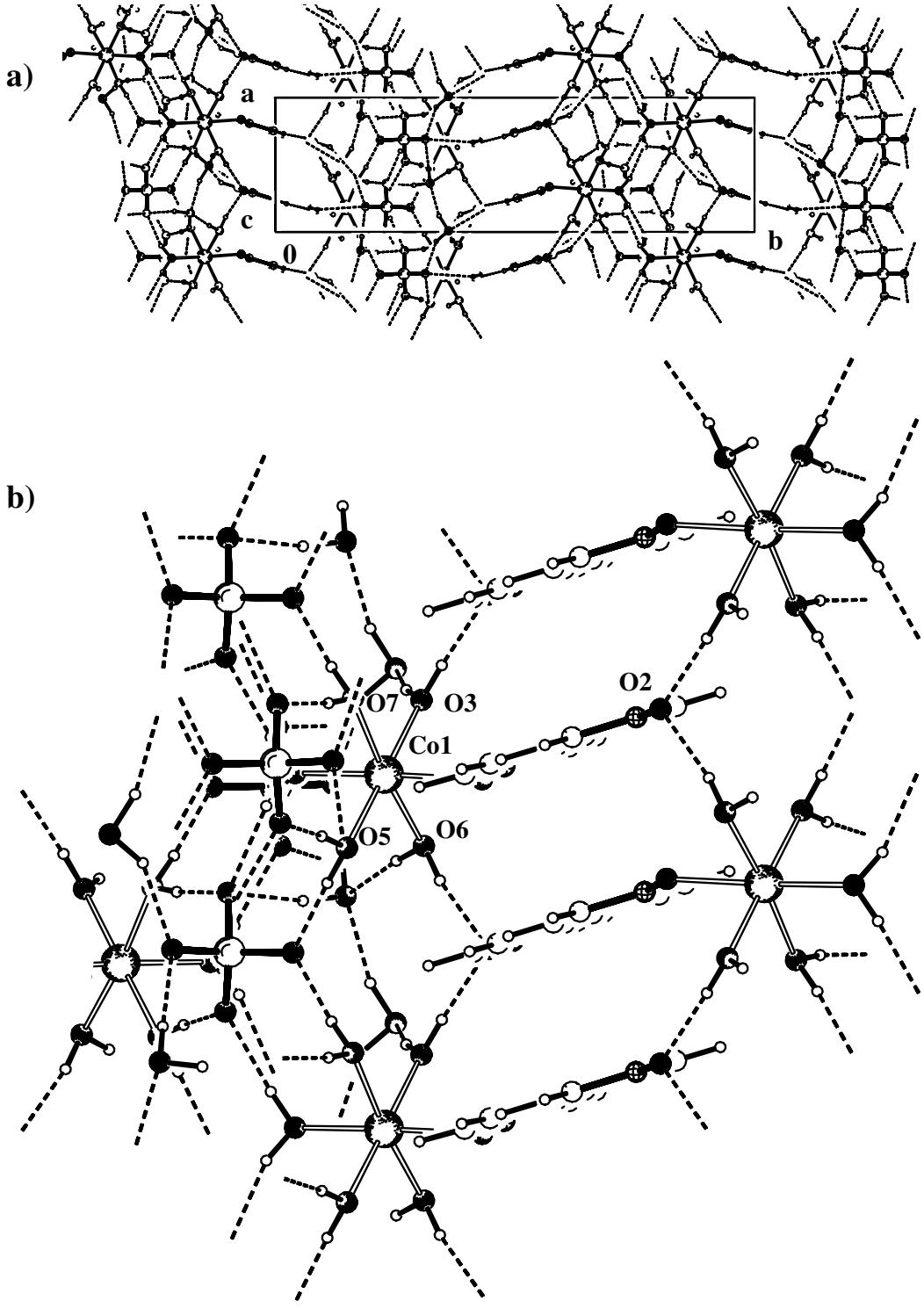

Figure 3.8 a) A crystal packing diagram for complex **C18; b)** details of the hydrogen bonding (dashed lines).

3.2.5 {[Ni (dpdo) (H_2O)$_5$] (SO_4) (H_2O)$_2$}: C19

As stated for the Co^{II} complex, **C16**, when the synthesis of **C17** was performed with NiS_2O_6 in aqueous solution (Reaction 3.5), the result is a mononuclear compound, which has been denoted as **C19** (Figure 3.9).

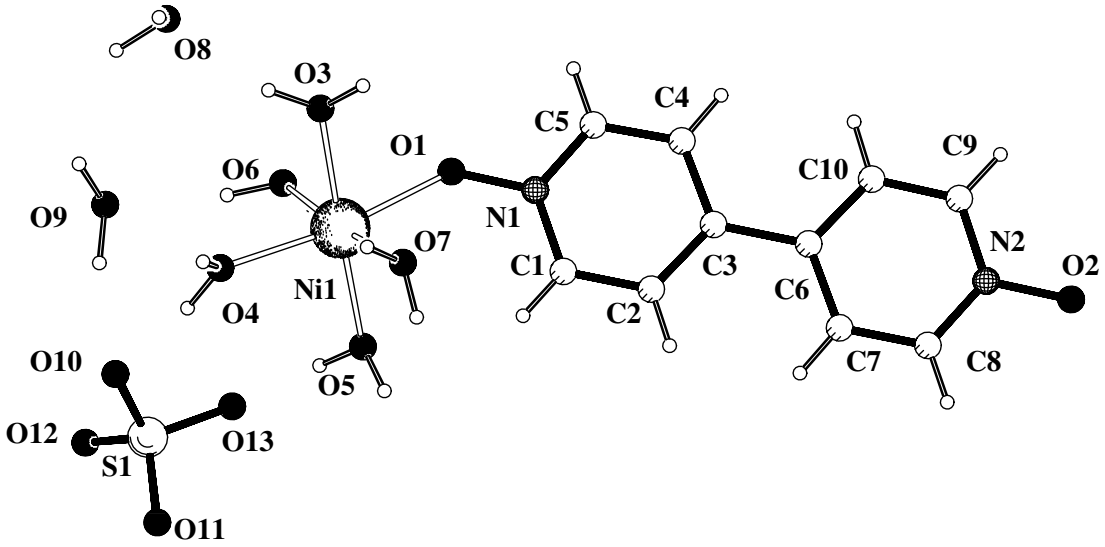

Figure 3.9 Ni^{II} coordination sphere for complex **C19**

$$NiS_2O_6 + dpdo \xrightarrow{EtOH/H_2O} \{[Ni(H_2O)_5(dpdo)](SO_4)(H_2O)_2\} + SO_2$$

Reaction 3.5

Crystals of **C19** can also be obtained directly by using the metal sulphate in either an ethanolic or an aqueous solution. Pale green needle-like crystals were obtained after several days. This compound crystallized in the monoclinic crystal system, space group $P2_1/n$, with a = 7.1380(8) Å, b = 25.244(3) Å, c = 10.211(1) Å, β = 92.173(9), Z = 4, V = 1838.5(4) $Å^3$, R1 = 0.0314, wR2 = 0.0861.

Complexes **C18**, **C19** and the Fe^{II} mononuclear complex already cited [16] are isomorphous. The Ni^{II} ions are coordinated by five water molecules and one dpdo ligand in an axial position, resulting in an octahedral environment (Table 3.9). In the dpdo

ligand coordinated to the metal ion the pyridine rings are twisted with respect to one another, with a dihedral angle between rings (N1 C1 C2 C3 C4 C5) and (N2 C6 C7 C8 C9 C10) of 2.15(12)°. There are two water molecules of crystallization per molecule of complex.

Table 3.9 Selected bond distances (Å) and bond angles (°) for **C19** ($P2_1/n$)

Bond	**Length (Å)**	**Angle**	**Angle (°)**
Ni1-O1	2.081(2)	O1-Ni1-O3	85.54(7)
Ni1-O3	2.040(2)	O1-Ni1-O4	171.35(7)
Ni1-O4	2.056(2)	O1-Ni1-O5	93.09(7)
Ni1-O5	2.048(2)	O1-Ni1-O6	82.63(7)
Ni1-O6	2.043(2)	O1-Ni1-O7	93.91(7)
Ni1-O7	2.045(2)	O3-Ni1-O4	89.44(8)
Angle	**Angle (°)**	O3-Ni1-O5	178.63(7)
O4-Ni1-O7	92.85(8)	O3-Ni1-O6	89.54(6)
O5-Ni1-O6	90.38(6)	O3-Ni1-O7	86.82(6)
O5-Ni1-O7	93.18(6)	O4-Ni1-O5	91.93(8)
O6-Ni1-O7	175.16(7)	O4-Ni1-O6	90.30(8)

The neighbouring dpdo ligands interact weakly *via* π-π stacking interactions resulting in the formation of a ladder-like motif. These ladders are extended into a 2D sheet by hydrogen bonds. Finally, SO_4^{2-} anions and crystal lattice water molecules link these sheets into a 3D network through hydrogen bonds (Figure 3.10, Table 3.10). The hydrogen bonding being identical to that for compound **C18**, cf. Figure 3.8b.

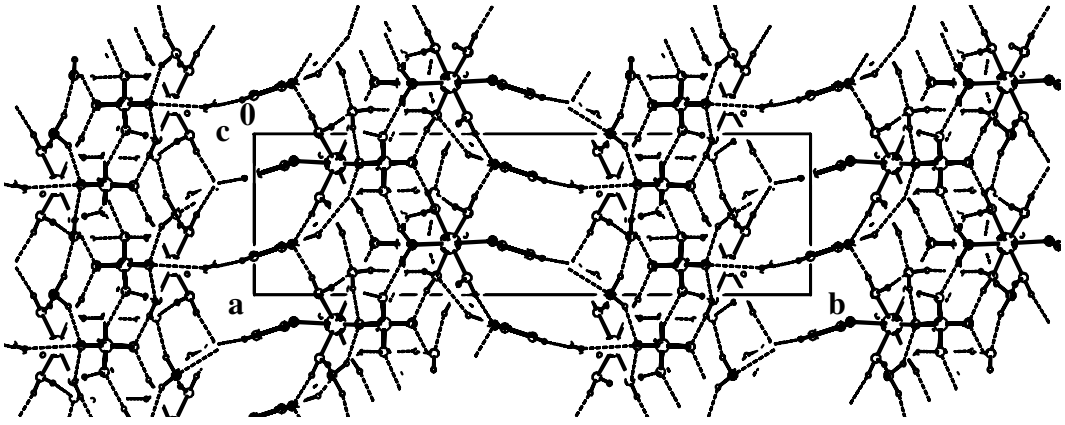

Figure 3.10 A crystal packing diagram for complex **C19**

Table 3.10 Hydrogen bonds for **C19** ($P2_1/n$)

Hydrogen Bond	D–H (Å)	H···A (Å)	D···A (Å)	D–H···A (°)	Symmetry operation
O3–H11···O8	0.90(2)	1.92(2)	2.786(3)	160(2)	
O3–H12···O2[a]	0.92(2)	1.81(2)	2.720(2)	173(3)	
O4–H13···O10	0.88(3)	1.93(3)	2.789(3)	165(3)	
O4–H14···O12[b]	0.88(2)	1.86(2)	2.745(3)	177(2)	
O5–H15···O12[c]	0.88(2)	1.82(2)	2.696(3)	172(2)	
O5–H16···O13	0.90(2)	1.78(3)	2.677(2)	177(3)	[a]) 1-x,-y,1-z
O6–H17···O9	0.87(2)	1.90(2)	2.764(3)	170(2)	[b]) -1+x,y,z
O6–H18···O2[d]	0.90(2)	1.80(2)	2.689(2)	167(2)	[c]) -1/2+x, -1/2-y, 1/2+z
O7–H19···O10[c]	0.87(2)	1.84(2)	2.692(3)	164(3)	[d]) 2-x,-y,1-z
O7–H20···O13[b]	0.92(2)	1.75(2)	2.658(2)	168(2)	[e]) -1/2+x,-1/2-y,-1/2+z
O8–H21···O9[b]	0.93	1.91	2.803(3)	157	[f]) 1-x,-y,-z
O8–H22···O11[e]	0.92	2.00	2.844(3)	149	[g]) x,y,-1+z
O9–H23···O11[e]	0.92	1.86	2.784(3)	168	[h]) x,y,1+z
O9–H24···O10	0.95	1.92	2.860(3)	165	[i]) 1-x,-y,1-z
C1–H1···O5	0.92	2.56	3.305(3)	136	
C2–H2···O11[c]	0.93	2.56	3.228(3)	128	
C4–H4···O8[f]	0.93	2.59	3.494(3)	162	
C5–H5···O2[g]	0.93	2.32	3.250(3)	175	
C8–H8···O1[h]	0.92	2.31	3.246(3)	174	
C9–H9···O7[i]	0.93	2.43	3.247(3)	145	

3.3 References

[92] Ma B.-Q., Gao S., Sun H.-L., Xu G.-X., *J. Chem.Soc., Dalton Trans.*, 130-133, **2001**.

[93] Nedelcu A., Zak Z., Madalan A. M., Pinkas J., Andruh M., *Polyhedron*, 22, 789-794, **2003**.

[94] Ma B.-Q., Sun H.-L., Gao S., *Chem. Commun.*, 2164-2165, **2003**.

[95] Ma B.-Q., Sun H.-L., Gao S., *Inorg. Chem.*, 44(4), 837-839, **2005**.

[96] Ghosh A. K., Ghoshal D., Zangrando E., Ribas J., Chaudhuri N. R., *Inorg. Chem.*, 44(11), 3880-3889, **2005**.

[97] Bruda S., Andruh M., Roesky H. W., Journaux Y., Noltemeyer M., Rivière E., *Inorg. Chem. Commun.*, 4, 111-114, **2001**.

[98] Long D.-L., Blake A. J., Champness N. R., Schröder M., *Chem. Commun.*, 2273-

2274, **2000**.

[99] Hill R. J., Long D.-L., Turvey M. S., ,Blake A. J., Champness N. R., Hubberstey P.,Wilson C., Schröder M., *Chem. Commun.*, 1792-1739, **2004**.

[100] Long D.-L., Blake A. J., Champness N. R., Schröder M., *Chem. Commun.*, 1369-1370, **2000**.

[101] Long D.-L., Blake A. J., Champness N. R., Wilson C., Schröder M., *Chem. Eur. J.*, 8, 2026-2033, **2000**.

[102] Roesky H. W., Andruh M., *Coord. Chem. Rev.*, 236, 91-119, **2003**.

[103] Addison A. W., Rao T. N., Reedijk J., Rijn J. van, Verschoor G. C., *J. Chem. Soc. Dalton Trans.*, 7, 1349-1356, **1984**.

[104] Ma B.-Q., Sun H.-L., Gao S., Xu G.-X., *Inorg. Chem.*, 40, 6247-6253, **2001**.

[105] Plater M. J., Foreman M. R. St. J., Slawin A. M. Z., *Inorg. Chim. Acta*, 303, 132-136, **2000**.

[106] Blake A. J., Champness N. R., Khlobystov A. N., Long D.-L., Wilson C., Schröder M., *Chem. Commun.*, 2258-2259, **2001**.

[107] Ma B.-Q., Gao S., Sun H.-L., Xu G.-X., *Cryst. Eng. Comm.*, 35, 1-5, **2001**.

4. Synthesis of Some Aromatic Diimides: A Green Chemistry Approach

4. Synthesis of Some Aromatic Diimides: A Green Chemistry Approach

4.1 Aromatic Diimides

The development of sustainable energy production is a topic of growing importance in view of the limited supply of fossil fuels, and the financial and environmental costs of the alternatives. One possible sustainable energy sources would be the sun, which makes the development of photovoltaic devices extremely interesting. For organic solar cells good electron donors are known whereas the development of good acceptors has progressed rather less. A class of highly interesting electron acceptors are aromatic diimides (i.e. *N*-alkyl-substituted perylene diimide derivatives) [1, 2].

Diimides of 1,2,4,5-benzenetetracarboxylic acid (abbreviated herein as pyromellitdiimides) constitute a group of heteroaromatic compounds of ever increasing importance in organic, medicinal, physical, supramolecular and materials chemistry [3-6]. Molecular structures composed of covalently linked electron donor and acceptor moieties have received considerable attention and a large number of examples incorporating pyromellitdiimide moieties as the electron acceptor have been reported [7-11] (Figure 4.1).

On the other hand, the conventional organic synthesis of these aromatic diimides involves the utilization of organic solvents, high temperatures and long reaction times [12-14]. In this chapter, an easier and environmental-friendly manner to synthesize this kind of compound is described.

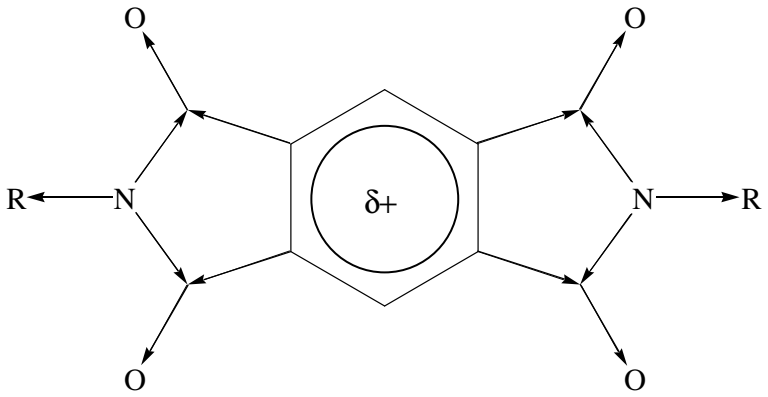

Figure 4.1 Main directions of polarisation for a pyromellitdiimide [12]

4.2 Green Method to Synthesize Pyromellitdiimides

The synthesis of three pyromellitdiimides, bis(pyridyl)phenyldiimide, bis(pyrazyl)phenyldiimide and bis(2-Chloro-pyridyl)phenyldiimide (**pyIMID**, **pyzIMID** and **ClpyIMID**, respectively), was carried out *via* a solvent-free two step synthesis described in Scheme 4.1.

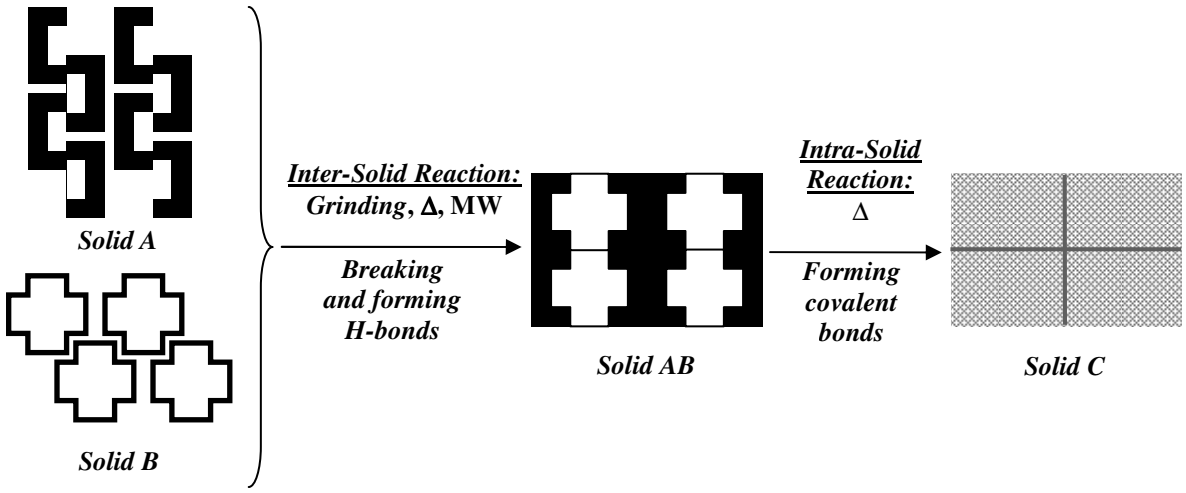

Scheme 4.1 Solvent-free synthesis steps

As Solid A three differents amines, 4-aminopyridine "Apy", 2-aminopyrazine "Apyz" and 4-amino-2-chloropyridine "ClApy", were used. As Solid B benzene-1,2,4,5-tetracarboxylic acid (H_4-BCTA) was used in all the cases (Scheme 4.2).

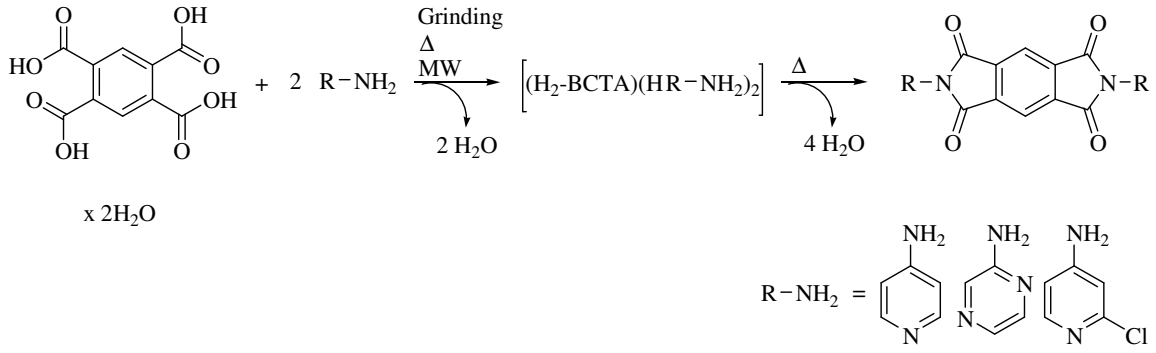

Scheme 4.2 Synthesis of the pyromellitdiimides **pyIMID**, **pyzIMID** and **ClpyIMID**

The first step is the formation of an intermediate compound [15-17], formed after grinding both starting materials in the correct ratio until a homogeneous mixture was obtained. XRPD analyses demonstrated that the process occurs even at room temperature but the transformation is very slow and diffractograms showed a mixture of products. This process can be accelerated by heating or using Microwave irradiation. The XRPD diffractograms then showed the formation of organic salts with the starting materials connected via strong hydrogen bonds.

The second step involves the condensation of the starting materials resulting in the formation of the pyromellitdiimides already cited. This solid state transformation was followed by thermogravimetry (Figure 4.2). The samples obtained were analysed by XRPD without any purification or recrystallization. The quality of all the powder diffractograms, for the intermediate and final products, allowed structure solution and Rietveld refinement.

The thermogravimetric curves, Figure 4.2, showed two weight loss steps for each reaction mixture. The first step corresponds to the loss of water molecules of crystallization of H_4-BCTA and surface humidity of the samples. Organic salts were formed at 120 °C [(H_2-BCTA)(H-Apyz)$_2$], at 180 °C [(H_2-BCTA)(H-Apy)$_2$] and [(H_2-BCTA)(H-ClApy)$_2$]. These compounds were also obtained by exposing the respective mixtures of starting materials to MW irradiation (600 W, 90 min). After that, the intermediate products loose four water molecules to form the corresponding diimides.

Pyromellitdiimides were formed at 190 °C for **pyzIMID**, 260 °C for **pyIMID** and 220 °C for **ClpyIMID**.

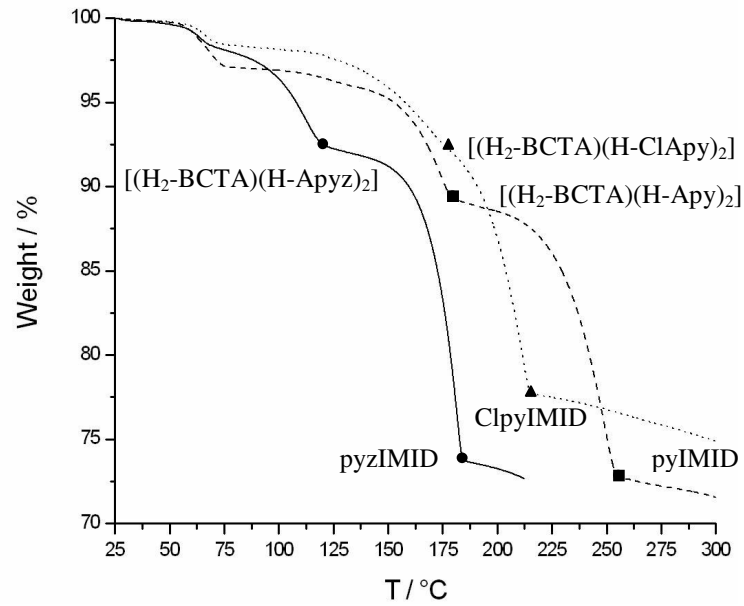

Figure 4.2 TG curves showing the two step synthesis for **pyIMID**, **pyzIMID** and **ClpyIMID**

4.2.1 [(H$_2$-BCTA)(H-Apy)$_2$] Organic Salt and pyIMID

On heating the previously ground mixture of Apy (m.p. 155-158 °C) and H$_4$-BCTA (m.p. 281-284 °C), the organic salt [(H$_2$-BCTA)(H-Apy)$_2$] and the symmetric diimide **pyIMID** were obtained in two separate steps at different temperatures, 180 °C and 260 °C, respectively (Reaction 4.1).

$$2\ \text{Apy} + \text{H}_4\text{-BCTA} \xrightarrow[\text{MW 90 min, 600 W}]{\Delta\ 180^\circ\text{C}} [(\text{H}_2\text{-BCTA})(\text{H-Apy})_2] \xrightarrow{\Delta\ 260^\circ\text{C}} \text{pyIMID}$$

$$- 2\ \text{H}_2\text{O} \qquad\qquad - 4\ \text{H}_2\text{O}$$

Reaction 4.1

The sample collected at 180 °C, [(H$_2$-BCTA)(H-Apy)$_2$], was a white crystalline powder suitable for XRPD. This intermediate product (Figure 4.3) crystallized in the

triclinic crystal system, space group $P\bar{1}$, with a = 11.3988(2) Å, b = 11.8643(2) Å, c = 3.8023(1) Å, α = 96.365(1) °, β = 95.906(1) °, γ = 108.898(1) °, Z = 1, V = 478.21(2) $Å^3$, D_c = 1.536 g/cm^3, R_p = 0.038, R_F = 0.064. The acid is centrosymmetric with C_i symmetry.

The starting material, H_4-BCTA·$2H_2O$, has the carboxylate groups twisted by about 19.2° and 72.5° with respect to the aromatic system [18]. However, the carboxylate groups forming the intermediate compound, [(H_2-BCTA)(H-Apy)$_2$], are planar with the benzene ring and present not only intermolecular hydrogen bonds but also intramolecular hydrogen bonds between two adjacent carboxylate groups ($S_1^1(7)$ motif) (Table 4.1) [19-20]. The classical hydrogen bonds generated a centrosymmetric graph set for [(H_2-BCTA)(H-Apy)$_2$], N_1= $C_3^3(12)$ $R_1^2(4)$ $R_4^4(12)$ $R_4^4(28)$ $R_6^4(20)$, resulting in the formation of a 2D layer. Non-classical hydrogen bonds, C–H···O, link these layers to give finally a 3D structure.

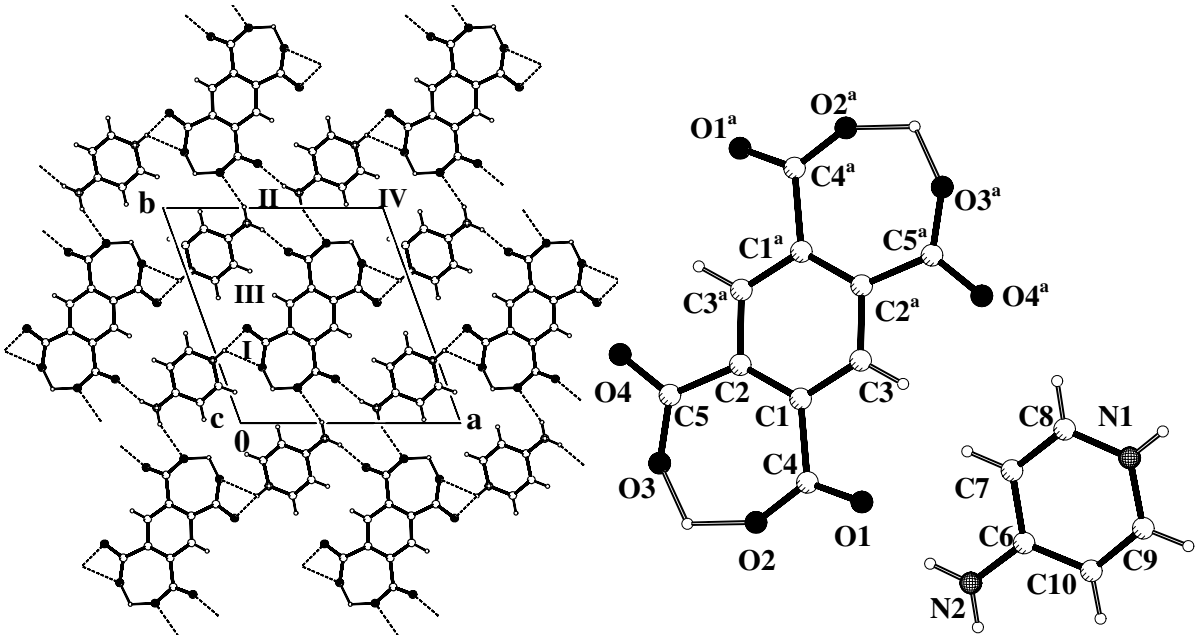

Figure 4.3 Crystal packing diagram for organic salt [(H_2-BCTA)(H-Apy)$_2$]; [a]) 1-x,1-y,1-z. Ring motifs (I):R_1^2 (4), (II):R_4^4 (12), (III):R_4^4 (28) and (IV):R_6^4 (20).

The carboxylate bond distances for [(H_2-BCTA)(H-Apy)$_2$] are: C4-O1 1.255(5) Å, C4-O2 1.296(5) Å, C5-O3 1.301(4) Å and C5-O4 1.258(5) Å.

Table 4.1 Hydrogen bonds for [(H_2-BCTA)(H-Apy)$_2$] (P-1)

Hydrogen Bond	D–H (Å)	H···A (Å)	D···A (Å)	D–H···A (°)	Symmetry operation
N1–H1···O3[b]	0.87	2.48	3.051(5)	124	
N1–H1···O4[b]	0.87	1.89	2.758(5)	173	
N2–H2A···O2[c]	0.86	2.31	3.115(4)	155	[a]) 1-x,1-y,1-z
N2–H2B···O1[d]	0.86	2.00	2.819(4)	159	[b]) 1+x,y,1+z
C3–H3···O1	0.93	2.37	2.720(4)	102	[c]) 1-x,-y,-z
C3–H3···O4[a]	0.93	2.29	2.678(5)	104	[d]) x,y,-1+z
C8–H8···O4[a]	0.93	2.58	3.360(4)	142	
C9–H9···O3[b]	0.93	2.50	3.066(5)	120	

The arrangement of the molecules in the crystal packing showed well defined stoichiometric amounts of the two molecular species (Figure 4.3).

The protonation of the pyridine nitrogen atom and the deprotonation of the H_4-BCTA, giving H_2-BCTA, in the solid state was observed. Comparatives studies were performed with similar known systems in the Cambridge Crystallographic Database (CCSD) [18, 21-25] and by IR spectroscopy [26-30].

The bond distances, C=O and C=N, in the organic salt are larger than those found for the tetraacid H_4-BCTA [18] and for Apy [22] because of the electronic delocalisation in the conjugated bonds (Table 4.2). Likewise, the angle C–N–C increases with the formation of the pyridinium cation. This effect has already been observed for this kind of pyridine/pyridinium systems [21-23].

In the region 3400-3200 cm^{-1} the N–H and O–H stretching vibration bands are shifted with respect to those of the initial aromatic systems probably due to the hydrogen-bonding arrangement present in the crystal. The C=N and the C=O vibration bands are shifted towards lower wavenumbers. The range 1700-400 cm^{-1} is dominated by the stretching and bending vibration bands of the pyridinium and benzene aromatic systems.

Table 4.2 Selected bond distances, bond angles and vibration bands for the starting materials and the organic salt [(H_2-BCTA)(H-Apy)$_2$]

	Bond	Length (Å)	ν (cm^{-1})	Angle	Angle (°)
H_4-BCTA[18]	C═O	1.212(2) 1.219(2)	1700 (br,s)		
Apy[22]	C═N	1.352 1.338	1648 (s)	C–N–C	115.05
[(H_2-BCTA)(H-Apy)$_2$]	C4-O1 C5-O4 C9-N1 C8-N1	1.255(5) 1.258(5) 1.362(3) 1.352(3)	1655 (s) 1616 (m)	C8–N1–C9	121.4(2)

The formation of the intermediate product, [(H_2-BCTA)(H-Apy)$_2$], is necessary for the synthesis of pyromellitdiimides by this *green* method. Experiments carried out with the pyromellitic dianhydride instead of H_4-BCTA did not provide any satisfactory results. The anhydride did not react with the amine.

The sample collected after heating to 260 °C, **pyIMID** (Reaction 4.1, Figure 4.4), was a pale yellow crystalline powder suitable for XRPD. This compound crystallized in the orthorhombic crystal system, space group Cmca, with a = 34.586(2) Å, b = 5.7132(1) Å, c = 8.0155(1) Å, Z = 4, V = 1583.82(8) $Å^3$, D_c = 1.553 g/cm^3, R_p = 0.041, R_F = 0.069. This molecule possesses symmetry D_{2h}.

This compound was synthesized for the first time in 1971 [12] using dry N-methyl-2-pyrrolidone as solvent and heating to 200 °C for 2-3 hours. However, the *green* method is environmental-friendly, economically efficient and time-saving. Furthermore this method is quantitative and does not produce any side products and no purification steps are necessary.

The pyromellitdiimide **pyIMID** (Figure 4.4), has the pyridine rings and the aromatic diimide system twisted with respect to one another, with a dihedral angle between ring 1 and ring 2 (N1 C2 C3 $C2^a$ $C3^a$ and N2 C4 C5 C6 $C5^a$ $C6^a$, respectively) of 57.9(2)° [symmetry operation ^{a}) x,-y,-z].

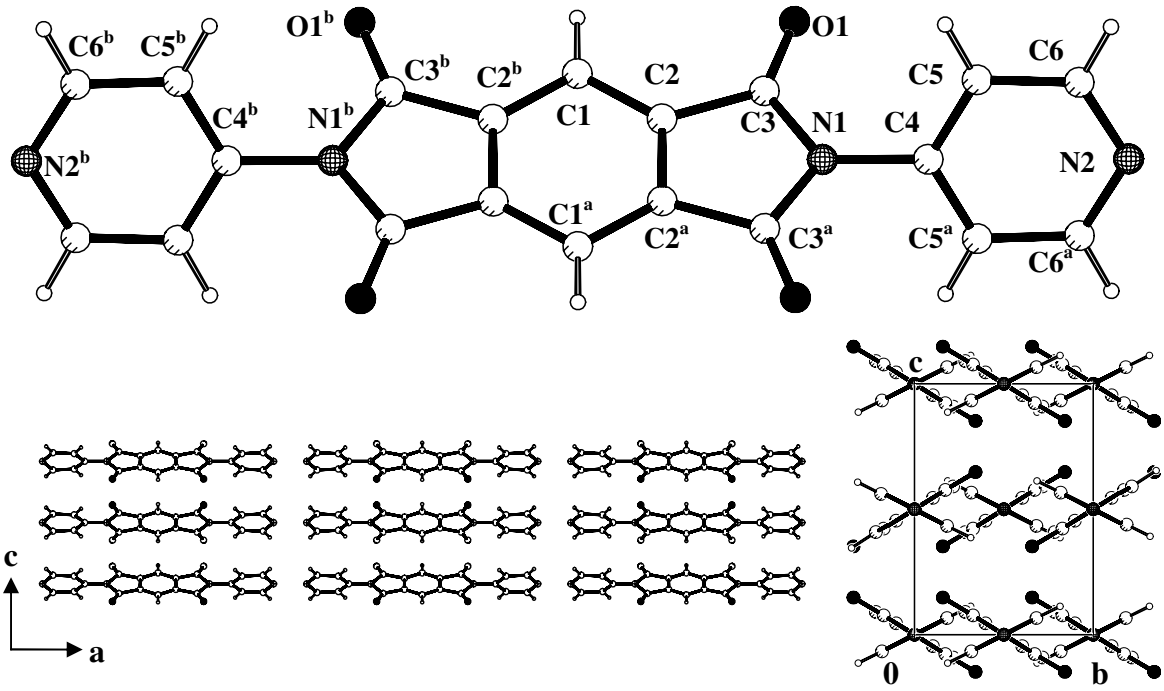

Figure 4.4 Molecular structure and crystal packing diagram of **pyIMID**; [a]) x, -y, -z, [b]) 1-x,-y,-z

The distances and angles are normal for this type of organic compound [31]. The absence of hydrogen donor functions in the molecule, such as N-H or O-H, excludes hydrogen bonding in the crystal packing. There are no π–π stacking interactions between molecules in the crystal.

4.2.2 [(H_2-BCTA)(H-Apyz)$_2$] Organic Salt and pyzIMID

Heating a ground mixture of Apyz (m.p. 118-120 °C) and H_4-BCTA (m.p. 281-284 °C) (2:1), [(H_2-BCTA)(H-Apyz)$_2$] the organic salt and the symmetric diimide **pyzIMID** were obtained at 120 °C and 190 °C, respectively (Figure 4.2, Reaction 4.2).

$$2\ \text{Apyz} + \text{H}_4\text{-BCTA} \xrightarrow[\text{MW 90 min, 600 W}]{\Delta\ 120^\circ\text{C}} [(\text{H}_2\text{-BCTA})(\text{H-Apyz})_2] \xrightarrow{\Delta\ 190^\circ\text{C}} \text{pyzIMID}$$

$$- 2\ \text{H}_2\text{O} \qquad\qquad - 4\ \text{H}_2\text{O}$$

Reaction 4.2

The sample collected at 120 °C, [(H_2-BCTA)(H-Apyz)$_2$], was a white crystalline powder suitable for XRPD. The powder crystallized in the monoclinic crystal system, space group $P2_1/c$, with a = 11.2777(6) Å, b = 12.8578(5) Å, c = 6.4718(2) Å, β = 94.697(4) °, Z = 2, V = 935.30(5) Å^3, D_c = 1.578 g/cm^3, R_p = 0.052, R_F = 0.048. The acid has C_i symmetry.

The crystal packing diagram (Figure 4.5) shows that the H_2-BCTA and H-Apyz ions are connected *via* strong hydrogen bonds (Table 4.3) which generate a 2D structure. The adjacent carboxylic groups have an intramolecular hydrogen bond forming a $S_1^1(7)$ motif. The classical hydrogen bonds generated the graph set containing five motifs, N_1= $C_3^3(10)$ C(5) $R_1^2(4)$ $R_3^3(17)$.

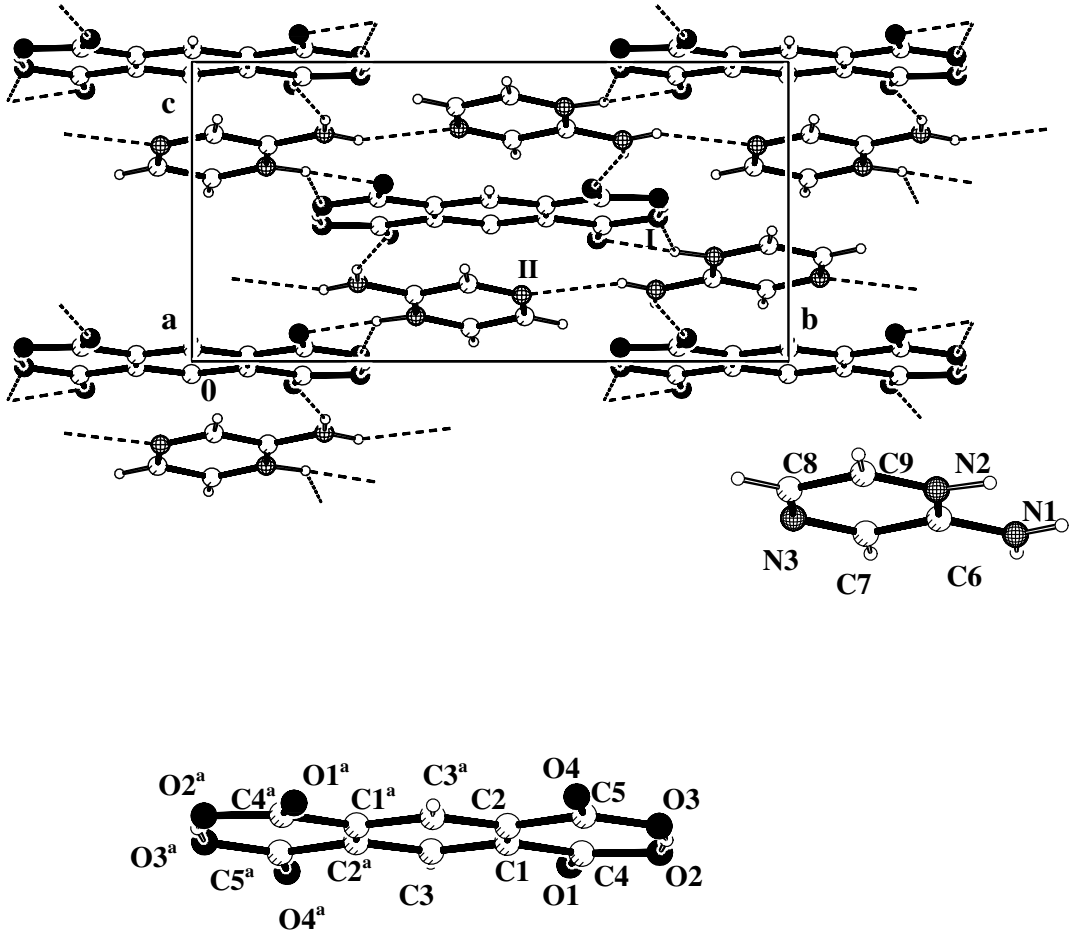

Figure 4.5 Crystal packing diagram for organic salt [(H_2-BCTA)(H-Apyz)$_2$]; [a]) 1-x,-y,-z. Ring motifs (I): $R_1^2(4)$, (II): $R_3^3(17)$.

Table 4.3 Hydrogen bonds for [(H_2-BCTA)(H-Apyz)$_2$] ($P2_1/c$)

Hydrogen Bond	D–H (Å)	H···A (Å)	D···A (Å)	D–H···A (°)	Symmetry operation
N1–H1A···N3[b]	0.86	2.30	2.916(7)	128	
N1–H1B···O1[c]	0.86	2.03	2.849(9)	159	
O2–H2···O3[d]	1.00	1.32	2.312(5)	169	[a]) 1-x,-y,-z
N2–H1N···O3[d]	0.99	2.30	3.038(7)	130	[b]) -x,1/2+y,3/2-z
N2–H1N···O4	0.99	1.76	2.722(8)	164	[c]) -x,1/2+y,1/2-z
C3–H3···O1	0.93	2.29	2.669(7)	104	[d]) 1-x,1-y,1-z
C3–H3···O4[a]	0.93	2.34	2.713(8)	103	[e]) x,y,1+z
C7–H7···O1[c]	0.93	2.39	3.170(8)	141	
C8–H8···O2[e]	0.94	2.56	3.395(8)	148	

The NH_2 function links the planar H_2-BCTA ions and they are titled with respect to one another by 10.0(2)°. The carboxylic bond distances found for this organic salt are: C4-O1 1.296(3) Å, C4-O2 1.294(3) Å, C5-O3 1.292(3) Å and C5-O4 1.296(3) Å.

No significant shifts were found in the IR spectrum for the C=N and the C=O vibration bands. The N–H and O–H stretching vibration bands are shifted with respect to those of the initial aromatic systems probably due to hydrogen-bonding interactions (Figure 4.5).

The sample collected after heating to 190 °C, **pyzIMID** (Reaction 4.2, Figure 4.6), was a pale pink crystalline powder suitable for XRPD. This compound crystallized in the orthorhombic crystal system, space group $Pca2_1$, with a = 9.6229(1) Å, b = 17.8130(4) Å, c = 9.2418(1) Å, Z = 4, V = 1584.16(4) Å^3, D_c = 1.561 g/cm^3, R_p = 0.048, R_F = 0.077.

The compound **pyzIMID** crystallizes in a non-centrosymmetric space group with one molecule per asymmetric unit. The pyrazine rings and the aromatic diimide system are twisted with respect to one another. The dihedral angle between ring 1 (N1 N3 N4 C11 C12 C13 C14) and diimide system is 42.6(2)°, and the dihedral angle between ring 2 (N2 N5 N6 C15 C16 C17 C18) and diimide system is 87.1(1)° (Figure 4.6).

The distances and angles are normal for this kind of organic compound. As a consequence of the absence of any N-H or O-H functions in the molecules, the **pyzIMID** crystal packing is controlled by C–H···N hydrogen bonds only (Table 4.4).

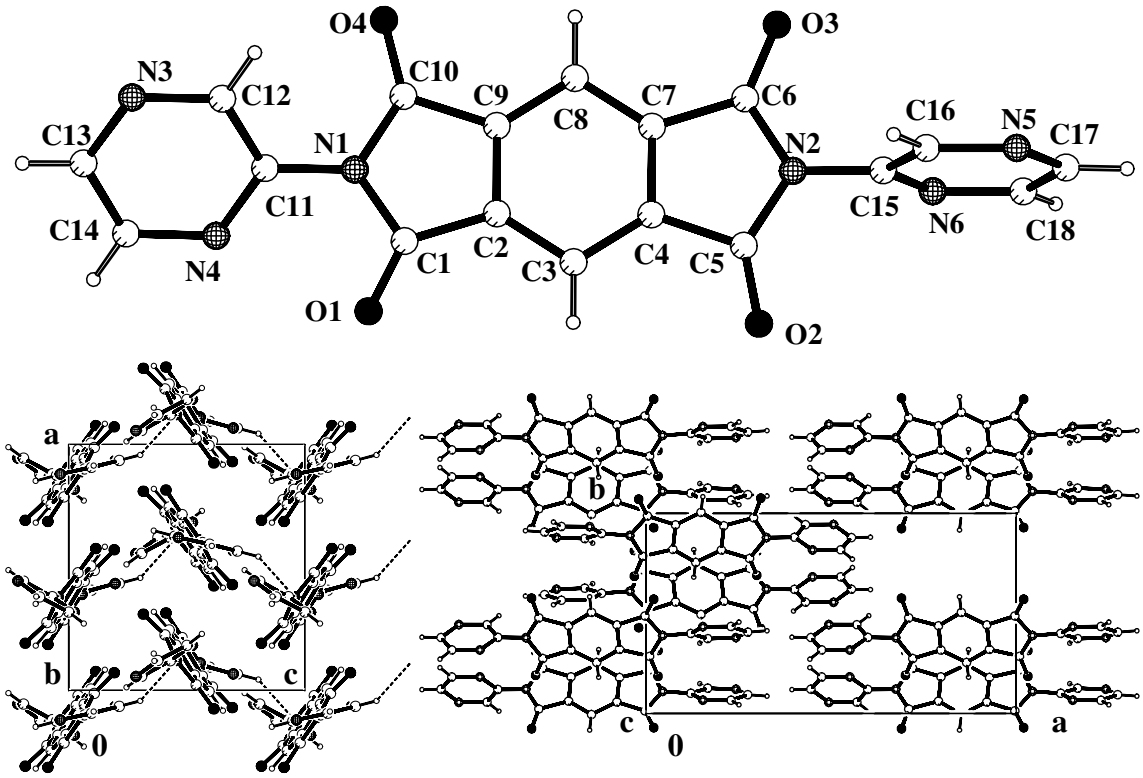

Figure 4.6 Molecular structure and crystal packing diagram of **pyzIMID**

Table 4.4 Hydrogen bonds for **pyzIMID** ($Pca2_1$)

Hydrogen Bond	D–H (Å)	H···A (Å)	D···A (Å)	D–H···A (°)	Symmetry operation
C14–H14···N2[a]	0.93	2.51	3.341(4)	150	[a]) -x,-y,1/2+z

As occurs for **pyIMID**, the *green* synthesis of **pyzIMID** requires the utilisation of H_4-BCTA as a starting material since the direct synthesis using piromellitic dianhydride did not work as expected.

4.2.3 [(H_2-BCTA)(H-ClApy)$_2$] Organic Salt and ClpyIMID

On heating the previously ground mixture of ClApy (m.p. 90-94 °C) and H_4-BCTA (m.p. 281-284 °C), the organic salt [(H_2-BCTA)(H-ClApy)$_2$] and the diimide denoted as **ClpyIMID** were obtained in two separate steps at different temperatures, 180 °C and 220 °C, respectively (Reaction 4.3).

$$2\ \text{ClApy} + \text{H}_4\text{-BCTA} \xrightarrow[\text{MW 90 min, 600 W}]{\Delta\ 180^\circ\text{C}} [(\text{H}_2\text{-BCTA})(\text{H-ClApy})_2] \xrightarrow{\Delta\ 220^\circ\text{C}} \text{ClpyIMID}$$

$$- 2\ \text{H}_2\text{O} \qquad\qquad - 4\ \text{H}_2\text{O}$$

Reaction 4.3

The sample collected after heating to 180 °C was a white crystalline powder suitable for XRPD. The powder crystallized in the monoclinic crystal system, space group $P2_1/n$, with a = 22.384(1) Å, b = 3.9587(1) Å, c = 11.6243(7) Å, β = 98.094(5) °, Z = 2, V = 1019.78(9) Å^3, D_c = 1.665 g/cm^3, R_p = 0.056, R_F = 0.050. The acid possesses C_i symmetry.

The crystal packing of this intermediate compound clearly shows hydrogen bonds between the protonated aromatic amine and H_2-BCTA ions (Table 4.5). The hydrogen bonding produces a very dense 3D structure. The carboxylate groups in H_2-BCTA are planar (Figure 4.7) probably due to the presence of an intramolecular bond with $S_1^1(7)$ motif. The graph set contains seven motif descriptors, N_1= $C_4^3(14)$ $C_4^4(24)$ $R_2^2(4)$ $R_2^2(4)$ $R_1^2(4)$ $R_6^4(24)$ $R_4^4(28)$.

The carboxylate bond distances found for [(H_2-BCTA)(H-ClApy)$_2$] are: C4-O1 1.23(1) Å, C4-O2 1.28(1) Å, C5-O3 1.28(1) Å and C5-O4 1.24(1) Å.

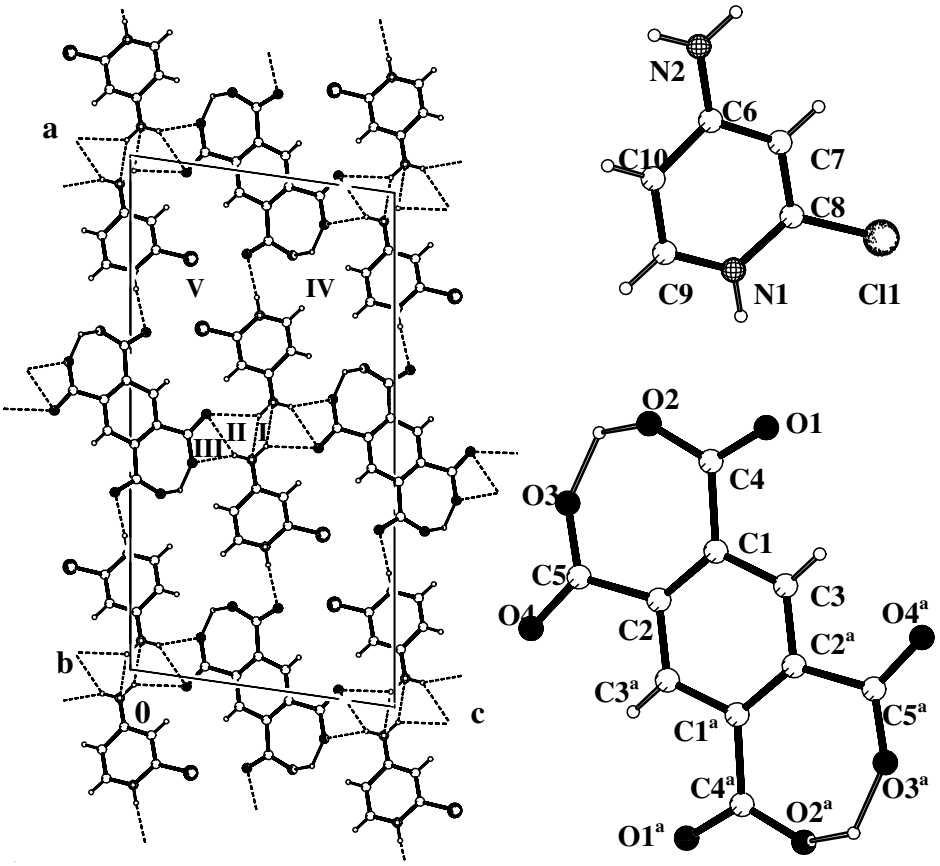

Figure 4.7 Crystal packing diagram for co-crystals [(H_2-BCTA)(H-ClApy)$_2$]; [a]) -x,1-y,1-z. Ring motifs (I) and (II):$R_2^2(4)$, (III):$R_1^2(4)$, (IV):$R_6^4(24)$ and (V):$R_4^4(28)$.

Table 4.5 Hydrogen bonds for [(H_2-BCTA)(H-ClApy)$_2$] ($P2_1/n$)

Hydrogen Bond	D–H (Å)	H···A (Å)	D···A (Å)	D–H···A (°)	Symmetry operation
N1–H1···O1	0.85(1)	1.96(1)	2.790(11)	164.8(9)	
N2–H2A···N2[b]	0.86(1)	2.59(1)	3.209(9)	129.6(10)	
N2–H2A···O4[c]	0.86(1)	2.40(2)	3.029(11)	130.5(9)	[a]) -x,1-y,1-z
N2–H2B···O3[d]	0.86(1)	2.26(1)	3.070(12)	157.1(11)	[b]) 1-x,2-y,1-z
N2–H2B···O4[d]	0.86(1)	2.45(1)	3.173(11)	142.6(11)	[c]) 1/2+x,3/2-y,1/2+z
C3–H3···O1	0.90(1)	2.33(1)	2.725(10)	106.8(7)	[d]) 1/2-x,3/2+y,1/2-z
C3–H3···O4[a]	0.90(1)	2.35(1)	2.727(9)	105.2(8)	
C7–H7···O4[c]	0.89(1)	2.56(1)	3.186(10)	127.4(7)	

As found for the previous structure, in the organic salt [(H_2-BCTA)(H-ClApy)$_2$] the pyridine nitrogen atom is protonated. Comparatives studies with similar systems in the Cambridge Crystallographic Data Centre CCDC were also carried out (Table 4.6).

The bond distances, C=O and C=N and the angle C–N–C, in the organic salt are larger than those found for the tetraacid H_4-BCTA [18] and for ClApy [32]. The variations in the bond distances (Table 4.6) are not so pronounced as those found for the 4-aminopyridinium cation (Table 4.2), probably due to the electronic influence of the chlorine atom in the pyridinium system.

In the region 3400-3200 cm^{-1} in the IR spectrum, the N–H and O–H stretching vibrational bands are shifted with respect to those of the initial aromatic systems. The C=N and the C=O vibration bands are shifted towards lower wavenumbers as shown in Table 4.6. This confirms the partial double-bond character of these bonds in the [(H_2-BCTA)(H-ClApy)$_2$] organic salt.

Table 4.6 Selected bond distances, bond angles and vibration bands for the starting materials and organic salt [(H_2-BCTA)(H-ClApy)$_2$]

	Bond	Length (Å)	ν (cm^{-1})	Angle	Angle (°)
H_4-BCTA[18]	C═O	1.24(1) 1.219(2)	1700 (br,s)		
ClApy[32]	C═N	1.340 1.338	1657 (s)	C–N–C	116.8
[(H_2-BCTA)(H-ClApy)$_2$]	C5-O4 C4-O1 C9-N1 C8-N1	1.24(1) 1.23(1) 1.339(9) 1.358(9)	1645 (s) 1608 (m)	C8–N1–C9	122.0(6)

The sample collected after heating to 220 °C, **ClpyIMID** (Reaction 4.3), was a pale yellow crystalline powder suitable for XRPD. This compound crystallized in the monoclinic crystal system, space group $P2_1/c$, with a = 7.8867(5) Å, b = 7.5288(6) Å, c = 14.3507(9) Å, β = 93.163(7)°, Z = 2, V = 850.8(1) $Å^3$, D_c = 1.714 g/cm^3, R_p = 0.048, R_F = 0.037.

The pyromellitdiimide **ClpyIMID** possesses C_i symmetry (Figure 4.8). The pyridine rings and the aromatic diimide system are twisted with respect to one another with a dihedral angle between, rings 1 and 2 (N1 C2 C3 C4 C5 and N2 C6 C7 C8 C9 C10, respectively) of 20.2(2)°.

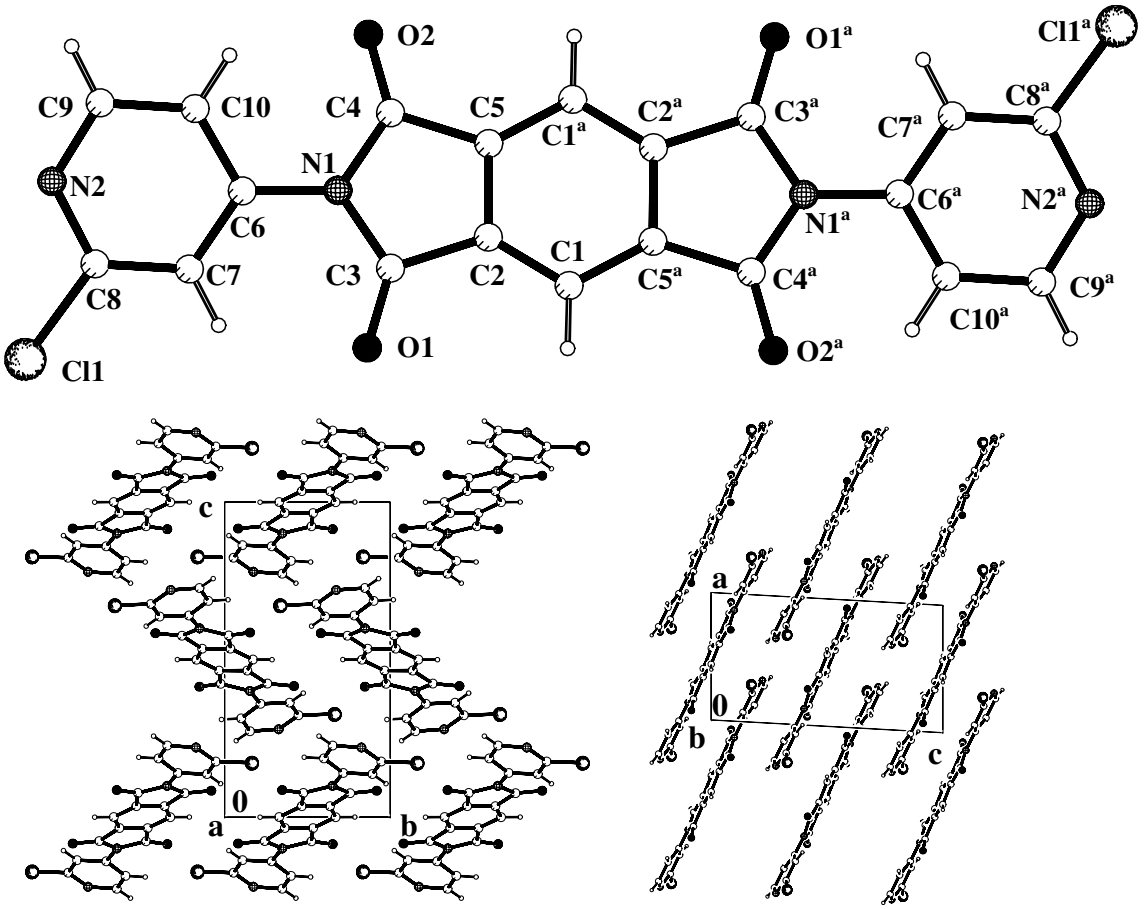

Figure 4.8 Molecular structure and crystal packing diagram of **ClpyIMID**; [a]) 1-x,-y,1-z

The X-Ray analysis showed that only the conformational *anti* stereoisomer is obtained; the chlorine atoms are on opposite sites of the diimide surface. It has been reported that piromellitdiimides can adopt stable *syn*- and *anti*-conformations [33-35]. The stability of these conformers arises from restricted rotation about the two N_{imide}-C_{aryl} single bonds. There are some examples where the resulting conformers are stable at room temperature but interconvert on heating [33], being more stable as the *anti*-stereoisomer ($\Delta G \approx 30$ kcal/mol). As **ClpyIMID** was synthesized at high temperature this may explain the fact there is a single conformer since the rotational energy barrier of the N_{imide}-C_{aryl} bonds, ≈ 4 kcal/mol (calculated value from the rotational energy of the N-C bond using PCModel 9.0 (Serena Software, Bloomington, Indiana, USA), could be easily exceeded.

4.2.4 Mixed Pyromellitdiimides

In order to synthesize new diimides by this *green* method, mixtures of two different amines and H_4-BCTA were first ground and then heated (Scheme 4.3).

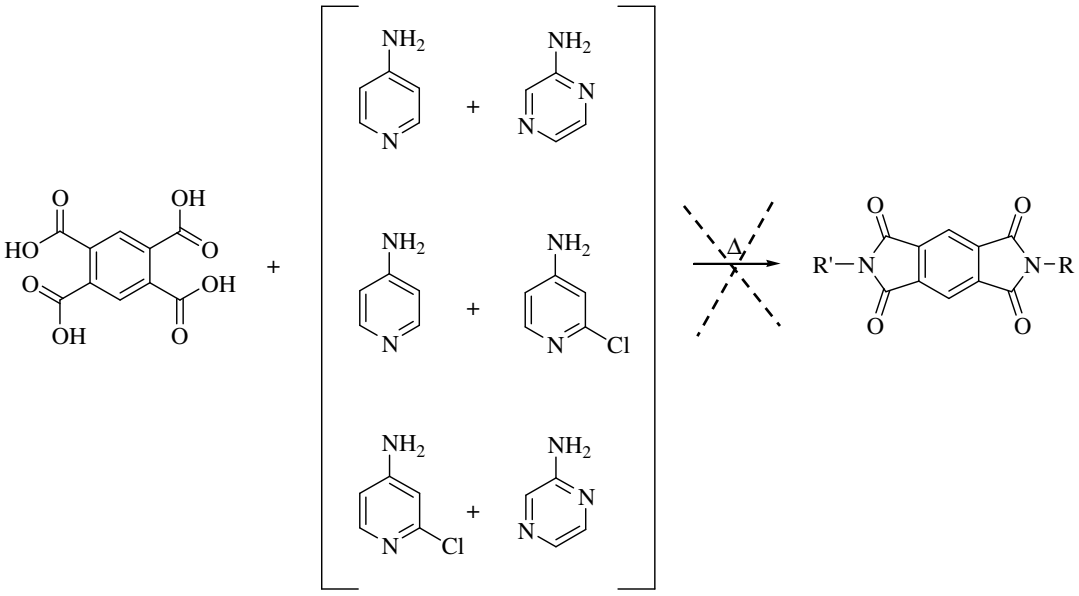

Scheme 4.3 Mixtures prepared using different amines and H_4-BCTA

The XRPD patterns showed in every case a mixture of piromellitdiimides but not the desired mixed-diimide. This is probably a consequence of the different temperatures required to form the diimides.

Certainly, the synthesis of new diimides, especially asymmetric ones, is an open subject but requires further research.

4.3 Hydrolysis of Pyromellitdiimides

4.3.1 Pyromellitamic Diacids H_p-pyIMID and H_m-pyIMID

The partial hydrolysis of **pyIMID** in HCL 0.5N produced two different kinds of crystals, needle-like and plate-like, which correspond to the hydrochloride salts of the *para* and *meta* diacids derived from **pyIMID**, respectively.

4.3.1.1 H_p-pyIMID

The colourless needle-like crystals correspond to the chloride salt with the carboxylic groups *para* to one another (Figure 4.9), abbreviated herein as **H_p-pyIMID**. This compound crystallized in the monoclinic crystal system, space group $P2_1/n$, with a = 9.5979(15) Å, b = 9.2863(10) Å, c = 11.3231(18) Å, β = 101.806(12)°, Z = 2, V = 987.9(2) $Å^3$, D_c = 1.611 g/cm^3, R1 = 0.0319, wR2 = 0.0842. The molecule has C_i symmetry.

The nitrogen atoms of the two pyridine groups are protonated. The neutral form of this organic cation was already synthesized in 1988 [36] by reaction of 4-aminopyridine with pyromellitic dianhydride but crystallographic data were not given.

The substituents, amide and carboxylic groups, are twisted with respect to the benzene ring. The dihedral angle between plane 1 and plane 2 (C1 C2 C3 $C1^a$ $C2^a$ $C3^a$ and O1 N1 C3 C4 C5, respectively) being 68.9(1)°, and that between plane 1 and plane 3 (C1 C2 C3 $C1^a$ $C2^a$ $C3^a$ and O2 O3 C2 C10, respectively) being 22.2(1)° [symmetry operation ^{a}) -x,1-y,-z].

The crystal packing is controlled by strong hydrogen bonds between the chlorine atoms and the diacid systems resulting in the formation of a 2D structure (Table 4.7). The motif generated is $C_3^2(12)$. Then non-classical hydrogen bonds link the adjacent layers.

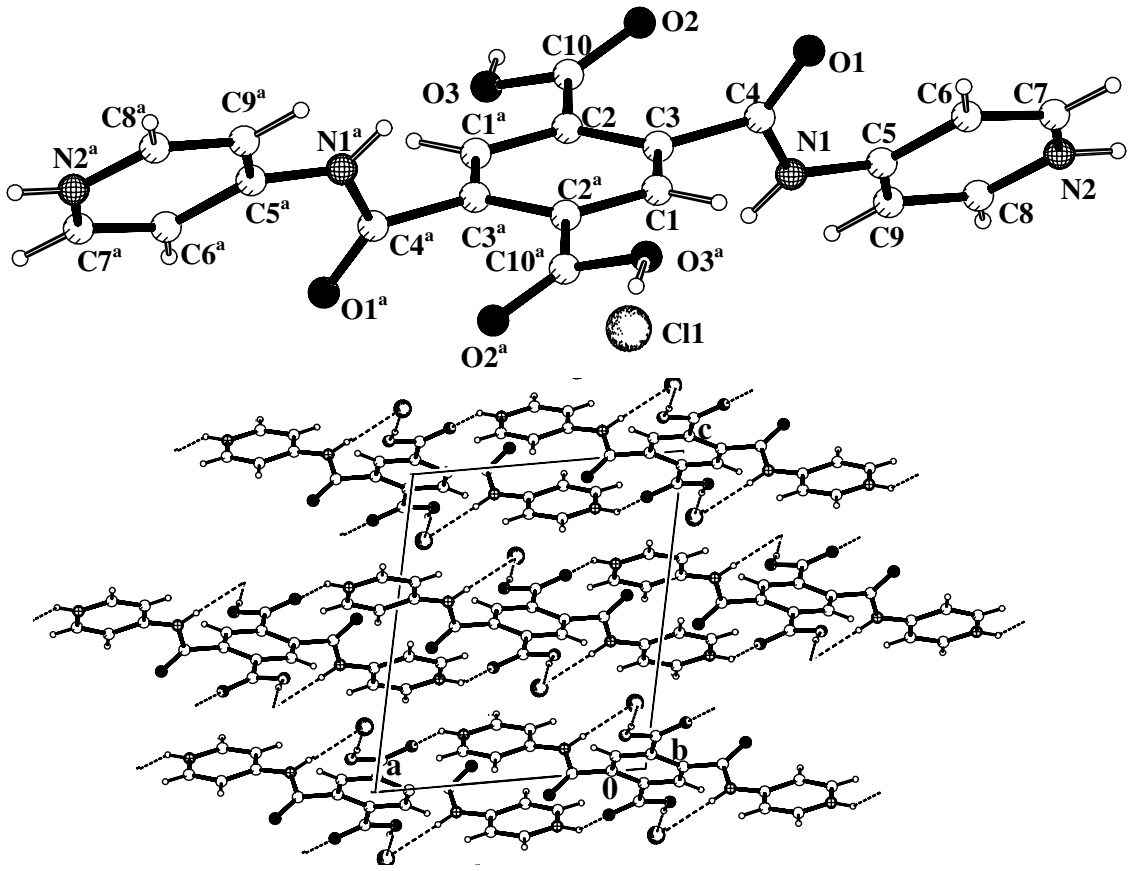

Figure 4.9 Molecular structure and crystal packing of **H_p-pyIMID**; [a]) -x,1-y,-z

Table 4.7 Hydrogen bonds for **H_p-pyIMID** ($P2_1/n$)

Hydrogen Bond	D–H (Å)	H···A (Å)	D···A (Å)	D–H···A (°)	Symmetry operation
N1–H1···Cl1	0.84(3)	2.34(3)	3.176(2)	179(3)	
O3–H1···Cl1[b]	0.96(4)	2.00(4)	2.949(2)	173(3)	[b]) -x,-y,-z
N2–H2···O2[c]	0.86(3)	2.00(3)	2.726(2)	141(3)	[c]) 1-x,-y,-z
C1–H1···Cl1[d]	0.95	2.80	3.614(2)	144	[d]) -1/2+x,1/2-y,-1/2+z
C6–H6···O1	0.95	2.27	2.834(3)	118	[e]) 1-x,1-y,-z
C6–H6···O1[e]	0.95	2.34	3.174(2)	147	

4.3.1.2 H_m-pyIMID

The plate-like crystals that were obtained correspond to the chloride salt with the carboxylic groups *meta* to one another (Figure 4.10), abbreviated herein as **H_m-pyIMID**, with again the nitrogen atoms of the two pyridine groups being protonated. This

compound crystallized in the monoclinic crystal system, space group C2/c, with a = 9.389(1) Å, b = 15.719(2) Å, c = 14.054(2) Å, β = 101.341(9)°, Z = 4, V = 2033.7(4) $Å^3$, D_c = 1.565 g/cm^3, R1 = 0.0492, wR2 = 0.1062. The molecule possesses C_2 symmetry, with atoms C1 and C4 lying on the 2-fold axis.

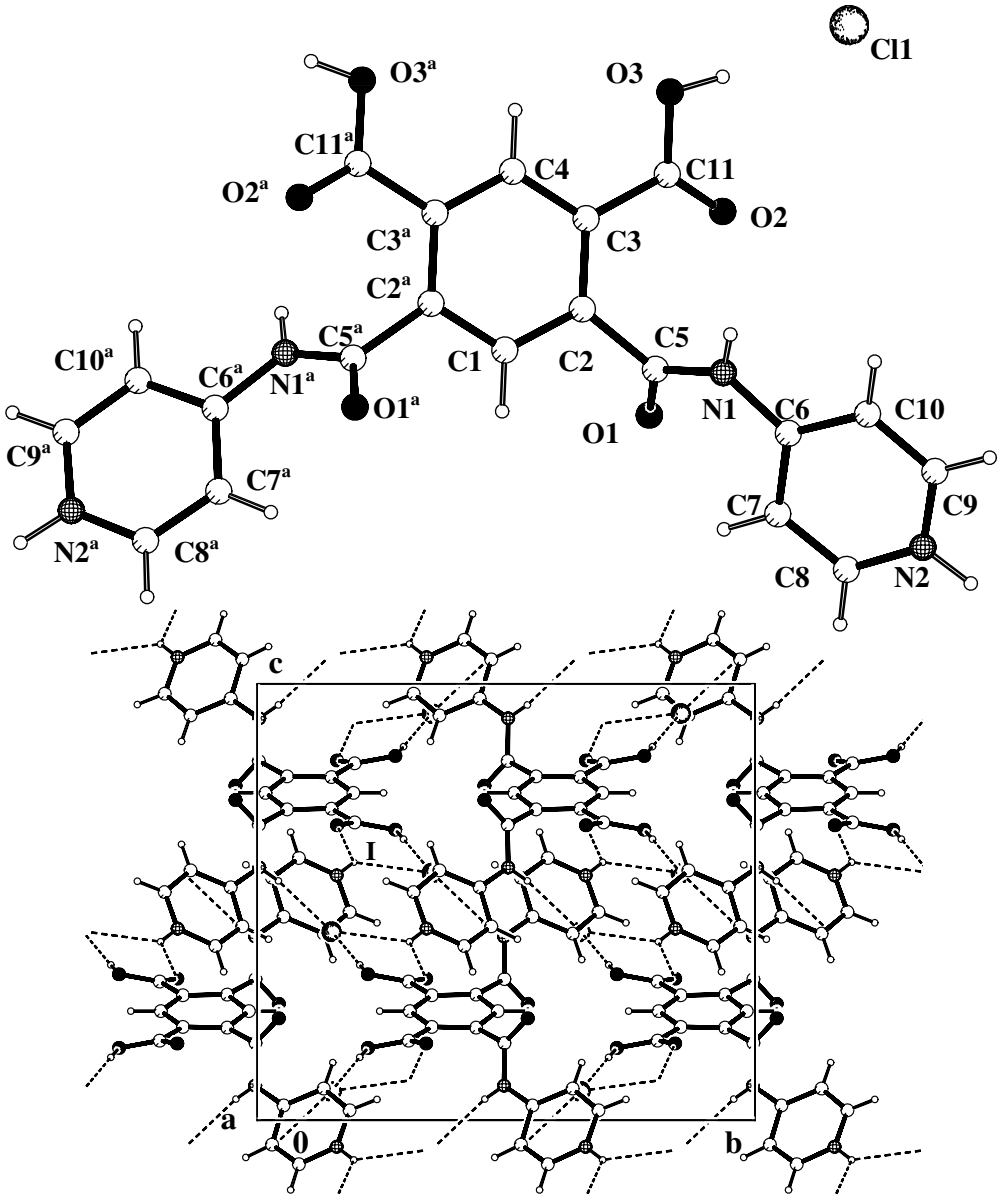

Figure 4.10 Molecular structure and crystal packing of **H_m-pyIMID**; [a]) 1-x,y,3/2-z. Ring motif (I):$R_2^2(6)$

For this *meta* isomer, the amide and carboxylic groups are twisted with respect to the benzene ring. The dihedral angle between plane 1 and plane 2 (C1 C2 C3 C4 $C2^a$ $C3^a$

and O1 N1 C5 C6, respectively) being 65.2(1)° and that between plane 1 and plane 3 (C1 C2 C3 C4 C2[a] C3[a] and O2 O3 C3 C11, respectively) being 17.8(1)° [symmetry operation [a]) 1-x, y, 3/2-z].

The crystal structure of **H_m-pyIMID** shows strong hydrogen bonds between the meta-linked units and the chlorine atoms resulting in the formation of a 3D structure (Table 4.8). The graph set generated for this compound was, $N_1 = C_2^1(13)\,R_2^2(6)$.

Table 4.8 Hydrogen bonds for **H_m-pyIMID** (C2/c)

Hydrogen Bond	D–H (Å)	H···A (Å)	D···A (Å)	D–H···A (°)	Symmetry operation
N1–H1···Cl1[b]	0.78(3)	2.42(3)	3.188(2)	172(3)	[b]) 3/2-x,1/2-y,1-z [c]) 2-x,-y,1-z [d]) x,-y,-1/2+z
O3–H1···Cl1	0.89(4)	2.14(4)	3.004(2)	166(4)	
N2–H2···Cl1[c]	0.94(4)	2.54(5)	3.225(2)	130(3)	
N2–H2···O2[c]	0.94(4)	2.11(4)	2.813(2)	131(4)	
C7–H7···O1	0.95	2.25	2.762(3)	113	
C8–H8···Cl1[c]	0.95	2.81	3.362(3)	118	
C9–H9···O1[d]	0.95	2.49	3.093(3)	121	
C10–H10···O1[d]	0.95	2.57	3.137(3)	118	

The XRPD study carried out with the mixture of these two compounds showed that the ratio of the *para* and *meta* isomers present in the sample was 70 and 30 %, respectively. When the mixture was heated to 260°C the crystalline powder obtained corresponded to **py-IMID**, as confirmed by XRPD.

This kind of salt-like compounds, is an intermediate product in the synthesis of the corresponding diimides by classical methods, but the most cases they were not isolated [37-39].

4.3.2 Pyromellitic Diacid H-pyzIMID

The partial hydrolysis of **pyzIMID** in concentrated HCl produced the corresponding organic salt, with the carboxylic groups *para* (Figure 4.11) only. After three weeks a white crystalline powder was obtained. This compound crystallized in the

monoclinic crystal system, space group $P2_1/c$, with a = 5.7393(1) Å, b = 9.2402(1) Å, c = 20.2312(4) Å, β = 93.102(2)°, Z = 2, V = 1071.34(3) $Å^3$, D_c = 1.591 g/cm^3, R_p = 0.0374, R_F = 0.0492. The molecule possesses C_i symmetry.

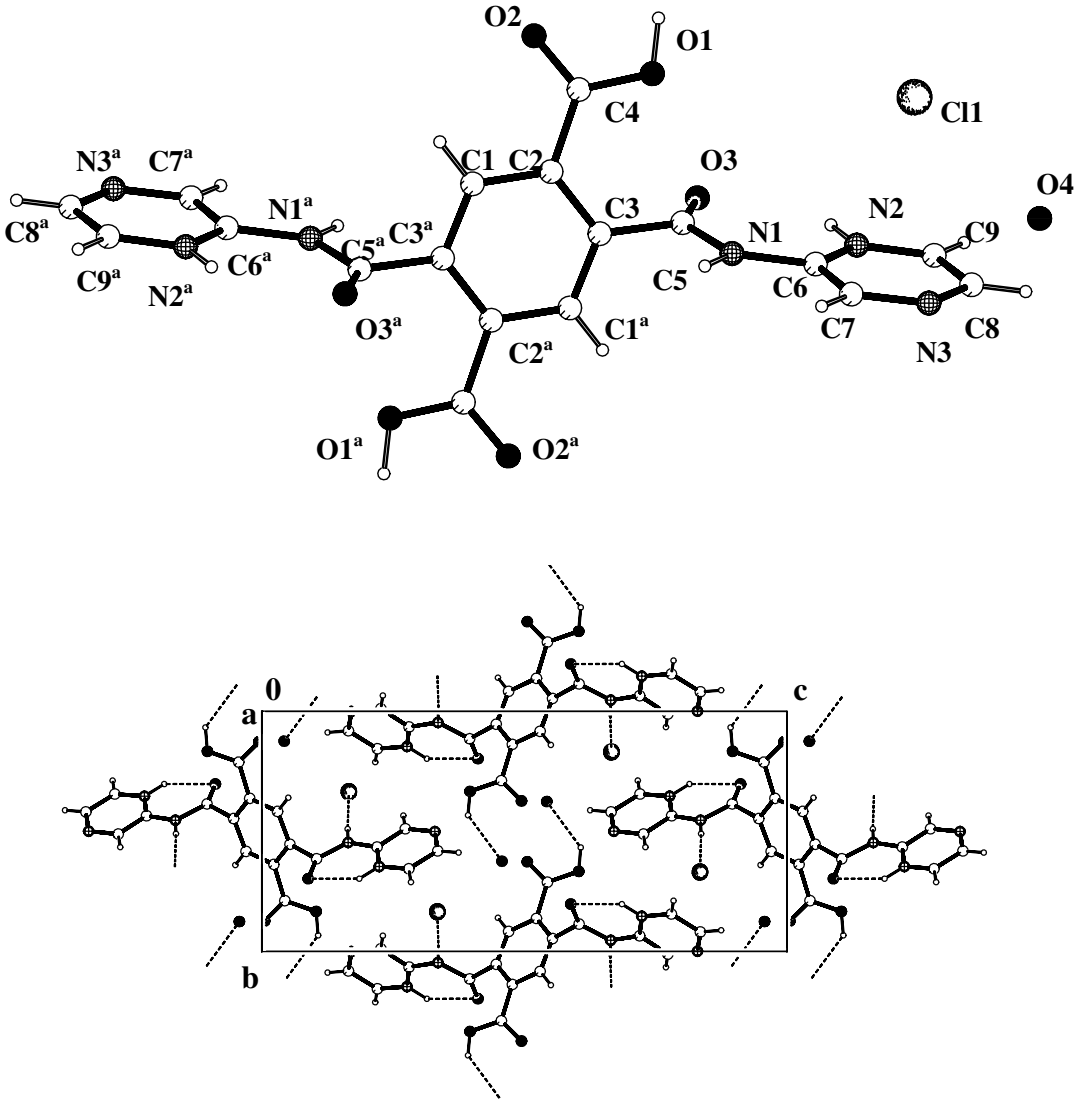

Figure 4.11 Molecular structure and crystal packing of **H-pyzIMID**; [a]) 1-x,-y,1-z

The protonation of the molecules takes place on the ortho nitrogen atom of the pyrazine substituent. Two chloride anions and two water molecules are co-crystallized per di-cation.

The *para* isomer has the substituents twisted with respect to the benzene ring. The dihedral angle between plane 1 and plane 2 (C1 C2 C3 C1^{a} C2^{a} C3^{a} and O3 N1 N2 N3 C5 C6 C7 C8 C9, respectively) being 74.7(2)° and that between plane 1 and plane 3 (C1 C2 C3 C1^{a} C2^{a} C3^{a} and O1 O2 C2 C4) being 22.3(3)° [symmetry operation ^{a}) 1-x, -y, 1-z].

The arrangement of the organic salt molecules in the crystal packing of the structure is directed by C-H···Cl hydrogen bonds which link the adjacent units resulting in the formation of a 2D structure (Table 4.9). The pyrazine and the amide group are planar due to an intramolecular hydrogen bond with $S_1^1(6)$ motif, N2–H2···O3 (Figure 4.11).

Table 4.9 Hydrogen bonds for **H-pyzIMID** ($P2_1/c$)

Hydrogen Bond	D–H (Å)	H···A (Å)	D···A (Å)	D–H···A (°)	Symmetry operation
N1–H1N···Cl1^{b}	0.951(7)	2.340(7)	3.287(5)	147.1(7)	^{b}) 1-x,-1/2+y,1/2-z
O1–H1O···O4^{c}	0.961(7)	2.587(8)	3.377(7)	139.7(7)	^{c}) 1-x,1/2+y,1/2-z
N2–H2N···O3	0.952(8)	2.344(9)	2.930(7)	119.4(7)	^{d}) -1+x,y,z
C9–H9···Cl1^{d}	0.936(6)	2.076(7)	2.953(5)	155.4(9)	

4.4 Complexation Tests and Precursers Syntheses

In preliminary studies, a *green* method to coordinate the diimides to a metal centre was chosen since most polyimides are difficult to handle due to their insolubility. **pyIMID**, **ClpyIMID** and **pyzIMID** are soluble in THF, DMSO or ethylene glycol only at reflux temperature.

Every diimide was mixed with copper(II) acetate or copper(II) chloride (2:1). Three series of experiments were performed, that is

- Grinding
- Grinding + MW irradiation
- Grinding + Δ

In all the cases, the XRPD studies showed that there were no reactions between the metal salts and the diimide ligands.

A second set of essays was carried out with mixtures of H_4-BCTA, each amine, and copper(II) acetate or copper(II) chloride. The aim was to synthesize the diimide *in situ* and to force coordination to the metal centres. Then, the same series of experiments already mentioned were performed. The XRPD studies showed the formation of the diimides but no coordination to the metal ions was observed.

Finally, two precursers, **P1** and **P2**, were synthesized to work as building blocks for these reactions.

Dark-blue block-like crystals of **P1** {[Cu $(Apy)_4$] Cl_2} (Figure 4.12) were obtained by diffusion of an methanolic solution of Apy into an aqueous solution of copper(II) chloride dihydrate (4:1). This compound crystallized in the monoclinic crystal system, space group $P2_1/a$, with a = 9.700(1) Å, b = 14.117(1) Å, c = 10.753(1) Å, β = 108.60(1)°, Z = 2, V = 1395.5(3) $Å^3$, R1 = 0.0558, wR2 = 0.1440. The complex possesses C_i symmetry.

The Cu^{II} has square planar geometry and its coordination sphere is defined by four Apy ligands. The Cl···Cu distances, 3.153(1) Å, are too long to be considered as coordination bonds (Table 4.10).

The hydrogen bonding 3D network is formed by the hydrogen bonds between the amine groups, the chlorine atoms and the solvent molecules (Figure 4.12, Table 4.11).

Table 4.10 Selected bond distances (Å) and bond angles (°) for **P1** ($P2_1/a$)

Bond	**Length (Å)**	**Angle**	**Angle (°)**
Cu1-N1	2.003(4)	N1-Cu1-N3	92.09(14)
Cu1-N3	2.049(3)	N1-Cu1-N3[a]	87.92(14)
[a]) 1-x,-y,1-z			

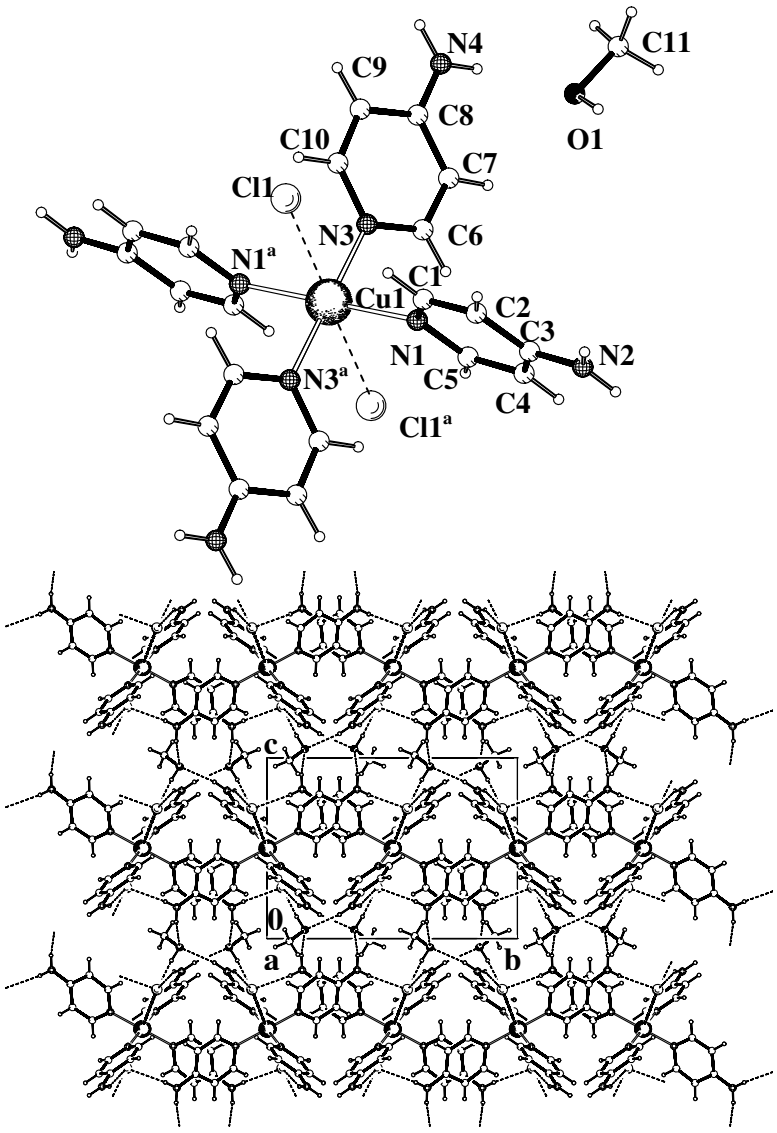

Figure 4.12 Cu^{II} coordination sphere and crystal packing diagram for **P1**; [a]) 1-x,-y,1-z

Table 4.11 Hydrogen bonds for **P1** ($P2_1/a$)

Hydrogen Bond	D–H (Å)	H···A (Å)	D···A (Å)	D–H···A (°)	Symmetry operation
N2–H2A···O1[b]	0.88	2.19	3.059(5)	168	
N2–H2B···Cl1[c]	0.88	2.52	3.350(4)	157	[a]) 1-x,-y,1-z
N4–H4A···O1	0.88	2.26	3.042(5)	149	[b]) x,y,-1+z
N4–H4B···Cl1[d]	0.88	2.52	3.381(4)	168	[c]) 1+x,y,z
O1–H12···Cl1[e]	0.92(6)	2.13(6)	3.037(3)	168(6)	[d]) 1/2-x,1/2+y,1-z
C5–H5···Cl1[a]	0.95	2.83	3.458(4)	125	[e]) 1/2+x,1/2-y,1+z
C6–H6···Cl1[a]	0.95	2.55	3.406(5)	150	
C10–H10···Cl1	0.95	2.70	3.472(5)	139	

Green block-like crystals of **P2** [Cu $(ClApy)_2$ Cl_2] (Figure 4.13) were synthesized by diffusion of a solution of ClApy in methanol into a solution of copper(II) chloride dihydrate in ethanol. This compound crystallized in the monoclinic crystal system, space group $P2_1/n$, with a = 6.1942(8) Å, b = 7.7079(7) Å, c = 15.049(2) Å, β = 97.77(2)°, Z = 2, V = 711.9(2) $Å^3$, R1 = 0.0685, wR2 = 0.1736. The complex has C_i symmetry.

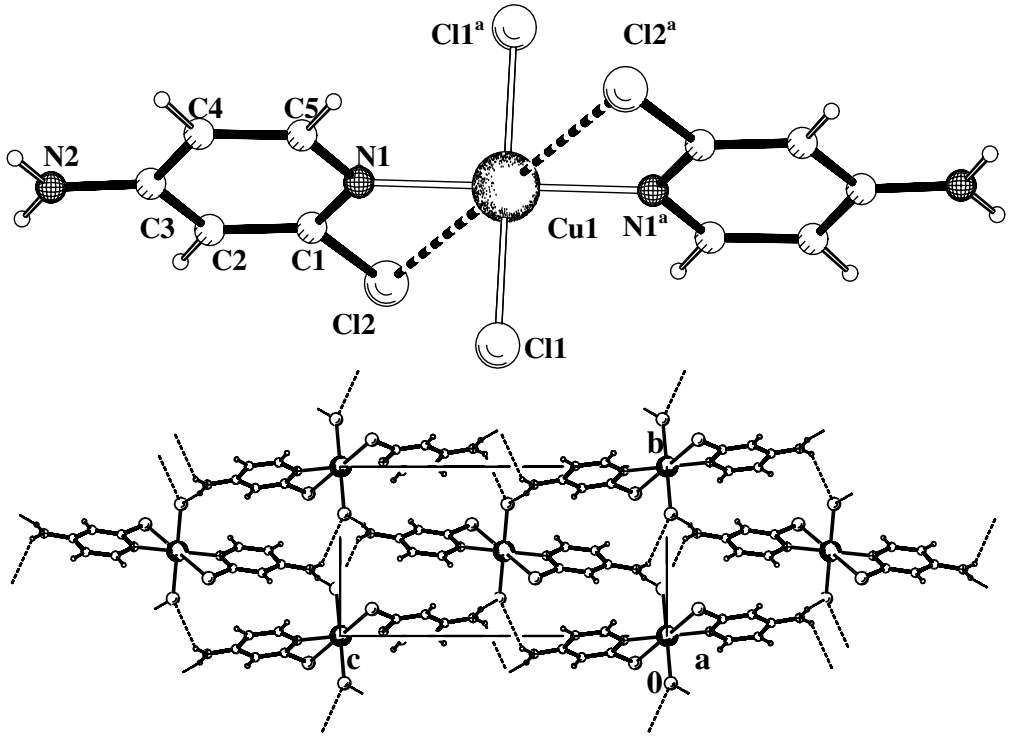

Figure 4.13 Cu^{II} coordination sphere and crystal packing diagram for **P2**; [a]) -x,-y,-z

The square planar Cu^{II} coordination sphere is defined by two ClApy ligands and two chlorine anions (Table 4.12). The Cu1···Cl2 distances are 3.158(2) Å.

Table 4.12 Selected bond distances (Å) and bond angles (°) for **P2** ($P2_1/n$)

Bond	Length (Å)	Angle	Angle (°)
Cu1-Cl1	2.268(2)	Cl1-Cu1-N1	90.69(16)
Cu1-N1	1.990(4)	Cl1-Cu1-N1[a]	89.31(16)
[a]) -x,-y,-z			

The 3D network structure is formed by hydrogen bonds between the amine groups and the chlorine atoms (Figure 4.13, Table 4.13).

Table 4.13 Hydrogen bonds for **P2** ($P2_1/n$)

Hydrogen Bond	D–H (Å)	H···A (Å)	D···A (Å)	D–H···A (°)	Symmetry operation
N2–H2A···Cl1[b]	0.88	2.77	3.496(6)	141	[b]) 1/2-x,1/2+y,1/2-z
N2–H2B···Cl1[c]	0.88	2.48	3.333(6)	164	[c]) -1/2+x,-1/2-y,1/2+z

Precursers **P1** and **P2** were mixed with H_4-BCTA and the samples were ground and heated. The XRPD patterns showed the formation of **pyIMID** for the **P1**/H_4-BCTA mixture (1:2) and the formation of **ClpyIMID** for the **P2**/H_4-BCTA mixture (1:1), plus $CuCl_2$. The diimides were not coordinated to the metal centres. During the heating process the energy communicated to the system it is enough to break the coordination bonds.

All the reactions and tests performed are summarised in Scheme 4.4.

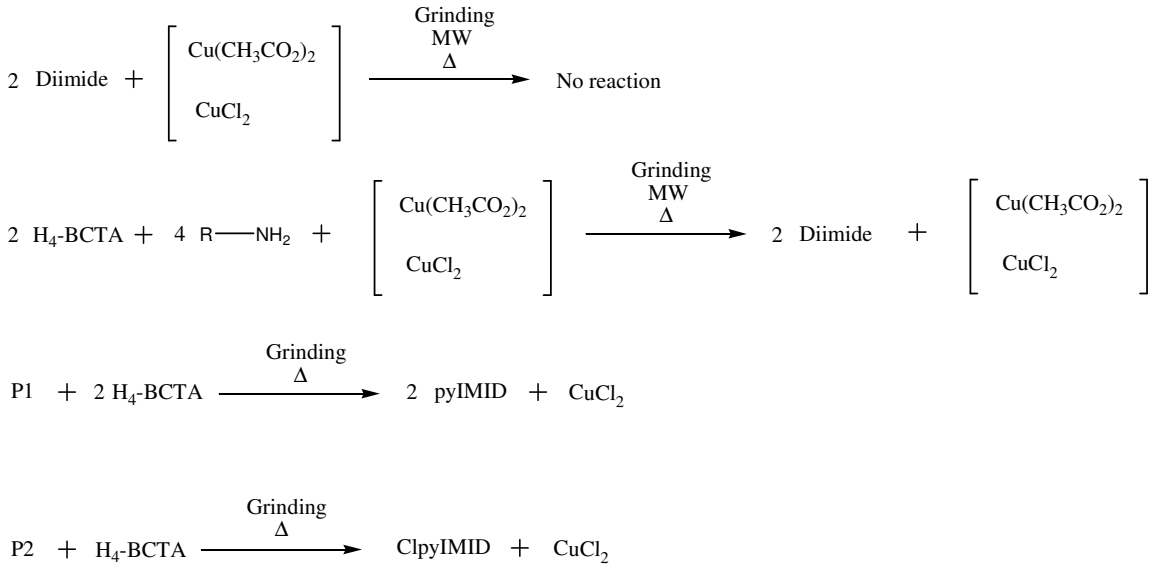

Scheme 4.4 Complexation tests

The complexation of the diimides using a *green* methodology did not give satisfactory results to date. This could be due to different factors:

- The metallic system was not appropriated. This means other metallic salts with different anions or metals could work under these conditions.
- The *green* conditions are not adequate to obtain a metal complex with the diimides. In this case, a conventional synthesis may resolve the problem.

Dinolfo et al. [31] have shown that a supramolecular complex of **pyIMID** can be obtained. Equivalent quantities of $[Re(CO)_4]_2$(2,2'-bisbenzimidazolate) and **pyIMID** were refluxed in THF for 48h to give a tetrametallic complex. Single imides usually form complexes by refluxing in a solvent [14] therefore this could be a possible way to continue this research.

4.5 References

[108] Struijk C. W., Sieval A. B., Dakhorst J. E. J., van Dijk M., Kimkes P., Koehorst R. B. M., Donker H., Schaafsma T. J., Picken S. J., van de Craats A. M., Warman J. M., Zuilhof H., Sudhölter E. J. R., *J. Am. Chem. Soc.*, 122, 11057-11066, **2000**.

[109] Schlettwein D. Wöhrle D., Karmann E., Melville U., *Chem. Mater.*, 6, 3-6, **1994**.

[110] Bockstahler E. R., Weaver L. C., Wright D. L., *J. Med. Chem.*, 11, 603-606, **1968**.

[111] Gawronski J., Brzostowska M., Gawronska K., Koput J., Rychlewska U., Skowronek P., Nordén B., *Chem. Eur. J.*, 8, 2484-2494, **2002**.

[112] Hansen J. G., Feeder N., Hamilton D. G., Gunter M. J., Becher J., Sanders J. K., M., *Org. Lett.*, 2, 449-452, **2000**.

[113] Kishikawa K., Tsubokura S., Kohmoto S., Yamamoto M., *J. Org. Chem.*, 64, 7568-7578, **1999**.

[114] Nakajima K., Tanaka K., Yamabe T., *Synth. Met.*, 62, 91-95, **1994**.

[115] Hansen J. G., Bang K. S., Thorup N., Becher J., *Eur. J. Org. Chem.*, 2135-2144, **2000**.

[116] Kaiser G., Jarrosson T., Otto S., Ng Y.-F., Bond A. D., Sanders J. K. M., *Angew. Chem. Int. Ed.*, 43, 1959-1962, **2004**.

[117] Zhang Q., Hamilton D. G., Feeder N., Teat S. J., Goodman J. M., Sanders J. K. M., *New J. Chem.*, 23, 897-903, **1999**.

[118] Pascu S. I., Jarrosson T., Naumann C., Otto S., Kaiser G., Sanders J. K. M., *New J. Chem.*, 29, 80-89, **2005**.

[119] Dine-Hart R. A., Wright W. W., *Die Makromolekulare Chemie*, 143, 189-206, **1971**.

[120] Dokoshi N., Tohyama S., fujita S., Kurihara M., Yoda N., *J. Polym. Sci., Part A: Polym. Chem.*, 8, 2197-2217, **1970**.

[121] Banthia S., Samanta A., *Inorg. Chem.*, 43, 6890-6892, **2004**.

[122] Aakeröy C. B., Salmon D. J., *Cryst. Eng. Comm.*, 7, 439-448, **2005**.

[123] Desiraju G. R., *Cryst. Eng. Comm.*, 5, 466-467, **2003**.

[124] Dunitz J. D., *Cryst. Eng. Comm.*, 5, 506, **2003**.

[125] Dale S. H., Elsegood M. R. J., *Acta Crystallogr., Sect. E: Struct. Rep. Online*, 59, o1087, **2003**.

[126] Etter M. C., MacDonald J., *Acta Cryst.*, B46, 256-262, **1990**.

[127] Bernstein J., Davis R. E., Shimoni L., Chang N.-L., *Angew. Chem. Int. Ed.*, 34, 1555-1573, **1995**.

[128] Sugiyama T., Mang J., Matsuura T., *Acta Crystallogr., Sect. C: Cryst. Struct. Commun.*, 58, o242, **2002**.

[129] Chao M., Schempp E., *Acta Crystallogr., Sect. B: Struct. Crystallogr. Cryst. Chem.*, 33, 1557, **1997**.

[130] Teulon P., Delaplane R. G., Olovsson I., Roziere J., *Acta Crystallogr., Sect. C: Cryst. Struct. Commun.*, 41, 479, **1985**.

[131] Noshchenko G. V., Mykhalichko B. M., Davydov V. N., *Russ. J. Coord. Chem.*, 30, 349-354, **2004**.

[132] Shi J. M., Zhang F. X., Lu J. J., Liu L. D., *Acta Crystallogr., Sect. E*, 61, m1181, **2005**.

[133] Roman P., Sertucha J., Luque A., lezama L., Rojo T., *Polyhedron*, 15, 1253-1262, **1996**.

[134] Roman P., Beitia J. I., Luque A., Gutiérrez-Zorrilla J. M., *Mat. Res. Bull.*, 27, 339-347, **1992**.

[135] Czupinski O., Jakubas R., Pietraszko A., *J. Mol. Struct.*, 704, 117-187, **2004**.

[136] Kotrla J., Florian J., Kubelkova L., fraissard J., *Collect. Czech. Chem. Commun.*,

60, 393-402, **1995**.

[137] Cook D., *Can. J. Chem.*, 39, 2009-2024, **1961**.

[138] Dinolfo P. H., Williams M. E., Stern C. L., Hupp J. T., *J. Am. Chem. Soc.*, 126, 12989-13001, **2004**.

[139] Parthasarathi V., Wolfrum S., Noordik J. H., Beurskens P. T., Smith G., O'Reilly E. J., Kennard C. H. L., *Cryst. Struct. Commun.*, 11, 1519, **1982**.

[140] Degenhardt III C., Shortell D. B., Adans R. D., Shimizu K. D., *Chem. Commun.*, 929-930, **2000**.

[141] Colquhoun H. M., Zhu Z., Cardin C. J., Gan Y., *Chem. Commun.*, 2650-2652, **2004**.

[142] Degenhardt III C., Smith M. D., Shimizu K. D., *Org. Lett.*, 4, 723-726, **2002**.

[143] Al-Azzawi M. J., Atto A. T., Al-Ahdami B. W., Ali I. T., *J. Biol. Sci. Res.*, 19, 85-93, **1988**.

[144] Mallakpour S., Shahmohammadi H. M., *J. Appl. Polym. Sci.*, 92, 951-959, **2004**.

[145] Faghihi K., Zamani K., Mirsamie A., Mallakpour S., *J. Appl. Polym. Sci.*, 91, 516-524, **2004**.

[146] Faghihi K., Zamani K., Mirsamie A., Mallakpour S., *Polym. Int.*, 53, 1226-1234, **2004**.

5. Conclusions and Further Investigations

5. Conclusions and Further Investigations

The aim of this work was to synthesize new metal-organic compounds, especially nanoporous solids for adsorption, using the principals of *Crystal Engineering* and, to synthesize, via a *green* route, new diimides as bridging ligands.

In the first part of this work, several metal-organic polymers containing 4,4'-bpy were synthesized. This ligand shows good coordination behaviour, as shown previously [see Chapter 2]. Several of these compounds were obtained by simply changing the reaction conditions; varying the solvent or the anion involved, for example. The presence of water during the reaction seems to be a limiting factor for the formation of 3D networks. This is the case for the metal complexes **C1** and **C2**, **C8** and **C9**, **C11** and **C11-1a,b,c** and finally **C10** and **C14**.

The anions SiF_6^{2-}, $S_2O_6^{2-}$ and SO_4^{2-} have similar behaviour and produce 3D and 2D network structures. However, the dithionate salts are difficult to handle since their solubility in methanol or ethanol is very poor and they are not stable in aqueous solution or upon heating.

Some of these new metal-organic compounds show anion-exchange properties in the presence of halide salts or potassium cyanate. This is the case for compounds **C1**, **C2**, **C8**, **C9**, **C11** and **C12**. These solid state transformations are usually associated with a change of colour of the solid, which is produced when a different anion coordinates to the metal centre.

Three metal-organic frameworks, that is **C1**, **C8** and **C11**, have been studied and characterized by adsorption isotherms and immersion calorimetry. The logarithmic plot of the DRK equation for these three compounds indicated coherence for the adsorption of the different vapours, within the framework of Dubinin's theory. Since the size of the pores is similar, the energy values $E_{C_6H_6}$ obtained (20 kJ/mol on **C1**, 18 kJ/mol on **C8,** and 12 kJ/mol on **C12** solid) are a direct consequence of the chemical composition of the pores.

The size of the molecule adsorbed, the presence of groups suitable to give interactions with the atoms forming the pores and the temperature have a significant influence on the adsorption processes, as was shown by the gravimetric isotherms and the immersion calorimetric experiments.

Although the dpdo ligand also works well in this kind of system, the influence of the presence of water in the medium is even more radical than found for 4,4'-bpy. The 3D networks obtained in ethanol decompose to give mononuclear compounds when water is used to dissolve the metal salt. In addition, the dithionate anions decompose to sulphate anions under the same conditions. When an ethanolic solution of the metal sulphate is used, the result is also the formation of a mononuclear compound. It may be assumed that sulphate anions do not work well as counteranions for the synthesis of 3D networks under these conditions.

It is important to note that to build up metal-organic frameworks, templating is very important. For this reason, the development of polydentate organic ligands, inorganic anions and metal centres, and the effect produced when one of the components is changed, must be studied to use *Crystal Engineering* as an efficient tool.

The last part of this work was the synthesis of some pyromellitdiimides via a *Green Chemistry* process. The *green* method is environmental-friendly, economically efficient and time-saving. Furthermore, this method is quantitative and does not produce any side products, hence no purification steps are necessary.

Other diimides may be obtained by changing the amines or the tetraacid used in the synthetic process. For instance, H_4-BCTA could be replaced by pyrazine-2,3,5,6-tetracarboxylic acid, and the amines used could be replaced by 3,4-diaminopyridine, 4-amino-3-nitropyridine, 3-aminopyridine, 5-aminopyridine-2-carbonitrile, etc., to give similar systems.

The experiments to complex these diimides with some metal ions, using *Green Chemistry* (i.e. grinding or for heating), were not successful. This is a domain that it would be interesting to investigate further by changing the metal ions and the nature of the counteranions, or trying conventional ways to synthesize these complexes. Also, it may be interesting to use the new organic ligands, that have been obtained by hydrolysis of the pyromellitdiimides, for the construction of new porous materials.

6. Experimental Section

6. Experimental Section

6.1 Solvents and Gases

Solvents for synthesis, calorimetric and isotherms experiments were of technical grade and were purified by distillation under nitrogen atmosphere and dried according to standard laboratory practices [1]. The doubly distilled water used was further purified with a Ministil P6 system (Christ Aqua ecolife AG, Aesch, Switzerland). Laboratory gases were purchased from Carbagas and used directly from the cylinders without further purification.

6.2 Starting Materials

All reagents employed were commercially available reagent grade materials from Aldrich Chemicals Co., Merk, Acros and Fluka Chemie AG and were used as received, without further purification. Dithionate salts were synthesized by the Inorganic Chemistry Department of the University of Kiev.

6.3 Instrumentation and Analyses

6.3.1 Infrared Spectroscopy

Infrared spectra were recorded with a Perkin-Elmer 1720X FT-IR spectrometer and with a Perkin-Elmer Spectrum One spectrometer in transmission mode where the

absorptions are given in reciprocal centimetres (cm^{-1}). Intensity data are described with the following abbreviations: br (broad), s (strong), m (medium) and w (weak).

All compounds were prepared as KBr pellets (solids) or just applied between two KBr windows (liquids). A standard press was used to produce KBr pellets. In cases where the samples were expected to change their composition in KBr pellets, data were collected as nujol mulls. In those cases mostly both KBr pellet and nujol mull spectra are presented to indicate the differences.

6.3.2 Elemental Analyses

The C, H and N elemental microanalysis were performed by the Microanalysis service of the Laboratory of pharmaceutical and organic propedeutical Chemistry at the University of Geneva (Switzerland), or the Department of Chemistry of the Engineer School in Fribourg.

6.3.3 Mass Spectra

ESI mass spectra were measured using a LCQ Finnigan spectrometer and EI mass spectra were performed on a Finnigan Polaris Q mass spectrometer by the mass service of the University of Neuchâtel (Switzerland). The electron beam energy used to carry out the EI was 70 eV.

6.3.4 Thermogravimetric Analyses

The TG curves were recorded using a METTLER 4000 thermogravimetric module. A sample of about 20 mg was put in a closed aluminium oxide crucible and heated at a rate of 10 $°Cmin^{-1}$ and/or 2$°Cmin^{-1}$ under nitrogen (gas flow 150 $mlmin^{-1}$) at atmospheric pressure.

6.3.5 Microwave Reactions

All the microwave-assisted reactions described here were performed in open glass vessels with MIO STAR MW2 Microwave System at a frequency of 2450 MHz (130–800 W).

6.3.6 X-Ray Single Crystal Structure Analysis

Intensity data were collected using a STOE IPDS (Image Plate Diffraction System) with graphite monochromated Mo Kα X-radiation (λ = 0.71073 Å), mostly at 153 ± 2 K. The structures were solved by Direct methods using the program SHELXS-97 [2]. The refinement and all further calculations were carried out using SHELXL-97 [3]. The H atoms were either located from difference Fourier maps and refined isotropically, or included in calculated positions and treated as riding atoms using SHELXL default parameters. When H-atoms of water molecules could be located from difference Fourier maps, they were included in the refinement and either refined isotropically without any constraints or refined with O-H distance restrained to be 0.95 Å. Weighted full-matrix least squares refinement on F^2 was used. Neutral atomic scattering factors were taken from International Tables for X-ray Crystallography [4]. The values R1 and wR2 given have been calculated as follows:

$$R1 = \frac{\left\| F_0 \right| - \left| F_c \right\|}{\left| F_0 \right|}$$

$$wR2 = \sqrt{\frac{w\left(F_0^2 - F_c^2\right)}{\left(wF_0^4\right)}}$$

with $w = 1/\left[\sigma^2(F_0^2) + (AP)^2 + BP\right]$ and $P = \left(F_0^2 + 2F_c^2\right)/3$

The goodness of fit ratio is given by:

$$GoF = \sqrt{\frac{w\left(F_0^2 - F_c^2\right)}{n - p}}$$

with n = number of reflections, p = number of refined parameters.

Figures were drawn using the programs PLUTON/PLATON-97 [5], ORTEP [6] and Mercury 1.4 [7].

6.3.7 X-Ray Powder Diffraction Analysis

The powder samples were inserted in glass capillaries of 0.5 mm diameter. The X-ray powder data were collected on a computer controlled STOE-STADIP focusing powder diffractometer [8] equipped with a curved Ge(111) monochromator, where the CuKα1-line could be well separated (λ=1.5404Å). A STOE linear position sensitive detector [9] was used. All compounds were measured in the range of $8° \leq 2\theta \leq 90°$ using a step width of 0.01°. The indexing procedure was performed using ITO [10] in WinXPow [11] or TREOR [12] in the program EXPO2004 [13]. Structure solutions for complexes were carried out using the program EXPO2004. These structural models were used for Rietveld refinement in GSAS/EXPGUI [14-15]. After the initial refinement of the scale, background, and unit cell constants, the atomic positions were refined using soft constraints defining the geometry of the ligand molecules within some allowable errors [4]. Subsequent Rietveld refinement was carried out using gradually relaxing bond restraints. The metal atom positions were refined anisotropically, while the rest of the non-hydrogen atoms were refined isotropically applying an overall temperature factor for the C, N, O atoms. The temperature factor of the H-atoms was fixed. In the final cycles of refinement, the shifts in all parameters were less than their estimated standard deviations. Neutral atom scattering factors were used for all atoms. No corrections were made for anomalous dispersion, absorption effects, or preferred orientation.

$$R_p = \sum |I_0 - I_c| / \sum I_0$$

$$R_F \langle |F_0| - |F_c| \rangle / \langle |F_0| \rangle$$

6.4 Characterization of Porous Materials

6.4.1 Immersion Calorimetry

Immersion calorimetry experiments were carried out at 293 K on samples of 0.100-0.150 g using a TIAN-CALVET type calorimeter (Figure 6.1) [16-18]. The out-gassed samples were placed in the calorimetric cells (E) and they were immersed into a water bath (A) controlled by a thermo-regulator system LUDA MS. The thermal flow was provided by 180 thermocouples of Cu/constantan (D) connected to a nanovoltmeter PREMA 8017 (B). The integral of the curve, $V=f(t)$, is proportional to the energy generated during the immersion process, $\Delta_i H$, typically between $|1|$ and $|10|$ J. The data were processed by a computer (C). The normal calibration of the calorimetry system was carried out with an electric resistance.

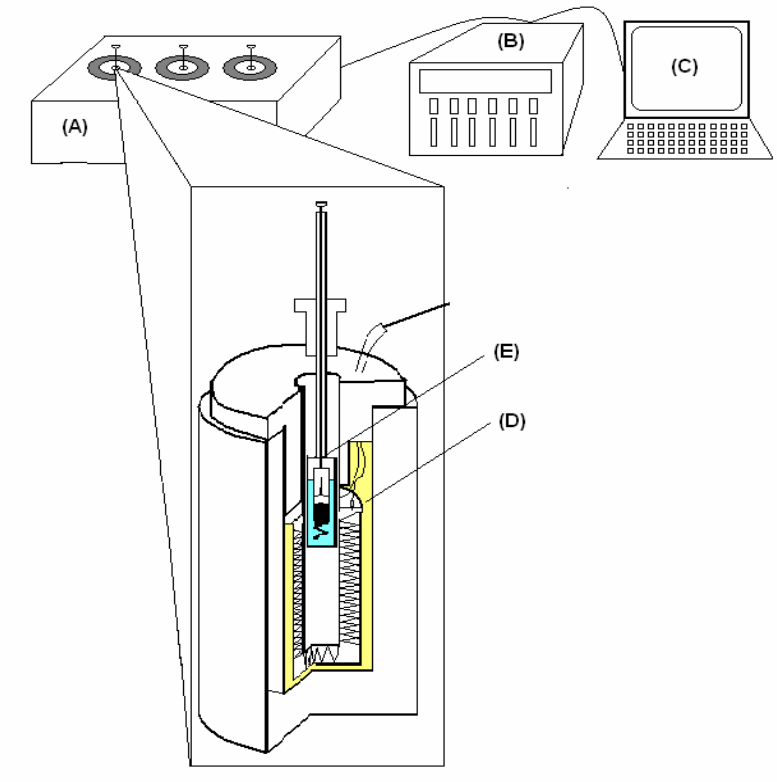

Figure 6.1

Different low polar organic solvents were used with the aim of testing the size of the nanopores. On the other hand, the water immersion experiments provide the value of the enthalpy of decomposition of the three dimensional network into a two dimensional network.

The accuracy varies between 3 and 4 % depending on the absolute energy liberated in the process and on the amount of solid used. The enthalpy of immersion was calculated within the framework of Dubinin's theory [16,19-21].

6.4.2 Gravimetric Isotherms

The adsorption isotherms were determined gravimetrically [16,19] at different temperatures in the range of relative pressures $10^{-4} < p/ps^{-1} < 0.2$. The gravimetric system is schematically illustrated in the Figure 6.2. The Mac Bain type balance (D) with a quartz spring is heated to 310 K by an external water circuit. The sample (~ 0.20 g) is placed into a cylindrical aluminium cell (A) and it is out-gassed in the same conditions as used in calorimetric immersion. Finally the system is heated to the desired temperature by another external water circuit (B). The system is in the initial stage (Step 1, Figure 6.2).

An out-gassed organic solvent vapour is introduced in the system (Step 2, Figure 6.2) and part of this vapour is adsorbed by the sample. The sample weight increases leading to stretching of the spring (Step 3, Figure 6.2) [18].

The adsorption process is a dynamic and microscopic process and it needs some time to attain the equilibrium state. Once the process has attained equilibrium, the change in the spring length is measured by a mobile micrometric magnified glass LEITZ (C).

The steps 2 and 3 were carried out until the system pressure reaches the saturation pressure of the absorbate.

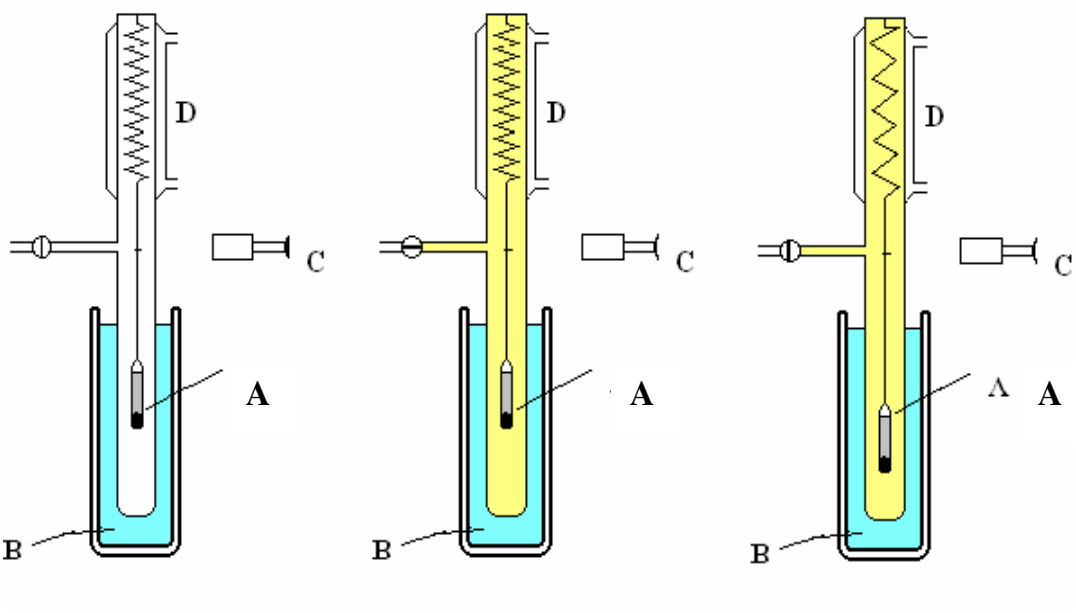

Step (1) Step (2) Step (3)

Figure 6.2

6.5 Complexes with 4,4'-Bipyridine

6.5.1 {[Cu (4,4'-bpy)$_2$ (SiF_6)] (H_2O)$_8$}$_n$: C1

This compound was synthesised following the method described in the literature [22].

Elemental analysis (%) calcd for $C_{20}H_{16}CuSiF_6N_4$: C 46.36, H 3.09, N 10.82; found: C 45.56, H 3.91, N 10.29. The elemental analysis was carried out with an out-gassed sample.
IR (nujol mull): $\tilde{\nu}$ = 3306(s,br), 3109(s), 2453(w), 1982(w), 1612(s), 1538(m), 1494(m), 1427(s), 1229(s), 1089(s), 885(m), 867(m), 829(s), 686(s), 646(s), 570(m), 513(m), 477(m) cm^{-1}.
IR (KBr pellet) : $\tilde{\nu}$ = 3369(s,br), 2945(s), 2878(m), 1611(m), 1534(w), 1494(m), 1459(m), 1411(m), 1222(m), 1087(s), 1043(s), 884(m), 813(s), 741(s), 645(m), 618(m), 482(s) cm^{-1}.

6.5.2 {[Cu (4,4'-bpy)$_2$ (H_2O)$_2$] (SiF_6)}$_n$: C2

This compound was synthesized by exposing the compound **C1** to water.

Elemental analysis (%) calcd for [$C_{20}H_{20}CuO_2SiF_6N_4$] × H_2O: C 41.98, H 3.85, N 9.80; found: C 41.90, H 3.82, N 9.50. This compound is hygroscopic; therefore one additional water molecule has been taken into account.
IR (nujol mull): $\tilde{\nu}$ = 3392(m), 3219(w), 3105(m), 3085(m), 2460(w), 1980(w), 1926(w), 1723(w), 1634(m), 1610(s), 1535(m), 1491(m), 1414(m), 1323(w), 1222(m), 1150(w), 1067(m), 1014(w), 967(w), 852(m), 810(m), 747(m), 685(m), 669(m), 644(m), 611(m), 499(w), 480(w), 463(w) cm^{-1}.
IR (KBr pellet) : $\tilde{\nu}$ = 3431(br, s), 3107(m), 3070(m), 3046(m), 3017(w), 2460(w), 2230(w), 2183(w), 1956(w), 1928(w), 1843(w), 1635(m), 1611(s), 1536(m), 1492(m), 1415(m), 1384(w), 1339(w), 1324(w), 1222(m), 1123(w), 1099(w), 1077(w), 1067(m), 1046(w), 1014(w), 995(w), 967(w), 853(m), 811(s), 748(s), 688(s), 670(m), 644(m), 616(s), 507(w), 499(w), 483(s), 464(w) cm^{-1}.

6.5.3 [Cu F_2 (4,4'-bpy)]$_n$: C3

This compound was synthesized from a **C1** or a **C2** sample put in a closed aluminium oxide crucible and heated at a rate of 2 °Cmin^{-1} until 300 °C under nitrogen (gas flow 150 $mlmin^{-1}$) at atmospheric pressure.

Elemental analysis (%) calcd for $C_{10}H_8CuF_2N_2$: C 46.59, H 3.11, N 10.97; found: C 43.96, H 3.42, N 10.10.
IR (nujol mull): $\tilde{\nu}$ = 3435(w), 3401(w), 3105(w), 3036(w), 2669(w), 1973(w), 1635(w), 1610(s), 1537(w), 1490(m), 1414(m), 1323(w), 1237(w), 1223(w), 1151(w), 1116(w), 1092(w), 1067(w), 1048(w), 1012(w), 967(w), 853(w), 840(w), 811(w), 754(m), 728(m), 688(w), 670(w), 642(w), 616(w), 500(w), 480(w), 460(w) cm^{-1}.

6.5.4 [Cu (OCN)$_2$ (4,4'-bpy)]$_n$: C4

This compound was synthesized by immersion of a solid sample of **C1** or **C8** into a KOCN saturated aqueous solution. After several hours, the solid colour changed from violet to pale-blue. Later on, a filtration was performed and the solid was analyzed by XRPD.

Elemental analysis (%) calcd for $[C_{12}H_8CuN_4O_2] \times 4H_2O$: C 38.34, H 4.26, N 14.91; found: C 38.65, H 2.54, N 14.14.
IR (nujol mull): $\tilde{\nu}$ = 3522(w), 3355(m), 3157(m), 3097(m), 3072(m), 2678(w), 2494(w), 2354(w), 2233(br, s), 1951(w), 1850(w), 1634(m), 1611(s), 1538(m), 1495(m), 1416(s), 1342(s), 1332(m), 1300(m), 1222(s), 1207(m), 1170(w), 1098(w), 1017(m), 1008(m), 891(w), 860(w), 831(w), 815(s), 728(m), 702(w), 676(w), 646(m), 622(s), 613(s), 554(w), 506(w), 497(m) cm^{-1}.

6.5.5 $\{[Ag\ (4,4'\text{-}bpy)]_2\ (SiF_6)\ (HOCH_2CH_2OH)_2\ (H_2O)_2\}_n$: C5

This compound was prepared by the diffusion of an aqueous ethylene glycol solution (1:3) containing a mixture of $Ag(BF_4)$ (0.5 mmol) and $(NH_4)_2SiF_6$ (0.5 mmol) into an ethylene glycol solution of 4,4'-bpy (1 mmol) using a straight-type tube at room temperature. Two weeks later, white needle-like crystals appeared between the layers. The complex is a linear polymer and shows a remarkable stability to light.

Elemental analysis (%) calcd for $C_{24}H_{32}Ag_2O_6SiF_6N_4$: C 34.71, H 3.86, N 6.75; found: C 34.66, H 4.03, N 6.62.
IR (KBr pellet): $\tilde{\nu}$ = 3385(br,s), 2936(m), 1599(s), 1527(w), 1410(m), 1220(m), 1089(s), 1042(s), 1002(w), 883(w), 807(s), 738(s), 621(m), 564(w), 511(w), 482(m) cm^{-1}.

6.5.6 $\{[Co\ (4,4'\text{-}bpy)_3\ (H_2O)_2]\ (BF_4)_2\ (4,4'\text{-}bpy)\ (H_2O)_9\}_n$: C6

This compound was synthesized by adding a water/acetone (1:3) solution containing a mixture of $Co(BF_4)_2 \cdot 6H_2O$ (0.5 mmol) and $(NH_4)_2SiF_6$ (0.5 mmol) to an acetone solution of 4,4'-bpy (1 mmol). A pink precipitate was formed on mixing the two solutions. The precipitate was filtered off and the filtrate allowed to stand for two weeks. Orange block-like crystals were obtained.

Elemental analysis (%) calcd for $C_{40}H_{54}CoO_{11}B_2F_8N_8$: C 45.52, H 5.12, N 10.62; found: C 44.79, H 4.55, N 10.41.
IR (KBr pellet): $\tilde{\nu}$ = 3100(br,s), 1601(s), 1535(m), 1490(m), 1409(s), 1324(w), 1288(w), 1224(m), 1065(br, s), 805(s), 730(m), 625(m), 572(w), 494(w), 468(w) cm^{-1}.

6.5.7 {[Co (4,4'-bpy) $(H_2O)_4$] $(BF_4)_2$ (4,4'-bpy)$_2$ $(H_2O)_2$}$_n$: C7

This product was synthesized by the same procedure as for **C6**.

Elemental analysis (%) calcd for $[C_{30}H_{36}CoO_6B_2F_8N_6] \times 2H_2O$: C 42.63, H 4.77, N 9.94; found: C 42.32, H 4.47, N 10.32. This compound is hygroscopic and contains two more water molecules of crystallization.
IR (KBr pellet): $\tilde{\nu}$ = 3435(br, s), 3063(m), 1949(w), 1610(s), 1600(s), 1537(m), 1491(w), 1410(m), 1384(m), 1323(w), 1299(w), 1220(w), 1084(br, s), 1035(s), 1001(m), 809(m), 731(w), 669(w), 635(w), 622(m), 573(w), 533(w), 522(w), 500(w), 467(w) cm^{-1}.

6.5.8 [Cu (S_2O_6) (4,4'-bpy)$_2$] $(H_2O)_{20}$}$_n$: C8

To an ethylene glycol solution of 4,4'-bpy (1 mmol) (a) was added a methanolic solution of $CuS_2O_6 \cdot 6H_2O$ (0.5 mmol) (b) with stirring at room temperature. After filtration, a violet crystalline powder was obtained suitable for powder X-ray analysis. Single crystals of **C8** suitable for X-ray analyses were obtained by diffusion of (b) into (a).

Elemental analysis (%) calcd for $[C_{20}H_{16}CuO_6S_2N_4] \times 5[OH(CH_2)_2OH]$: C 42.57, H 5.44, N 6.62; found: C 42.06, H 5.46, N 6.81. Elementary analysis carried out for **C8** crystalline powder showed five ethylene glycol solvent molecules instead of twenty water molecules crystallized per fundamental unit.
IR (nujol mull): $\tilde{\nu}$ = 3391(br,s), 3108(m), 3056(m), 2461(w), 1961(w), 1614(s), 1538(m), 1495(m), 1419(s), 1256(s), 1088(s), 990(s), 884(m), 863(w), 822(m), 729(m), 676(w), 646(m), 568(m), 507(w), 463(w), 455(w) cm^{-1}.
IR (KBr pellet): $\tilde{\nu}$ = 3368(br, s), 2944(s), 2877(s), 2342(w), 2183(w), 1930(w), 1648(m), 1610(s), 1599(s), 1534(m), 1493(m), 1457(m), 1410(s), 1385(m), 1338(m), 1248(s), 1215(s), 1087(s), 1043(s), 995(s), 883(m), 864(m), 812(s), 723(m), 678(m), 645(m), 617(m), 568(s), 519(s), 469(w) cm^{-1}.

6.5.9 {[Cu (4,4'-bpy)$_2$ $(H_2O)_2$] (S_2O_6)}$_n$: C9

This compound was synthesized by exposing compound **C8** to water. The initial dark purple powder changes its colour to sky blue, and the corresponding structural changes can be followed by XRPD studies. This compound was also obtained as a side product during the synthesis of **C8**.

Elemental analysis (%) calcd for $[C_{20}H_{20}CuO_8S_2N_4] \times 2H_2O$: C 39.50, H 3.95, N 9.22; found: C 39.51, H 4.00, N 8.53. Two water molecules were added to the formula of compound **C9** related to its hygroscopic behaviour.
IR (nujol mull): $\tilde{\nu}$ = 3400(br, w), 1637(m), 1604(m), 1533(m), 1491(m), 1412(m), 1323(w), 1204(s), 1066(m), 1012(m), 982(s), 813(m), 728(m), 676(w), 639(w), 555(m), 512(w), 468(w) cm^{-1}.
IR (KBr pellet): $\tilde{\nu}$ = 3420(br, s), 2450(w), 2183(w), 1639(m), 1607(s), 1533(m), 1492(w), 1413(m), 1384(w), 1323(w), 1250(s), 1222(s), 1208(s), 1112(w), 1069(m), 1046(w), 1011(w), 991(s), 858(w), 814(m), 729(w), 677(w), 642(m), 616(m), 583(m), 563(m), 514(m), 486(w), 469(w) cm^{-1}.

6.5.10 $\{[Co\ (4,4'\text{-}bpy)_2\ (H_2O)_2]\ (SO_4)\}_n$: C10

The reaction of an ethylene glycol solution of 4,4'-bpy (1 mmol) and a methanolic solution of $CoS_2O_6 \cdot 6H_2O$ (0.5 mmol) produced after several days light orange block-like crystals.

Elemental analysis (%) calcd for $[C_{20}H_{20}CoN_4O_6S] \times 8H_2O$: C 37.10, H 5.60, N 8.65; found: C 37.13, H 4.19, N 7.91. Eight water molecules were added to the formula of compound **C10** related to its hygroscopic behaviour.
IR (KBr pellet): $\tilde{\nu}$ = 3400(br, s), 2928(w), 2852(w), 2446(w), 2321(w), 2163(w), 2074(w), 1943(w), 1833(w), 1645(m), 1606(s), 1534(m), 1492(m), 1413(s), 1384(m), 1343(w), 1323(w), 1262(s), 1228(s), 1202(s), 1093(w), 1065(m), 1021(w), 1008(w), 988(s), 981(s), 867(w), 849(w), 811(s), 780(w), 731(m), 689(m), 654(w), 631(s), 561(s), 512(w), 504(w), 465(w) cm^{-1}.

6.5.11 $[Cu\ (SO_4)\ (4,4'\text{-}bpy)_2]\ (H_2O)_3\ (HOCH_2CH_2OH)_2\}_n$: C11

To an ethylene glycol solution of 4,4'-bpy (1 mmol) (a) was added a methanolic solution of $CuSO_4 \cdot 5H_2O$ (0.5 mmol) (b) with stirring at room temperature. After filtration, a blue crystalline powder was obtained suitable for powder X-ray analysis. Single crystals of **C11** suitable for X-ray analyses were obtained by diffusion of (b) into (a).

Elemental analysis (%) calcd for $C_{24}H_{34}CuO_{11}S_1N_4$: C 43.79, H 5.17, N 8.52; found: C 43.38, H 5.22, N 7.42.
IR (nujol mull): $\tilde{\nu}$ = 3271(br, m), 1611(s), 1536(m), 1418(m), 1225(m), 1015(m), 884(m), 823(m), 724(m), 644(m), 617(m), 571(w), 512(w), 487(w) cm^{-1}.

IR (KBr pellet): $\tilde{\nu}$ = 3400(br, s), 2945(w), 2878(w), 2081(w), 1643(m), 1610(w), 1535(w), 1492(w), 1411(m), 1384(m), 1338(w), 1222(m), 1111(s), 1089(s), 1044(m), 883(w), 812(m), 723(w), 678(w), 644(m), 617(s), 469(w) cm^{-1}.

6.5.12 {[Cu (SO_4) (H_2O)$_2$ (4,4'-bpy)][Cu (SO_4) (4,4'-bpy) ($HOCH_2CH_2OH$)$_2$]}$_n$:C12

When the crystalline powder of **C11** was allowed to stand in solution for a month, the dark blue powder changed into light blue cube-like crystals of **C12**.

Elemental analysis (%) calcd for $C_{24}H_{32}Cu_2O_{14}S_2N_4$: C 36.38, H 4.04, N 7.07; found: C 37.85, H 4.37, N 7.31.
IR (nujol mull): $\tilde{\nu}$ = 2000(w), 1956(w), 1651(w), 1611(m), 1569(w), 1538(m), 1418(s), 1334(m), 1300(m), 1152(s), 1076(s), 1015(s), 918(m), 890(m), 826(m), 728(m), 678(w), 646(m), 623(m), 590(m), 577(m), 547(m), 489(m) cm^{-1}.
IR (KBr pellet): $\tilde{\nu}$ = 3429(br, s), 2932(w), 2876(w), 2078(w), 1643(m), 1610(s), 1536(w), 1492(w), 1417(m), 1384(m), 1336(w), 1222(m), 1107(s), 1077(s), 1044(m), 963(w), 875(w), 813(m), 723(w), 678(w), 645(m), 617(s), 470(w) cm^{-1}.

6.5.13 [Cu (SO_4) (4,4'-bpy)]$_n$: C13

When samples of **C8**, **C9**, **C11**, and **C12** are heated up to 210-225 °C, the resulting green crystalline powder is the 3D polymer denoted as **C13**.

Elemental analysis (%) calcd for $C_{10}H_8CuO_4SN_2$: C 38.03, H 2.55, N 8.87; found: C 38.20, H 2.72, N 8.91.
IR (nujol mull): $\tilde{\nu}$ = 3141(w), 3104(w), 3088(w), 3065(w), 3036(m), 2670(w), 2472(w), 2238(w), 1972(w), 1879(w), 1742(w), 1677(w), 1610(s), 1544(w), 1490(m), 1413(m), 1305(w), 1238(w), 1153(w), 1092(m), 1048(w), 1011(w), 972(w), 891(w), 838(m), 729(m), 684(w), 642(m), 477(w), 459(w) cm^{-1}.
IR (KBr pellet): $\tilde{\nu}$ = 3436(br, s), 3075(w), 3038(w), 3017(w), 2093(w), 1643(m), 1610(s), 1545(w), 1490(w), 1413(m), 1384(m), 1237(w), 1216(w), 1092(w), 1048(w), 1012(w), 839(m), 813(w), 729(w), 643(m), 474(w), 459(w) cm^{-1}.

6.5.14 {[Co_2 (SO_4) (S_2O_6) (4,4'-bpy)$_4$] (H_2O)$_5$ }$_n$: C14

Compound **C14** was synthesized by diffusion of a methanolic solution of $CoS_2O_6 \cdot 6H_2O$ (0.5 mmol) into an ethylene glycol solution of 4,4'-bpy (1 mmol) under N_2 atmosphere. The solvents used were dried according to standard laboratory practices. Two weeks later, light orange block-like crystals appeared in the solution.

Elemental analysis (%) calcd for $[C_{40}H_{42}Co_2N_8O_{15}S_3] \times 16H_2O$: C 37.32, H 4.98, N 8.71; found: C 37.74, H 4.30, N 7.58. This compound is strongly hygroscopic; therefore sixteen water molecules have been taken into account.
IR (KBr pellet): $\tilde{\nu}$ = 3321 (br, s), 2953(m), 2935(m), 2880(m), 2330(w), 1646(m), 1607(s), 1537(m), 1491(m), 1454(w), 1414(s), 1384(w), 1374(w), 1338(w), 1260(m), 1221(s), 1186(s), 1115(s), 1076(s), 1065(s), 1036(s), 1008(m), 988(m), 959(m), 878(w), 835(w), 8067(m), 728(m), 697(m), 663(w), 633(s), 619(s), 562(m), 513(w), 479(w) cm^{-1}.

6.6 Complexes with 4,4′-Dipyridyl-N,N′-dioxide

6.6.1 $\{[Cu(H_2O)(dpdo)_2](S_2O_6)(H_2O)\}_n$: C15

A solution of $CuS_2O_6 \cdot 6H_2O$ (0.5 mmol) dissolved in 5 ml of ethanol was added to a solution of 4,4'-dpdo (1 mmol) dissolved in 5 ml of ethanol. A red precipitate was formed inmediatily. Upon slow evaporation of the solvent, green block-like crystals were obtained.

Elemental analysis (%) calcd for $[C_{20}H_{20}CuN_4O_{12}S_2] \times 7H_2O$: C 31.51, H 4.46, N 7.35; found: C 29.27, H 3.51, N 6.46. This compound is unstable and attracts water from the air during the decomposition process. Consequently, the elemental analysis has been calculated with an additional quantity of seven water molecules.
IR (KBr pellet): $\tilde{\nu}$ = 3421(br, m), 3127(br, s), 1644(m), 1594(m), 1512(w), 1470(w), 1400(s), 1214(m), 1182(m), 1118(w), 987(w), 858(w), 846(w), 795(w), 729(w), 607(w), 567(w), 508(w), 496(w) cm^{-1}.

6.6.2 $\{[Co(dpdo)_3](S_2O_6)(C_2H_5OH)_7\}_n$: C16

An ethanolic solution (10 ml) of $CoS_2O_6 \cdot 6H_2O$ (0.5 mmol) was gently added into an ethanolic solution (10ml) of 4,4'-dpdo (1 mmol). After one day, orange block-like crystals were obtained.

Elemental analysis (%) calcd for $[C_{30}H_{24}CoN_6O_{12}S_2] \times 6H_2O$: C 40.41, H 4.07, N 9.42; found: C 40.84, H 3.69, N 9.27. Crystals lost solvent of crystallization very rapidly attracting water from the air during the decomposition process.
IR (KBr pellet): $\tilde{\nu}$ = 3114(br, s), 2418(w), 1621(br,w), 1546(w), 1471(s), 1401(s), 1322(w), 1224(s), 1180(s), 1029(m), 984(m), 837(m), 700(w), 553(m), 511(w) cm^{-1}.

6.6.3 {[Ni (dpdo)$_3$] (S_2O_6) (C_2H_5OH)$_7$}$_n$: C17

An ethanolic solution (10 ml) of $NiS_2O_6 \cdot 6H_2O$ (0.5 mmol) was gently added into an ethanolic solution (10ml) of 4,4'-dpdo (1 mmol). After one day, orange needle-like crystals were obtained.

Elemental analysis (%) calcd for $[C_{30}H_{24}NiN_6O_{12}S_2] \times 6H_2O$: C 40.42, H 4.07, N 9.43; found: C 40.46, H 3.91, N 9.23. Crystals lost solvent of crystallization very rapidly attracting water from the air during the decomposition process.
IR (KBr pellet): $\tilde{\nu}$ = 3116 (br, s), 1621(br, w), 1546(w), 1470(s), 1401(s), 1322(w), 1222(s), 1177(s), 1028(m), 984(m), 836(m), 700(w), 552(m), 475(w) cm^{-1}.

6.6.4 {[Co (dpdo) (H_2O)$_5$] (SO_4) (H_2O)$_2$}: C18

An ethanolic solution (10ml) of 4,4'-dpdo (1 mmol) was gently added to an aqueous solution (10 ml) of $CoS_2O_6 \cdot 6H_2O$ (0.5 mmol). Upon slow evaporation, orange needle-like crystals were obtained. This compound can also be obtained using directly $CoSO_4$ instead of the corresponding dithionate salt following the same procedure.

Elemental analysis (%) calcd for $C_{10}H_{22}CoN_2O_{13}S$: C 25.59, H 4.73, N 5.97; found: C 24.6, H 4.29, N 5.48.
IR (KBr pellet): $\tilde{\nu}$ = 3132(br, s), 1636(br, w), 1550(w), 1474(m), 1400(s), 1325(w), 1237(m), 1185(m), 1090(w), 1031(w), 986(w), 839(m), 699(w), 559(w), 520(w), 485(w) cm^{-1}.

6.6.5 {[Ni (dpdo) (H_2O)$_5$] (SO_4) (H_2O)$_2$}: C19

An ethanolic solution (10ml) of 4,4'-dpdo (1 mmol) was gently added into an aqueous solution (10 ml) of $NiS_2O_6 \cdot 6H_2O$ (0.5 mmol). Upon slow evaporation, green needle-like crystals were obtained. This compound can also be obtained using directly $NiSO_4$ instead of the corresponding dithionate salt, following the same procedure.

Elemental analysis (%) calcd for $C_{10}H_{22}NiN_2O_{13}S$: C 25.61, H 4.73, N 5.97; found: C 25.12, H 4.63, N 5.80.

IR (KBr pellet): $\tilde{\nu}$ = 3128(br, s), 1650(br, w), 1549(w), 1475(m), 1400(s), 1324(w), 1242(w), 1188(w), 1115(m), 1030(w), 982(w), 840(w), 763(w), 698(w), 622(w), 559(w), 506(w), 489(w) cm^{-1}.

6.7 Synthesis of Organic Compounds

6.7.1 [(H_2-BCTA)(H-Apy)$_2$]

The organic salt [(H_2-BCTA)(H-Apy)$_2$] was synthesized by exposing the starting materials to microwave irradiation at 600W for 90 min. In a second way, [(H_2-BCTA)(H-Apy)$_2$] was synthesized at 180°C under nitrogen atmosphere and heated at a rate of 2 °Cmin^{-1} using a thermogravimetric module. The molar composition of the reaction mixture was 1 H_4-BCTA: 2 Apy. The starting materials were completely converted to the product as shown by XRPD.

Elemental analysis (%) calcd for $C_{20}H_{18}N_4O_8$: C 54.30, H 4.07, N 12.67; found: C 54.15, H 3.87, N 12.56.
IR (KBr pellet): $\tilde{\nu}$ = 3393(m), 3215(m), 3096(w), 3059(w), 2923(m), 2802(w), 2697(w), 1698(m), 1655(br,s), 1616(m), 1591(m), 1567(m), 1534(s), 1468(s), 1428(m), 1365(m), 1325(m), 1290(w), 1274(w), 1140(m), 1083(m), 1018(m), 961(w), 874(w), 821(m), 751(w), 694(m), 631(w), 558(w), 523(w), 497(w) cm^{-1}.

6.7.2 [(H_2-BCTA)(H-Apyz)$_2$]

Crystals of the organic salt [(H_4-BCTA)(Apyz)$_2$] were synthesized by exposing the starting materials to microwave irradiation at 600W for 90 min. In a second way, [(H_4-BCTA)(Apyz)$_2$] molecular crystals were synthesized at 120°C under nitrogen atmosphere and heated at a rate of 2 °Cmin^{-1} using a thermogravimetric module. The molar composition of the reaction mixture was 1 H_4-BCTA: 2 Apyz . The starting materials were completely converted to the product as shown by XRPD.

Elemental analysis (%) calcd for $C_{18}H_{16}N_6O_8$: C 48.61, H 3.60, N 18.90; found: C 48.42, H 3.26, N 18.21.
IR (KBr pellet): $\tilde{\nu}$ = 3333(m), 3101(m), 2507(w), 1992(w), 1895(w), 1701(m), 1661(br,s), 1614(m), 1579(s), 1488(s), 1458(s), 1349(s), 1287(m), 1243(w), 1215(m),

1139(s), 1110(s), 1037(s), 989(m), 957(w), 855(m), 828(m), 749(m), 721(m), 615(m), 562(m) cm^{-1}.

6.7.3 [(H_2-BCTA)(H-ClApy)$_2$]

The organic salt [(H_2-BCTA)(H-ClApy)$_2$] was synthesized by exposing the starting materials to microwave irradiation at 600W for 90 min. In a second way, [(H_2-BCTA)(H-ClApy)$_2$] was synthesized at 180°C under nitrogen atmosphere and heated at a rate of 2 °Cmin^{-1} using a thermogravimetric module. The molar composition of the reaction mixture was 1 H_4-BCTA: 2 ClApy. The starting materials were completely converted to the product as shown by XRPD.

Elemental analysis (%) calcd for $C_{20}H_{16}Cl_2N_4O_8$: C 46.97, H 3.16, N 10.96; found: C 46.70, H 3.11, N 9.75.
IR (KBr pellet): $\tilde{\nu}$ = 3393(m), 3307(m), 3198(m), 3099(m), 2924(w), 2856(w), 2617(w), 1909(w), 1712(m), 1645(br,s), 1608(m), 1581(s), 1539(s), 1464(s), 1421(s), 1360(s), 1319(s), 1280(m), 1240(m), 1182(m), 1129(m), 1077(m), 979(m), 919(m), 859(m), 815(m), 752(m), 722(w), 681(m), 605(w), 587(w), 527(w), 483(w) cm^{-1}.

6.7.4 pyIMID

The ligand py-IMID was synthesized at 260°C under nitrogen atmosphere and heated at a rate of 2°Cmin^{-1} using a thermogravimetric module. The molar composition of the reaction mixture was 1 H_4-BCTA: 2 Apy. The starting materials were completely converted to the product as shown by XRPD.

Elemental analysis (%) calcd for $C_{20}H_{10}N_4O_4$: C 64.87, H 2.72, N 15.13; found: C 64.48, H 2.90, N 15.04.
IR (KBr pellet): $\tilde{\nu}$ = 3488(w), 3037(w), 2517(w), 1953(w), 1831(w), 1787(w), 1725(br,s), 1702(s), 1588(m), 1570(m), 1504(m), 1468(w), 1452(w), 1416(m), 1400(m), 1250(w), 1222(m), 1193(w), 1160(w), 1127(s), 1077(m), 990(w), 958(w), 917(w), 857(m), 804(s), 730(w), 720(s), 680(w), 659(w), 625(w), 569(w), 523(m), 496(w), 456(m) cm^{-1}.
EI-MS: *m/z* 370.13 $[M]^+$.

6.7.5 pyzIMID

The ligand pyz-IMID was synthesized at 190°C under nitrogen atmosphere and heated at a rate of 2°Cmin^{-1} using a thermogravimetric module. The molar composition of the reaction mixture was 1 H_4-BCTA: 2 Apyz. The starting materials were completely converted to the product as shown by XRPD.

Elemental analysis (%) calcd for $C_{18}H_8N_6O_4$: C 58.06, H 2.15, N 22.58; found: C 57.04, H 2.10, N 21.08.
IR (KBr pellet): $\tilde{\nu}$ = 3487(w), 3040(w), 2923(w), 1946(w), 1784(m), 1738(br,s), 1717(s), 1578(w), 1550(w), 1523(w), 1480(m), 1456(w), 1416(s), 1366(s), 1316(w), 1297(w), 1217(w), 1185(w), 1151 (w), 1099(m), 1053(m), 1016(m), 922(w), 886(w), 863(w), 853(w), 826(m), 808(w), 752(w), 721(s), 669(w), 634(w), 617(w), 570(w) cm^{-1}.
EI-MS: *m/z* 372.78 $[M]^+$.

6.7.6 ClpyIMID

The ligand Clpy-IMID was synthesized at 220°C under nitrogen atmosphere and heated at a rate of 2°Cmin^{-1} using a thermogravimetric module. The molar composition of the reaction mixture was 1 H_4-BCTA: 2 ClApy. The starting materials were completely converted to the product as shown by XRPD.

Elemental analysis (%) calcd for $C_{20}H_8Cl_2N_4O_4$: C 54.68, H 1.82, N 12.76; found: C 54.67, H 2.04, N 12.55.
IR (KBr pellet): $\tilde{\nu}$ = 3487(w), 3137(w), 3111(w), 3097(w), 3044(w), 1947(w), 1780(m), 1733(br,s), 1711(s), 1584(s), 1544(m), 1468(s), 1386(s), 1351(s), 1290(m), 1201(s), 1136(w), 1090(m), 1068(s), 990(w), 927(w), 908(w), 871(w), 845(m), 829(m), 748(m), 725(m), 672(w), 615(m), 604(w), 574(w), 492(w) cm^{-1}.
EI-MS: *m/z* 437.74 $[M]^+$, *m/z* 439.75 $[M+2]^+$, *m/z* 441.77 $[M+4]^+$.

6.7.7 H-pyIMID

This organic compound was obtained by hydrolysis of **pyIMID** in HCl 0.5 N. After several days, colourless needles-like and plates-like crystals (*para* and *meta* form, respectively) were obtained (ratio 70:30).

Elemental analysis (%) calcd for $C_{20}H_{16}Cl_2N_4O_6$: C 50.12, H 3.36, N 11.69; found: C 49.20, H 3.62, N 11.40.
IR (KBr pellet): $\tilde{\nu}$ = 3415(br, m), 3107(m), 2923(m), 1702(s), 1634(s), 1601(s), 1556(s), 1502(s), 1417(s), 1318(s), 1233(s), 1193(s), 1133(m), 1104(s), 1008(m), 947(m), 914(w), 876(m), 807(m), 716(m), 671(w), 642(w), 624(w), 525(w) cm^{-1}.
EI-MS: *m/z* 515.83 $[(M+2)+Cl^-]^-$, *m/z* 517.83 $[(M+4)+Cl^-]^-$.

6.7.8 H-pyzIMID

This organic compound was obtained by hydrolysis of **pyzIMID** in HCl concentrated. After several days, colourless needles-like crystals (*para* form) were obtained.

Elemental analysis (%) calcd for $C_{18}H_{14}Cl_2N_6O_6$: C 44.92, H 2.93, N 17.46; found: C 46.75, H 3.31, N 17.46.
IR (KBr pellet): $\tilde{\nu}$ = 3117(br, s), 2805(m), 2541(br, m), 2100(w), 1722(m), 1687(m), 1622(w), 1593(w), 1543(s), 1494(m), 1449(m), 1400(s), 1349(m), 1289(m), 1273(m), 1261(m), 1242(m), 1199(m), 1131(w), 1107(m), 1062(w), 1001(w), 895(w), 821(m), 779(w), 717(w), 665(w), 647(w), 609(w), 534(w), 500(w), 493(w) cm^{-1}.
EI-MS: *m/z* 480.59 $[M]^-$, *m/z* 517.70 $[(M+2)+Cl^-]^-$.

6.8 Precursers

6.8.1 {[Cu (Apy)$_4$] Cl$_2$}: P1

Crystals of **P1** were obtained by diffusion of an methanolic solution of Apy (4 mmol, 10ml) into an aqueous solution of copper(II) chloride dihydrate (1 mmol, 10ml). After several days, dark-blue block-like crystals appeared at the bottom of the test tube.

Elemental analysis (%) calcd for $C_{20}H_{24}Cl_2CuN_8$: C 47.02, H 4.73, N 21.93; found: C 46.06, H 5.07, N 20.88.
IR (KBr pellet): $\tilde{\nu}$ = 3477(s), 3381(s), 3319(s), 3196(s), 2677(w), 2551(w), 2074(w), 1635(s), 1615(s), 1560(m), 1516(s), 1455(m), 1384(m), 1345(m), 1286(w), 1216(s), 1059(w), 1019(m), 854(w), 826(m), 732(w), 670(w), 621(w), 568(w), 530(m) cm^{-1}.

6.8.2 [Cu (ClApy)$_2$ Cl$_2$]: P2

Crystals of **P2** were synthesized by diffusion of an methanolic solution of ClApy (4 mmol, 10 ml) into an ethanolic solution of copper(II) chloride dihydrate (1mmol, 10 ml). After several days, green block-like crystals were obtained.

Elemental analysis (%) calcd for $C_{10}H_{10}Cl_4CuN_4$: C 30.67, H 2.57, N 14.31; found: C 30.65, H 2.72, N 14.27.
IR (KBr pellet): $\tilde{\nu}$ = 3426(s), 3319(s), 3240(m), 3210(m), 2924(w), 2802(w), 2700(w), 2599(w), 2563(w), 2343(w), 2076(w), 1943(w), 1913(w), 1626(s), 1614(s), 1541(s), 1505(s), 1443(m), 1385(m), 1360(m), 1301(m), 1264(m), 1141(m), 1086(m), 1027(m), 958(w), 922(m), 848(w), 826(s), 722(w), 611(w), 567(w), 457(w) cm^{-1}.

6.9 References

[1] W. L. F. Armarego, D. D. Perrin, *"Purification of Laboratory Chemicals"*, fourth edition, Butterworth-Heinemann, Oxford (UK), **1996**.

[2] Sheldrick, G.M. *SHELXS-97 Program for the Solution of Crystal Structures, Acta Crystallogr.*, *A46*, 467, **1990**.

[3] Sheldrick, G.M. *SHELXL-97*, *Program for the Refinement of Crystal Structures*, University of Göttingen, (Germany), **1997**.

[4] The International Union of Crystallography, *International Tables for Crystallography*, version 5.1, vol. C, Ed. Wilson, Kluwer Academic Publishers, Dorecht (Germany), **1995**.

[5] Spek, A.L. *Acta Crystallogr.*, *A46*, C-34, **1990**.

[6] L. Zsolnai, ZORTEP, *Molecular Graphics Program*, University of Heilderberg, (Germany), **1997**.

[7] *Mercury 1.4*, Cambridge Crystallographic Data Center, Cambridge (UK), **2001-2005**.

[8] Wolfel, E. R., *J. Appl. Crystallogr.*, 14, 291-296, **1981**.

[9] Wolfel, E. R., *J. Appl. Crystallogr.*,16, 341-348, **1983**.

[10] Visser, J. W., *J. Appl. Crystallogr.* 2, 89-95, **1969**.

[11] Stoe & Cie. WinXPow: STOE Powder Diffraction Software, Version 1.10. Stoe & Cie GmbH, Darmstadt, Germany, **2002**.

[12] Werner, P. E.; Eriksson, L.; Westdahl, M., *J. Appl. Crystallogr.*, 18, 367-370, **1985**.

[13] Altomare, A.; Camalli M.; Caliandro R.; Cuocci C.; Giacovazzo C.; Guagliardi A.; Moliterni A. G. G.; Rizzi R.: *EXPO2004. Program for Solving Crystal Structures from Powder Data by direct Methods*, **2004**.

[14] Larson, A.; Von Dreele, R.B., *GSAS*, *Generalized Structure Analysis System*, Los Alamos National Laboratory Report LAUR 86-748, Los Alamos, (NM), **2000**.

[15] Toby, B. H., *J. Appl. Cryst.*, 34, 210-213, **2001**.

[16] Bansal R. C., Donnet J. B., Stoeckli F., *Active Carbon*, Marcel Dekker, New York, 119 – 162, **1988**.

[17] Stoeckli F., Hugi-Cleary D., Centeno T. A., *J. Eur. Ceram. Soc.*, 18, 1177-1185, **1998**.

[18] Fernández Ibañez M. E., *Étude de la Carbonisation et l'Activation de Précurseurs Végétaux Durs et Mous*, Thèse de Doctorat, Université de Neuchâtel, Neuchâtel, **2002**.

[19] F. Stoeckli, *Porosity in Carbons*, (Ed.: J. Patrick), Arnold, London, 67 – 92, **1995**.

[20] F. Stoeckli, *Russ. Chem. Bull. Int. Ed.*, 50, 2265 – 2272, **2001**.

[21] Dubinin M. M., *Progress in Surface and Membrane Science*, Vol. 19 (Ed.: D. A. Cadenhead), Academic Press, London, 1 – 69, **1975**.

[22] Noro S., Kitagawa S., Kondo M., Seki K., *Angew. Chem., Int. Ed.* 39, 2082-2084, **2000**.